universität wien

MASTERARBEIT / MASTER'S THESIS

Titel der Masterarbeit / Title of the Master's Thesis

„Chitosan membranes for wastewater treatment"

verfasst von / submitted by

Jan Engelbert Janesch, BSc

angestrebter akademischer Grad / in partial fulfilment of the requirements for the degree of

Master of Science (MSc)

Wien, 2018 / Vienna 2018

Studienkennzahl lt. Studienblatt / degree programme code as it appears on the student record sheet:	A 066 862
Studienrichtung lt. Studienblatt / degree programme as it appears on the student record sheet:	Masterstudium Chemie
Betreut von / Supervisor:	Prof. Dr. Alexander Bismarck

Contents

Danksagung

Ich danke Prof. Alexander Bismarck für die Möglichkeit, die Masterarbeit in einer tollen, internationalen Arbeitsgruppe machen zu können.
Mein besonderer Dank geht an Dr. Andreas Mautner für seine Geduld, konstruktive Kritik und dafür, dass er sogar im Urlaub meine Masterarbeit korrekturgelesen hat.

Am meisten möchte ich meinen Eltern danken, die mich sowohl emotional als auch finanziell immer schon bei all meinen Projekten unterstützt haben.
Bedanken will ich mich auch bei meiner Freundin Vera, die es mir nie übel genommen hat, dass ich so manchen schönen Sommertag (und -abend) im Labor verbracht habe.

Ich danke des weiteren Mag. Johannes Theiner für die Durchführung der Elementaranalyse und FTIR-Spektroskopie und Dr. Markus Bacher für die NMR-Spektroskopie meiner Proben. Außerdem danke ich Agnes Wildauer für die Titration der Kupfernitrat-Lösungen und Manuel Holzmann für die Bereitstellung seiner Daten zur statischen Adsorption.

1 Introduction

Already today 1.2 billion people have to drink polluted water [1]. Unfortunately, in the decades to come the need for clean water will increase more than ever before [2] so that by 2025 more than half of the world's population is estimated to be living in areas with water scarcity [3]. This shortage is attributed to climate change, population rise, the expansion of cities, dietary changes [4], energy production, and industry [2].
By clean water becoming a rare and precious commodity in many parts of the world there is an urgent demand for the reuse of polluted water. Contrary to that, today more than 80% of the world's wastewater is directly released into the environment without prior treatment [2]. Besides the need to recycle wastewater, contaminated industrial process water poses a major threat to both the environment and our health.

Water pollutants may be of chemical or biological origin. The former class splits into inorganic compounds, such as heavy metals, and organic materials, which also include hormones and various toxins. Toxic dyes are extensively used in the textile, plastics and food industry [5]. Byproducts of synthetic dyes used as food dyes contain aromatic amines and phenolic compounds, which are often mutagenic and carcinogenic [6]. Biological pollutants often stem from faeces containing bacteria, viruses and parasites. Polluted drinking water is linked to the transmission with diseases such as cholera, diarrhoea, dysentery, hepatitis A, typhoid, and polio [3]. Among the industries producing the biggest share of water pollution are agriculture, mines, the petrochemical, steel and paper industry. Further causes for water pollution include urbanisation and energy production [7].

1.1 Waste water treatment

1.1.1 Filtration in wastewater treatment

A major challenge in wastewater treatment is the removal of small pollutants. One method to achieve this is the use of nanofiltration (NF) and ultrafiltration (UF) membranes. Both use the principle of size exclusion to reject matter bigger than the pore size of the filtration membrane. The pore size of UF membranes lies between 2 and 100 nm, which enables them to reject pollutants, such as bacteria, larger viruses and also bigger molecules, such as proteins. NF membranes have a smaller pore size (<2 nm) and are therefore able to remove all types of viruses as well as many inorganic and organic molecules such as divalent ions and dyes by size exclusion [8].
NF is also used for desalination of salt water [9] and for reducing water hardness [10]. Reverse osmosis (RO) membranes have a pore size even smaller than NF membranes and can reject salts and small organic molecules. An advantage of NF over RO is the smaller pressure at which the system can be operated. RO membranes need high pressure to achieve an accept-

able permeance [11]. While RO membranes can reject monovalent ions, NF membranes are more efficient at removing divalent ions.

One of the problems of NF membranes is that they are prone to fouling. This happens when particles clog the pores. This is a reason for high maintenance costs and thus one of the drawbacks of NF membranes. Membrane fouling is often caused by nonpolar compounds and can hence be reduced by making the membrane surface more hydrophilic. Such a surface will preferably be covered by a layer of water, instead of adsorbing nonpolar species forming a biofilm [12]. Membranes made of polysaccharides present hydroxyl functional groups on their surface, thus they are already polar. In addition to that, chitosan contains free amino groups. The hydrophilic properties of these membranes are therefore advantageous for filtration applications. Besides hydrophilicity a second parameter affecting fouling is the surface roughness. A rougher surface provides a greater area and more ways for mechanical locking of molecules [13]. Most nanofiltration membranes are based on polyamide or cellulose acetate. However, today many more polymeric materials are studied for their potential in this field [14] and renewable polymers are on the rise.

1.1.2 Adsorption of heavy metal ions in wastewater treatment

Heavy metals are defined as metals having a density greater than 5 g/cm^3. These include for example nickel(II), lead(II) [15], cadmium(II) and copper(II) [16], arsenic (II) [17] and mercury(II) which are all toxic to humans at low concentration. Heavy metals are among the most dangerous contaminants in water. Higher doses lead to damage of the brain, lungs, kidney, and liver [17]. They are released into the environment by mining or industrial processes. Absorbed by plants, they enter the food chain and have the tendency to accumulate in the organism [17]. Even though being an essential element for humans [18], Cu^{2+} is toxic above concentrations of 0.25 mg/L and is known for causing liver damage, Wilson disease and insomnia. Due to its easy bioaccumulation it is present throughout the food chain [19]. Adsorption is one of the most effective low-cost tools for the removal of heavy metal ions from industrial streams. This approach towards water treatment employs a material that interacts with pollutants, e.g. heavy metals, thereby removing them from water. The two possible adsorption processes are chemisorption through chemical bonding and physisorption only by van der Waals forces. One prominent adsorption technique is ion exchange, in which ions adsorbed to the substrate are exchanged with ions present in the solution. However, it has the problem that it cannot handle highly concentrated heavy metal solutions, and its effectiveness is strongly dependent on the pH value [20]. Zeolithes are often used for ion exchange due to their high surface area and affinity to heavy metals. They are formed of SiO_4 and AlO_4 and have high affinity towards cations because of their negative net charge [21]. Also clays are used for adsorption, although their adsorption capacity for metal ions is lower compared to zeolithes. Activated carbon is one of the classical adsorbents. It has a high surface area and may present functional groups such as carboxyl-, carbonyl-, phenol-, quinone-,

and lactone groups [22]. Because of the cost of coal based carbon agricultural waste, such as coconut buttons [23], rice husks [24] or sawdust, have been investigated [22, 25] for their potential as alternative sources for activated carbon.

Generally, as the demand for cheap adsorbers is greater than ever before, research focusses on the use of wasteproducts for water treatment applications. Many industrial waste products such as fly ash, blast furnace slag and sludge, black liquor lignin, red mud, and waste slurry may, especially if chemically modified, be used for the adsorption of heavy metal ions [26]. Furthermore, chitin and chitosan are good adsorbers for heavy metal ions. They can be extracted from fungal biomass, gained as a waste stream from industrial citric acid fermentation [27].

1.2 Biomaterials - the green alternative to fossil based materials

Biomaterials as alternative media for adsorption and filtration are attracting increasing interest [28]. They may be derived either from dead biomass, algal biomass or microbial biomass [22]. A big advantage of biopolymers such as cellulose and chitin is their renewability, additionally most biopolymers are also biodegradable. On the other hand, conventional membranes for water purification are often made from synthetic polymers using fossil resources [29] or ceramics requiring a lot of energy for their preparation.

Another big advantage of biopolymers is cost effectiveness owed to their high abundance and renewability. Socioeconomic factors play a significant role in wastewater cleaning. High-income countries treat about 70% of the wastewater they generate, whereas in low-income countries only 8% of wastewater is treated. Besides infrastructure and technical capacity also the financial aspect is a factor [2]. Cheap filtration systems are therefore in high demand [28]. Especially in nanofiltration the cost of membranes is critical and one of the reasons why NF is less widely used than UF and RO. For these reasons there is now an increasing number of biomaterials explored for nanofiltration and adsorption applications.

1.2.1 Nanocellulose and its potential use in water treatment

While there is a lot of literature on the use of cellulose acetate for ultrafiltration and nanofiltration [30], employing nanocellulose (NC) for this purpose is a relatively new approach [31, 32]. NC is the nanostructured form of cellulose and can be produced by mechanical or chemical treatment of cellulose, but can also be produced by bacterial fermentation [33]. NC is made of fibrils with diameters of 2 to 100 nm. Nanocellulose may appear in the form of bacterial cellulose, wood-derived nanocellulose, TEMPO-oxidized cellulose nanofibrils, and cellulose nanocrystals [33, 33]. A common way to obtain nanocellulose is the use of mechanical shear forces to separate the fibers of wood pulp into nanofibers. Chemical modification in a TEMPO-oxidation facilitates the splitting into NC fibrils. Cellulose nanocrystals are obtained from wood by acidic extraction. In addition to plant derived NC there is bacterial cellulose, which is a material excreted by certain types of bacteria.

Manufacturing of tight ultrafiltration (UF) membranes from all of these NC varieties has been proven to be feasible by Mautner et al. [34]. The molecular weight cut-offs were found in the range of 6 to 25 kDa corresponding to a pore size of only a few nanometers. It is noteworthy that the permeance was comparable to commercial NF membranes. This parameter was dependent on the type of NC (fibril diameter) and the grammage of the papers. RO membranes have also been produced using nanocellulose fibers as a support for interfacial polymerisation. The membranes were tested positivily for desalination applications [12].
Moreover, nanocellulose papers are good candidates for organic solvent filtration. Their advantages over polymer membranes, ceramics and organic–inorganic hybrid materials are their solvent stability, cost-effectiveness and environmentally friendly production [32]. Another big advantage of nanocellulose are its antifouling properties (see 1.1.1) [12]. Furthermore, it was found that chemically modified NC is also a good candidate for adsorption [35]. Functionalized NC-membranes can be used to remove heavy metal ions and organic dyes from water.

1.2.2 Chitin - an idle resource

Above we saw that biobased nanofibrils, such as NC, are capable of removing pollutants from water by size exclusion. In addition to that, NC can also be used for adsorption processes, if chemically modified. But what about using biobased nanofibrils that are already functionalised for the adsorption of pollutants? Chitin is a polymer that carries acetyl-groups and has been demonstrated to be able to remove ions from water [36]. Right after cellulose chitin is the second most abundant renewable biopolymer on the planet. It is insoluble in water and organic solvents. However, oligomers of chitin may be dissolved in water [37]. Furthemore it is possible to process chitin into hydrogels [38].
The structural similarity of chitin and cellulose can be seen in Figure 1. While cellulose consists of glucose monomers, chitin is formed of N-acetyl-D-glucosamine subunits connected through a β-1-4-linkage.

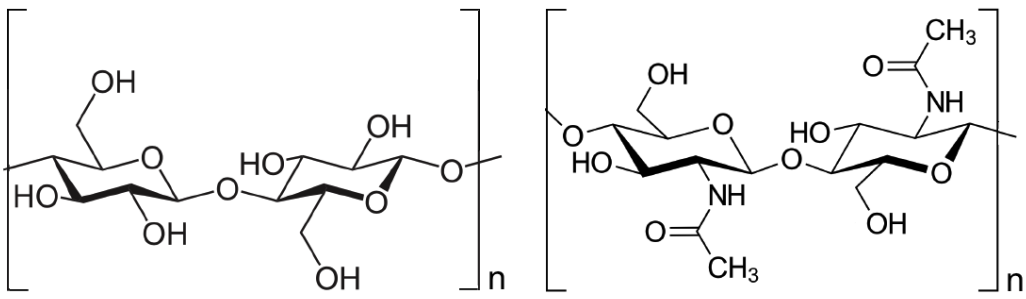

Figure 1: Cellulose (left) consists of glucose [39] and chitin (right) is a N-acetylglucosamine polymer [40].

In the animal kingdom chitin is found in the exoskeleton of arthropods, especially in that

of insects and crustaceans, such as shrimp and lobster, but also arachnids and myriapoda contain chitin. The two conformational isomers are α-chitin which is alligned in anti-parallel fashion and β-chitin, arranged in parallel [41]. Chitin in crustaceans and insects is in the α-form, while in molluscs such as squid it is present as β-chitin. The strong hydrogen bonding in α-chitin makes it more stable than the β-form [42]. Besides its presence in animals, chitin is also found in the fungal cell wall, where it is present as chitin-glucan.

Chitin contents vary a lot from species to species. The exoskeleton of shell waste usually comprises 30–40% proteins, 30–50% minerals and 20–30% chitin. The exoskeletons of lobster and shrimp are made of 69.8 and 17.8% chitin, respectively. While dried mycelium of *Aspergillus niger* contains 42% chitin the chitin content in Saccharomyces gutulata mycelium is only 2.3% [43].

Commercially available chitin is traditionally produced from waste of the shell fish industry, especially from that of crab and shrimp shells. In the exoskeleton of these animals chitin is present in crystalline form, with $CaCO_3$ incorporated into its structure [44]. The first step in the conventional method for extracting chitin from shellfish is an acid treatment for demineralisation of the material, followed by alkaline treatment to solubilize proteins. A final decolorization step is needed to obtain a white powdered chitin [45, 46].

1.2.2.1 Chitin-Glucan from fungi

Prof. Henri Braconnot in 1811 was the first to discover chitin in fungi [47], where it is the structural component in cell walls. Chitin is present in several fungal species such as *Aspergillus niger* [48], *Saccharomyces cerevisiae* [49] and *Agaricus bisporus*, the common champignon [50]. In fungi it usually occurs as α-chitin [51, 52] that is covalently bonded to β-glucan [53], a glucose polymer forming a chitin-glucan complex (CG). In all fungi, the glucan was found to predominantly exist in the form of β-1,3-/1,6-glucan, which is linked to chitin via a β-1,4 glycosidic bond [54]. Figure 2 shows the monomer unit of β-1,3-glucan.

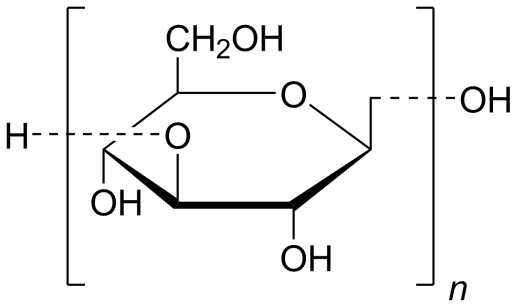

Figure 2: Chemical structure of β-1,3-glucan [55]

The structural components β-1,3-glucan, β-1,6-glucan, chitin, and mannoprotein are all linked together in the fungal cell wall [56]. Figure 3 (Beauvais et al. [52]) shows the design of the fungal cell wall and its components.

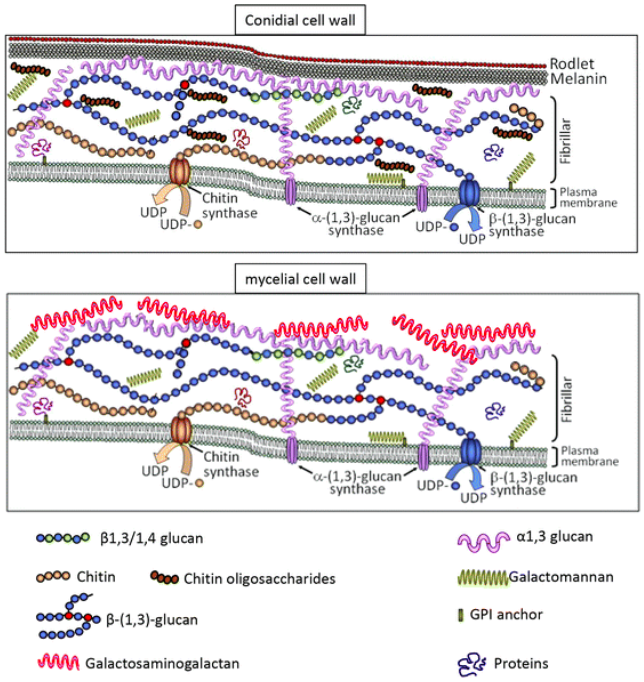

Figure 3: A schematic illustration of the fungal cell wall by Beauvais et al. [52].

Figure 4 depicts how chitin and glucan are organized in different types of fungi.

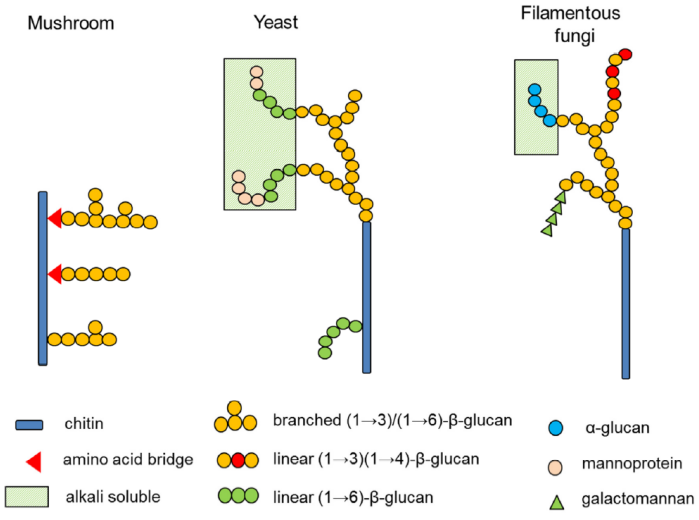

Figure 4: Assumed bonding between chitin and glucan in different types of fungi [57].

While β-glucan itself is soluble in water, the linkage to chitin renders it water-insoluble. Furthermore, CG is hygroscopic and has a high swelling capacity [58]. Because of its non-toxicity, biodegradability and its antibacterial properties, CG has found applications in cosmetics, such as skin care products and as anti-aging agent [59].

Shellfish chitin contains minerals [44], which is the cause for its stiffness. This is why the industrial production of chitin usually involves HCl in a demineralisation step. However longer acid treatment is known to cause degradation of polymeric chitin [60]. Because of the absence of minerals in fungal chitin-glucan, in the extraction of CG no acid treatment is required. Extraction was shown to be possible under mild alkaline conditions with 1 M NaOH solution at 80°C [57]. In this process CG is separated from the alkali soluble fraction, which also contains proteins and polysaccharides, such as mannans [54]. Figure 5 shows CG obtained by alkaline extraction of blended mushrooms (*Agaricus bisporus*).

Figure 5: CG suspension extracted from *Agaricus bisporus*.

Commercially available NF membranes are conventionally produced by composite membrane technique or interfacial polymerisation [12]. Using already nanostructured materials in a paper-making process, is a simple and cost-effective approach towards NF membrane production, as already shown for NC [34]. One advantage of CG over nanocellulose is, that it is by itself made up of nanofibers, hence no chemical or mechanical treatment is required to further break it down to nanosized material, which would make an industrial production more cost-efficient.

CG's adsorption capacity was proven to be useful for the removal of lead, iron, and cadmium from wine [61]. Furthermore, it has been demonstrated that it is possible to make nanopapers from CG through a simple filtration process [57]. Both, the CG suspended in water as well as the dried nanopapers were tested for their properties to remove Ca^{2+}, Mg^{2+} and Cu^{2+} [36] as well as Zn^{2+} [62] from an aqueous solution, with the adsorption capacity being highest for copper ions.

1.2.3 Chitosan - A versatile material

A very important property of chitin is its degree of deacetylation (DDA). It is defined as the number of monomers in a chitin macromolecule that lack an acetyl-group bonded to the amine [63]. If the DDA exceeds 50%, the number of glucosamine units is higher than the number of N-acetyl-glucosamine units and the molecule is then called chitosan (CS) [64].

Figure 6 shows the difference between chitosan and chitin.

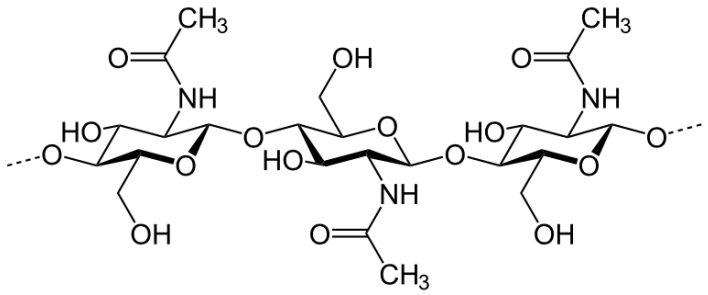

(a) Chitin: DDA <50%

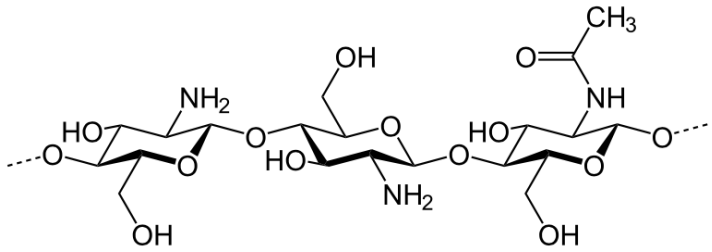

(b) Chitosan: DDA >50%

Figure 6: Chitin and chitosan and their degree of deacetylation (DDA) [65]

Chitosan (CS) is also found in nature, but is less abundant than chitin. Its biosynthesis involves chitin deacetylase enzymes (CDE), which are found in several insect and fungal species, such as *Mucor rouxii*, *Absidia coerulea* and *Aspergillus nidulans*. CDE produce chitosan by catalyzing the cleavage of chitin's acetyl group and often work in tandem with chitin synthetase, deacetylating freshly synthesized native chitin [37].

However, 90% of industrially produced chitosan is made in Japan from chitin isolated from shellfish wastes [37]. The deacetylation of chitin to chitosan can be achieved by alkaline or acidic treatment. As the latter may cause hydrolysis of glycosidic bonds, alkaline treatment is preferred. Many procedures concerning the production of chitosan from chitin through NaOH treatment can be found in the literature. The majority of publications describe procedures using dry chitin mostly from marine sources. Procedures for different kinds of chitin containing animals such as shrimp [66], fish (scales) [67] or field crickets [68] have been reported. The conventional way to obtain chitosan is the deacetylation of chitin with 40 - 60% NaOH [45, 67]. Temperatures are around 100°C and the reaction times vary between 1 and 5 h. The higher the reaction temperature the faster the deacetylation occurs. For 130 to 150°C, deactetylation was reported to be completed after 2h [69]. Also the reaction times were proven to affect the DDA: Treating chitin with 50 % (w/w) NaOH led to 82% DDA after 1 h and to 100% DDA after 48 h [70]. However, considering the large amount of time that is required to achieve complete deacetylation under these conditions, the use

of higher concentrations of NaOH seems more feasible. Furthermore, longer reaction times [70] as well as higher reaction temperatures [69] were reported to lead to a reduction of molecular weight. Table 1 is a reproduction from the literature [71]. It shows the effect of different reaction conditions on squid chitin.

Table 1: DDA after applying different deacetylation conditions to squid chitin [71].

c (NaOH) [%]	T [°C]	time [min]	DDA [%]
20	100	120	22.8
40	60	60	52.4
40	100	60	73.6
40	100	120	88.7
60	100	60	97.3

There is also literature concerning the deacetylation of the fungal CG complex. 1 g dried material and NaOH solution were stirred at 90°C for 5 h. The DDA was 42% and 78% for 20% NaOH and 60% NaOH, respectively. Figure 7 depicts the NaOH-concentration versus degree of deacetylation (DDA) achieved by Abdel-Mohsen [72] and shows that the relationship between the two quantities has a linear character.

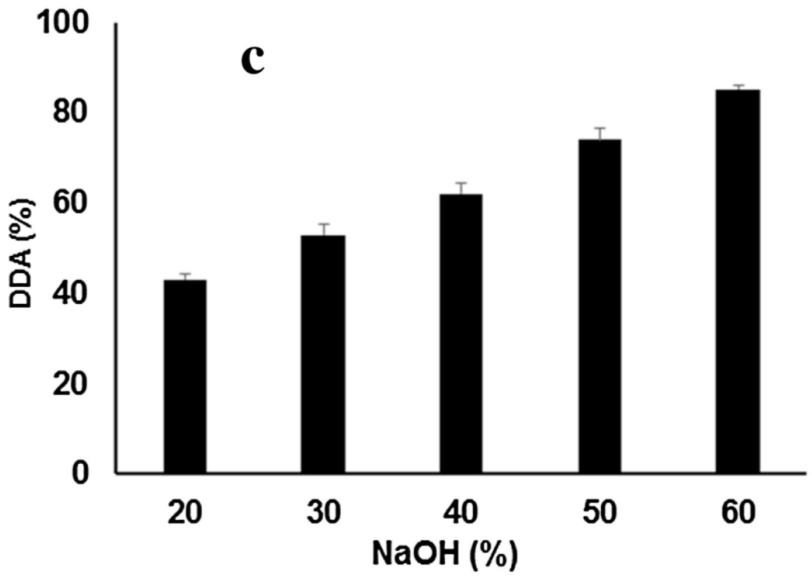

Figure 7: NaOH concentration and DDA for fungal CG from Abdel-Mohsen et al. [72].

Besides the conventional deacetylation using NaOH, research is directed for different approaches in order to produce chitosan. Thatat et al. [73] proved the possibility to achieve deacetylation under milder conditions by pretreatment of chitin with γ-radiation. Furthermore, heating by microwaves was shown to facilitate deacetylation [74]. Alternative routes such as enzymatic or fermentation methods completely omit the alkaline treatment. It was

shown that for material properties not only the DDA, but also the pattern of acetylation in the polymer chain plays an important role. Latest research has proven that this factor can be controlled by enzymatic deacetylation [75].

Because of its interesting physicochemical properties chitosan has been studied more extensively than chitin and has found several applications in industry. Its non-toxicity, excellent biodegradability and biocompatibility [76] as well as its outstanding material properties, as outlined in the following, have paved the way for a variety of biomedical applications. Chitosan's polycationic character enables it to form complexes with negatively charged species, such as DNA and many proteins. This makes it a vital candidate in drug or gene delivery applications [77]. Furthermore, it is used as a scaffold in tissue engineering [78]. In combination with anionic species chitosan can form dense hydrogels, which are able to mimic body tissue. In addition to that chitosan has the ability to promote rapid tissue growth [78] and is then eventually replaced by own body tissue [79]. An example where chitosan is useful in tissue engeneering is bone regeneration [80].

Another field were chitosan is just about to emerge is the food packaging industry [81, 82]. Increasing demand for renewable materials makes this whole industry sector now shifting towards biomaterials. Chitosan is an ideal candidate, because it is biodegradable and has excellent film formation properties. Because of its non-toxicity films from chitosan are edible [83, 84].

CS can be used in agriculture as a seed coating. It enhances the protective abilities of plants and may hence reduce the amount of pesticides. A chitosan coating on vegetables and fruits can increase their shelf life and maintain food quality [85]. Another reason why chitosan is promising in the field of food packaging is its antimicrobial activity [82]. This property is directly linked to chitosan's polycationic character and thus highly dependent on the pH. In acidic environment the free amino groups are positively charged and undergo electrostatic interactions with negatively charged bacterial cell walls and may disrupt them [86, 87].

1.2.3.1 Chitosan for adsorption of pollutants from wastewater

Chitosan is one of the most promising polymers for the removal of heavy metal ions from wastewater and is known for its outstanding adsorption properties [88–92]. This is due to the high abundace of amino- and hydroxyl functional groups [47, 93]. Chitosan has the advantage of being able to bind cations through metal chelation at neutral pH and anions through electrostatic interactions in acidic environment [90]. In addition to ions, also dyes and phenols can be removed from water [47]. In contrast to conventional adsorption systems such as activated carbon or synthetic resins chitosan is available at low cost as its precursor, chitin, is very abundant in nature.

Chitosan was proven to effectively remove Cu^{2+}, Cd^{2+}, Ni^{2+}, Pb^{2+} and Hg^{2+} from wastewater. The affinity of chitosan towards metal ions follows the order $Hg^{2+} > Cu^{2+} > Fe^{3+} > Ni^{2+} > Ag^{+} > Cd^{2+} > Mn^{2+} > Pb^{2+} > Co^{2+} > Cr^{3+}$ [94]. Values from around 80 mg/g

[95, 96] up to 485 mg/g [97] for chitosan's maximum capacity to remove Cu^{2+} have been reported. This outperforms many sorption media, such as activated carbon (21 mg/g at pH 6) [98], waste slurry (21.0 mg/g at pH 3) [99] or graphene oxide (45.2 mg/g at pH 5) [100, 101]. The maximum adsorption capacity of chitosan for copper ions is highly dependent on pH and was found to be highest at pH 4.5 [96].

The adsorption of metal ions on chitosan is complex and could be dominated by a combination of adsorption, ion-exchange and chelation [102]. Studies investigating the complex formation of copper ions and chitosan reported two complexes [103, 104]: The first one consisting of one Cu^{2+} ion bond to one amino group could be observed at a pH higher than 5.3. A second complex of one Cu^{2+} ion bond to the amino groups of two glucosamine subunits formed at pH 5.8. The two models, also called pendant model and bridge model, respectively, are depicted in Figure 8, a reproduction from literature [103].

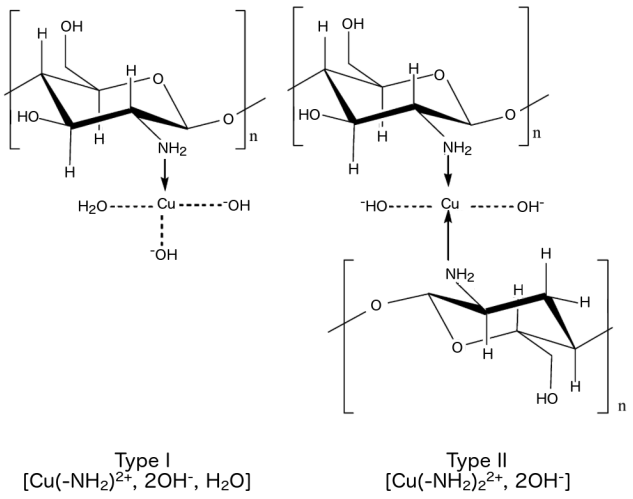

Figure 8: The pendant model (left) and the bridge model (right) are two proposed ways in which Cu^{2+} ions are adsorbed by CS. The Figure was copied from Rhazi et al. [103].

By functionalization of fungal CG and CSG (e.g. carboxymethylation or carboxyethylation) it is further possible to tailor the adsorption behaviour and make the adsorbent more specific for certain ions [62]. Besides this, copolymers of chitosan linked to other polymers and materials coated with chitosan have been developed. Some examples of such systems report the following adsorption capacities for copper ions: 87.9 mg/g for a chitosan coated PVC sorbent [105], 64.6 mg/g for chitosan beads, 31.2 mg/g for chitosan–GLA 1:1 beads [106], 227.3 mg/g for porous chitosan oxalate beads [107], 33.4 mg/g (Langmuir) and 21.6 mg/g (Freundlich) for pure chitosan beads and 47.9 mg/g (Langmuir) and 29.5 mg/g (Freundlich) for Chitosan/PVA beads [108]. The food industry employs CS as a clarifying agent for dehazing of fruit juices. Its coagulation and flocculation properties are used to remove proteins and lipids from foods or wastes [109].

One characteristic of chitosan is its solubility in acidic media. Most protocols to extract chitosan use dilute acetic acid [110, 111]. This behaviour is explained by protonation of the

amine groups. Unfortunately, the solubility of pure chitosan limits its applicability. Therefore CS is often crosslinked, e.g. by glutaraldehyde, which may however negatively affect the adsorption capacity [112].
The adsorption capacity of pure chitosan usually suffers from its high crystallinity. Because adsorption mainly occurs in amorphous regions, chitosan is often processed to chitosan beads which show a higher content of amorphous regions [113]. Chitosan beads have a higher surface area than chitosan flakes. Another problem of chitosan is its swelling. Crosslinked chitosan beads have lower swelling and can be used at different pH [114].

Chitosan bonded to glucan would potentially overcome some of these problems and omit the use of a crosslinking agent. So far it has been demonstrated that it is possible to obtain fungal CS by acidic extraction from CG, e.g. prepared from *Aspergillus niger* or *Mucor rouxii* [115, 116]. The chitosan was still linked to glucan and formed a chitosan-glucan complex (CSG). From this material physico-chemical properties, such as ion chelation, antioxidant activity, emulsifying activity, and antibacterial properties have been determined. Also fungal CSG has been prepared by deacetylation of CG (extracted from yeast) [72].
Due to glucan's film formation properties it may be possible to produce papers from CSG, as it has been demonstrated with CG. It can be assumed that CSG also comprises nanofibers. The resulting nanopapers may at best combine the filtration properties of CG nanpopapers with the high heavy metal affinity of chitosan.

2 Aim and objectives

The aim of this work is to develop water treatment nanopapers from biomaterials that can be used to remove viruses and heavy metal ions from water. To achieve this, the following objectives are defined:

1. Chitin-Glucan (CG) will be extracted from *Agaricus bisporus*, the common mushroom.
2. In a reaction with highly concentrated NaOH the material will be deacetylated to yield Chitosan-Glucan (CSG).
3. The resulting CSG will be characterized by elemental analysis, Fourier-transform infrared spectroscopy, ^{13}C-NMR spectroscopy, and thermogravimetric analysis.
4. From CSG, nanopapers will be prepared by a simple vacuum filtration process and subsequent pressing at elevated temperatures.
5. Surface morphology, fibril diameter, mechanical properties, water permeance, and the specific surface area will be determined in order to investigate the properties and characteristics of the nanopapers.
6. Furthermore, the ability to reject 10 nm gold nanoparticles and the adsorption capacity for Cu^{2+} ions will be evaluated.

3 Experimental

Agaricus bisporus was purchased in a local supermarket. All papermaking filtrations were performed with VWR qualitative filter paper, 413. For the extraction of CG and the production of CSG NaOH pellets (VWR, technical grade) were used. Ethylenediaminetetraacetic acid (EDTA) (0.1 M, Roth, analytical grade), murexide (Fluka), NH_4Cl (Roth), and ammonium hydroxide solution (25 %, Sigma Aldrich, analytical grade) were used in complexometric titration. For the determination of the pore size gold nanoparticles (Sigma Aldrich, OD 1, stabilized suspension in citrate puffer) of 10 nm in diameter were used. In all experiments pure water (purified with Elga - Purelab Classic) was used. All chemicals were used as received without further purification.

3.1 Chitin-Glucan extraction from *Agaricus bisporus*

1 kg of *Agaricus bisporus* was washed two times with 1 L of destilled water and blended in batches in a blender (Multiquick 5, Braun) with 3 L of water for 5 min. The NaOH solution was magnetically stirred for 30 min at 85°C and then centrifugated. The supernatant was removed and the precipitate was suspended into 3 L of 1 M NaOH-solution that had been preheated to 65°C. It was then magnetically stirred at this temperature for 3 h. The supension was centrifugated and washed with water for at least 6 times until neutral pH was reached. Centrifugation conditions in all steps were 9000 rpm for 15 min [57]. The procedure yielded a CG suspension with a consistency of 3%. It was stored at 4°C for further use.

3.2 Synthesis of Chitosan-Glucan from Chitin-Glucan

General Procedure

A predetermined amount of CG gel was placed into a piping bag and transferred to a 1000 mL round bottom flask together with a magnetic stirring rod. The flask was put into an oil bath (100°C). H_2O (15% of the mass of the CG suspension) and an appropriate amount of NaOH (Table 2, e.g. 47.8 g for CSG40 of 100 g CG-gel of 3% w/w) were added and the mixture was stirred with the help of a spatula until the material became less viscous and allowed the magnetic stirring rod to rotate. A reflux condensor was put onto the flask and the mixture was stirred for a certain amount of time (Table 2). It was then combined with 3 L of water and centrifuged for 15 min at 9000 rpm. Centrifugation and washing were repeated until the pH was neutral. Figure 9 shows the steps necessary for the production of CSG.

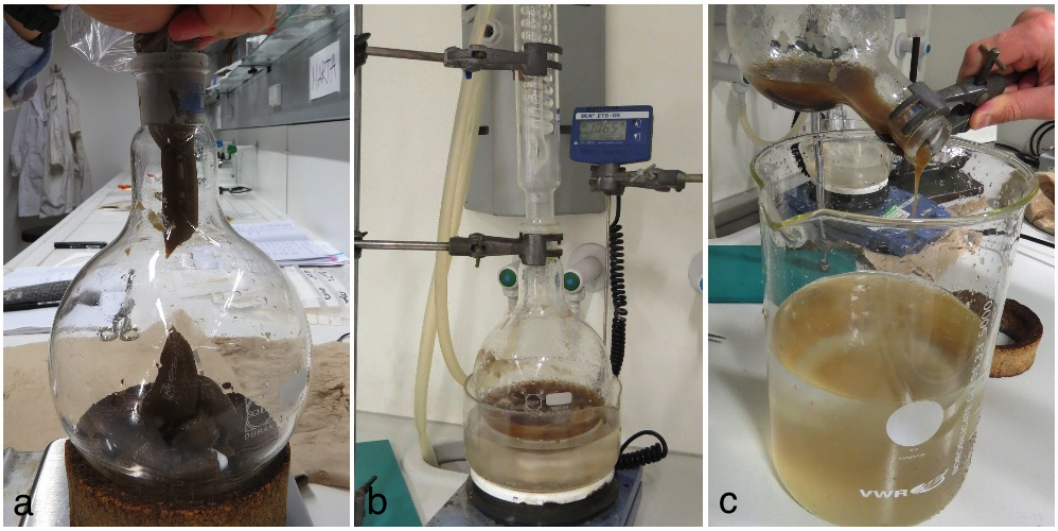

Figure 9: Production of CSG. a) Transfer of CG into the flask, b) magnetic stirring at 100°C, c) quenching the reaction with 3 L of water

The two parameters, stirring time and concentration of NaOH, were subject to variation. Table 2 summarizes the 5 used synthesis conditions. The left column lists the abbreviations for the respective chitosan-glucan (CSG) material that will be used throughout this thesis. The two right columns show the mass fraction w (third column) and the mass concentration β (fourth column) of the NaOH used in the protocols.

Table 2: Reaction conditions for chitosan-glucan production.

Method	**t [h]**	w **(NaOH) [% w/w]**	β **(NaOH) [% w/v]**
CSG20-1	1.0	17	20
CSG40-0.5	0.5	30	40
CSG40-1	1.0	30	40
CSG40-2	2.0	30	40
CSG60-1	1.0	42	60

3.3 Characterization of synthesized compounds

Fourier-transform infrared spectroscopy (Agilent Technology, Carry 630) and elemental analysis (EA 1108 CHNS-O, Carlo Erba) of CG and CSG were both carried out by Mag. Johannes Theiner (Mikroanalytisches Laboratorium, Universität Wien). Solid state ^{13}C-NMR spectroscopy of the samples was performed by Dr. Markus Bacher (University of Natural Resources and Life Sciences). The fraction of chitin in CG was calculated from the nitrogen content, as determined by elemental analysis.

3.4 Nanopaper preparation from chitosan-glucan (CSG)

3.4.1 Nanopaper preparation using an oven

First, a predetermined amount of CSG gel (e.g. 20.4 g of CSG 3% (w/w) for a nanopaper of 50 g/m^2) was blended with 300 mL of water for 5 min and vacuum filtered through a 125 mm VWR 413 filter paper. To achieve a homogeneous nanopaper the filter was balanced with a spirit level. When the surface of the filter cake was almost dry, the filter was removed with the help of a spatula. The filter cake was cold pressed between blotting paper and two metal plates under a 5 kg weight for several minutes. The blotting paper was exchanged twice. The nanopapers were put in an oven and pressed between two metal plates under a 5 kg weight for 3 h at 120°C. In order to prevent sticking, baking paper was used in addition to the blotting paper at the contact side with the filter cake. Figure 10 illustrates the paper making process. An example for the final nanopaper is shown in the last picture (h).

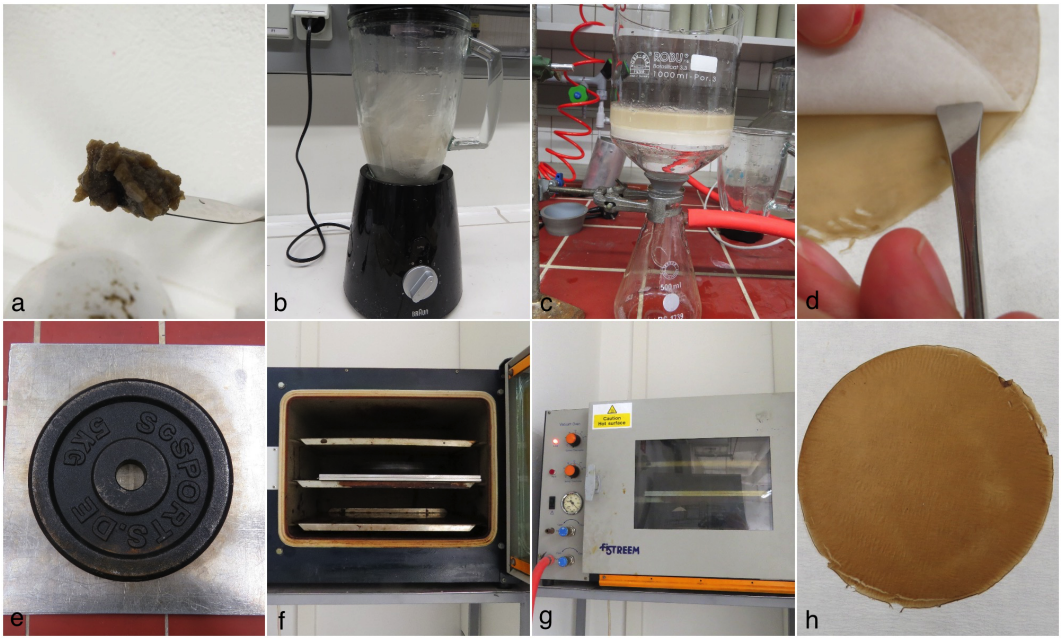

Figure 10: Paper making process. a) Chitosan-glucan gel, b) blending CG with water, c) vacuum filtration over filter paper, d) removing the filter paper from the CSG nanopaper, e) cold pressing under 5 kg weight, f) and g) heating at 120°C for 3 h in an oven, h) the final CSG paper

3.4.2 Nanopaper preparation in the hot press

In a second method, one CSG20-1 nanopaper was prepared by hot-pressing. Instead of pressing the nanopaper under 5 kg at 120°C, the nanopaper was pressed for 15 min at 120°C under a mass of 1 t. All other steps were as described in the previous chapter. Tensile tests were carried out to investigate the effect of the different pressing techniques on the mechanical properties.

3.5 Grammage, thickness and density of nanopapers

Discs of 49 mm in diameter were cut from the nanopapers, weighed and the thickness measured with a micrometer gauge at 20 distinct points. The grammage G, was calculated using equation 1

$$G = \frac{m}{r^2 \cdot \pi} \tag{1}$$

where m is the mass of the circle and r its radius in meters. The ratio between grammage and thickness d is the envelope density as given by equation 2:

$$\rho_{envelope} = \frac{G}{d} \tag{2}$$

The skeletal density $\rho_{skeletal}$ was determined by helium pycnometry (micromeritics AccuPyc II 1340 Gas Pycnometer). A cylindrical measurement cell with a volume of 1 cm^3 was filled with vacuum dried material (around 0.03 g). Evacuating the chamber and then draining it with helium allows to calculate the skeletal density from the mass of the sample and the required amount of helium.

3.6 Investigation of nanopaper surface morphology with SEM

Images of the microstructure of the nanopapers were made by scanning electron microscopy (Zeiss Supra 55 VP). Prior to imaging the samples were coated with a 10 nm layer of gold at 60 mA by a Vacuum Sputter Coater (Leica EM SCD050). The imaging was done at a voltage of 2 kV at the Faculty Center for Nanostructure Research (University of Vienna).

3.7 Determination of nanopaper permeance in a dead end cell

The permeance of water was determined by measuring the water flux in a dead end cell (HP4750, Sterlitech Corporation). In this method a paper is placed on top of a sintered stainless steel support and pressure forces a liquid through the paper. The amount of water that passes the paper per unit time is weighted. From this the permeance is calculated as the volume of water that passed the membrane per unit time, per unit area, per unit pressure $[L/m^2 \cdot h \cdot MPa]$. All tests were performed using nitrogen head pressure of 5 bar. The effective filtration diameter of the dead end cell was 43 mm.

3.8 Determination of the nanopaper's mechanical properties

The tensile test is a standardized method, in which a sample of defined length, width and thickness is stretched until failure. It is used to investigate typical material properties such as maximum tensile strength, elongation at break and Young's modulus.

Tensile tests were performed with an Instron 2580-106 universal test frame. For all measurements, specimen defined in EN ISO 527-1 with an overall length of 30 mm and a parallel

width of 2 mm were prepared. The thickness was measured at 5 points along the dog bone to calculate the cross-sectional area. For a measurement a specimen was clamped between two grips (20 mm in distance) in vertical position. Above the higher grip a load cell of 1 kN maximal strength measured the applied load during the test until failure. The tests were performed at a speed of 1 mm/min. Although the load frame already provides data on the elongation, evaluating a video is much more accurate, because it is possible to only take into account a defined area within the parallel region of the tested dog bone. The tensile test was therefore recorded by a camera (Blackfly - GigE PoE) installed around 1.5 m in front of the sample. The gauge length was set to 10 mm. To increase the contrast, the samples were marked with black points with a felt pen. The evaluation was done with a video gauge software. During the test the load cell registers the force acting on the specimen over the time. From this the stress was calculated as the force per area ($N/m^2 = Pa$). The stress was then plotted against the strain, which was obtained from the video extensiometer, to give a stress-strain curve. From the data of the stress-strain curve, the ultimate tensile strength and the elongation at break were extracted. The Young's modulus was calculated as the slope of the linear section of the stress-strain curve.

3.9 ζ-potential measurements to investigate the surface charge

The ζ-potential was measured by streaming potential measurements (SurPASS Electrokinetic Analyzer, Anton Paar) through remote control (Software: Attract2.1). For a measurement two specimen (30 x 10 mm) were fixed onto two rectangular specimen holders with the aid of double-sided adhesive tape. In the measurement unit the two specimen face each other with a gap of 100 µm, through which electrolyte solution (1 mM KCl in pure water) is pumped. The pH of the electrolyte solution was set to 10. The ζ-potential was determined, followed by titration of a defined amount of HCl (0.05 mM). This was repeated until a pH of 4 was reached.

3.10 Thermal stability measured by thermogravimetric analysis

Dried CG and CSG powder as well as nanopapers were analyzed by thermogravimetric analysis under both air and N_2 atmosphere. The materials were dried under vacuum over night before the measurements. An amount between 2 and 5 mg of material was put into a pan and weighted. After equilibration at 30°C the samples were heated to 600°C with an heating rate of 10°C/min followed by an isothermal for 10 min.

The mass loss with respect to temperature was recorded. From this data the onset-temperatures of mass loss were calculated by numerical derivation of the data points. The temperature where the mass loss per 1 °C did exceed 0.25% ($|\frac{dm}{dT}| > 0.25$) was taken as the onset temperature.

3.11 Surface area determined by iGC-measurements

The surface area was determined based on the BET model for gas adsorption. 200 mg of CSG nanopaper were packed into a column which was closed on both sides with glass wool. Measurements were performed with Surface Measurement System - iGC Surface Energy Analyzer using octane as probe molecule.

3.12 Determination of the pore size with gold nanoparticles

A dry CSG nanopaper was placed into a dead end cell in which 20 mL of a suspension of gold nanoparticles with 10 nm diameter was filled. Nitrogen head pressure of 5 bar was applied and the filtrate was collected in fractions of 2-3 mL. The adsorbance was measured with an UV/VIS photometer (Agilent 8453) and the relative concentrations were calculated from the absorbance at a wavelength of 520 nm.

3.13 Adsorption of copper ions in continuous adsorption measurements

A disc of 49 mm in diameter was placed into a dead end cell (effective diameter = 43 mm) with 20 mL 1.92 mM Cu^{2+}-solution on top of it. A nitrogen head pressure of 5 bar was applied and the permeate was collected in fractions of 2-3 mL. The concentration of each permeate fraction was analyzed by complexometric titration.

3.13.1 Complexometric titration to determine the Cu^{2+} concentration

Complexometric titration was performed with slight varation to literature [36]. 2-3 mL of the permeate (possibly containing Cu^{2+}) were put into a flask and mixed with 50 mL pure water. 5 mg of NH_4Cl and 12 drops ($\widehat{=}$ 0.6 mL) of NH_4OH were added to set the pH to 10. 5 mg of murexide were added as indicator. Titration was done with 0.5 mM EDTA until the transition point (color change from yellow/orange to pink) was reached. Assuming that one EDTA molecule can complex one Cu^{2+} ion the final concentration of Cu^{2+} ions in the solution is given by equation 3. $V_{\text{Titration}}$ is the volume of solution that is titrated.

$$Cu^{2+}\ [mmol \cdot L^{-1}] = \frac{0.5\ [mmol \cdot L^{-1}] \cdot V_{\text{EDTA}}\ [mL]}{V_{\text{Titration}}\ [mL]} \tag{3}$$

To calculate the amount of Cu^{2+} that has been adsorbed from a certain titration volume, equation 4 was used. 63.546 g/mol is the molar mass of copper.

$$m\ [mg] = c\ [mmol \cdot L^{-1}] \cdot 63.546\ [mg \cdot mmol^{-1}] \cdot V_{\text{Titration}}\ [mL] \tag{4}$$

From the mass adsorbed, the adsorption capacity in mass per area [mg/m^2] was derived by equation 6. The dead end cell has an effective diameter of 0.043 m ($\widehat{=}$ 0.00046225 m^2).

$$q_A\ [mg \cdot m^{-2}] = \frac{m\ [mg]}{0.00046225\ [m^2]} \tag{5}$$

The adsorption in mg/g was then calculated by dividing q_A [mg/m^2] by the grammage G:

$$q_e\ [mg \cdot g^{-1}] = \frac{A\ [mg \cdot m^{-2}]}{G\ [g \cdot m^{-2}] \cdot 1000\ [mg \cdot g^{-1}]} \tag{6}$$

4 Results and discussion

4.1 Preparation of Chitin-Glucan (CG)

CG was prepared from *Agaricus bisporus*. The mushrooms were blended to yield a homogeneous suspension. A hot water treatment was used to dissolve the water soluble components and separate them from the suspension through centrifugation. The precipitate was combined with 1 M NaOH to remove alkali soluble moietes, such as proteins and lipids. The procedure yielded a brown hydrogel of 97% water content (Figure 3). 1 kg of fresh mushrooms gave approximately 360 g CG gel or 10.8 g dried CG, respectively.

4.2 Preparation of Chitosan-Glucan (CSG)

4.2.1 Optimization of the procedure

In this work initially it was tried to perform the reaction with never-dried CG gels, which predominantly consist of water (97 - 97.5% w/w). This has the advantage that the drying step is omitted. No case of a direct use of CG suspension for deacetylation is mentioned in literature. However, to keep the reaction conditions close to standard protocols and keep the NaOH conc. as high as possible, the use of additional water to dilute the CG gel was avoided.

Therefore the highest concentrated possible aqueous solution of NaOH (52% w/v) was prepared and mixed with the CG gel. This proved impractical because of two reasons: Firstly, the suspension was very viscous and a lot of it stuck to the inner wall of the vessel, making it impossible to control the actual amount of NaOH added. Secondly, following this procedure still a lot of water was eventually added to achieve the desired concentrations.

For the reasons mentioned above a different method had to be developed. Instead of preparing a NaOH solution, sodium hydroxide pellets were added directly to CG gel. This approach turned out to be easily applicable, having only the slight disadvantage of not instantly reaching equilibrium concentration. This problem did arise because the CG suspension is a viscous gel and stirring was hindered. Nevertheless heating in an oil bath and the lower viscosity following the solubilisation of NaOH pellets promoted stirring, which could be achieved within approximately 5 min after addition of NaOH pellets. To further facilitate stirring a small amount of water (15% of CG's wet weight) was added and the ingredients were mixed with a spoon. One needs to be conscious of the fact that during this time frame the NaOH concentration was not the same everywhere in the material.

After the reaction a washing step was required to neutralize the material. Filtration was an obvious choice, but it proved to be too slow. Pore clogging by nanostructured CG/CSG may be the cause why filtration was taking up to three days. It was therefore omitted and replaced by centrifugation.

For practical reasons it was chosen to use the weight/weight ratio for calculating the required

amount of NaOH. 17%, 30% and 42% w/w correspond to approximately 20%, 40% and 60% w/v. These values were calculated from the density of NaOH solutions, listed in literature [117].

4.2.2 Products obtained from optimized CSG synthesis

Both, CG and CSG readily form hydrogels with brown color, which was always slightly darker for CG. Figure 11 gives an impression on what the products of the procedures described in chapter *3.2* looked like compared to CG. The first row shows the vacuum dried suspension. Dry CG and CSG are beige and do not differ much in terms of color. The dry weight after centrifugation was around 2.5 % (w/v) for CG and 4.0 % (w/v) for CSG, respectively.

Figure 11: Hydrogel (bottom) and dried material (top). From left to right: CG, CSG40-1, CSG40-2.

Longer reaction time and higher sodium hydroxide concentration did both have a negative effect on the yield, as shown in Table 3, whereby for 1 or 2 h (CSG40-1 and CSG40-2) almost no difference is detected.

Interestingly, already for the lowest NaOH concentration (20%) more than half of the material was lost. Because the alkali soluble fraction had already been separated during the CG extraction, this mass loss can best be explained by a partial destruction of the CG/CSG complex itself. At high molecular weight most β-glucans are water-insoluble, but their solubility increases with decreasing molecular weight [118]. The covalent bond to chitin further causes β-glucan to become insoluble. A possible explanation for the mass loss is, that some

of the glucan was cleaved off and then solubilised. However, a mass loss of more than 54% (as it is shown for all procedures in Table 3) can only be explained by cleavage of both, glucan and chitin/chitosan. This means that in addition to glucan also chitin/chitosan was lost in the procedure. These low molecular weight components could not be recovered using the applied centrifugation conditions.

Table 3: Yield of CSG for the optimized deacetylation procedures

method	**NaOH (w/v)**	**time [h]**	**yield**
CSG20-1	20%	1	**46%**
CSG40-0.5	40%	0.5	**43%**
CSG40-1	40%	1	**34%**
CSG40-2	40%	2	**33%**
CSG60-1	60%	1	**21%**

4.3 Characterization of synthesized compounds

Table 4 lists the results of elemental analysis for the 5 different CSG synthesis protocols.

Table 4: Elemental analysis of CG and CSG

Sample	%C	%H	%N	%O
CG	42.8	7.1	3.4	46.7
CSG20-1	44.0	7.2	5.0	43.8
CSG40-0.5	43.9	7.3	5.5	43.3
CSG40-1	44.0	7.4	6.2	42.4
CSG40-2	43.2	7.5	6.1	43.2
CSG60-1	42.6	7.4	6.2	43.8

4.3.1 Chitin and glucan content in CG calculated from elemental analysis (EA)

Elemental analysis (EA) of CG was performed to determine the relative contents of chitin and glucan in the material. The chitin content was calculated from the results of EA of vacuum dried CG suspension under the assumption that all nitrogen found in the analysis was stored in the chitin fraction and that all chitin subunits were fully acetylated.
The molecular formula of chitin is $[C_8H_{13}O_5N]_x$. For the example of 3.15 % N the percentages of elements present in the chitin fraction were calculated to be

$$\frac{3.15\%}{14\ g \cdot mol^{-1}} \cdot 12\ g \cdot mol^{-1} \cdot 8_{PartsCarbon} = 21.6\%\ C$$

$$\frac{3.15\%}{14\ g \cdot mol^{-1}} \cdot 1\ g \cdot mol^{-1} \cdot 13_{PartsHydrogen} = 2.93\%\ H$$

$$\frac{3.15\%}{14\ g \cdot mol^{-1}} \cdot 16\ g \cdot mol^{-1} \cdot 5_{PartsOxygen} = 18\%\ O$$

$$\frac{3.15\%}{14\ g \cdot mol^{-1}} \cdot 14\ g \cdot mol^{-1} \cdot 1_{PartNitrogen} = 3.15\%\ N$$

giving a total chitin content of 45.7% of CG's mass. Hence, 54.3% glucan are contained in this CG batch.

The calculated chitin contents were 48.6%, 45.7%, and 43.2% for three different CG-batches, respectively. These results are in accordance with EA results found in literature [36, 57]. The variation of the chitin content among different batches shows that CG, although from mushrooms of the same species, is not a material with clearly defined composition. Age, size,

growing conditions, and the time of harvesting are among the factors causing the difference.

4.3.2 Elemental analysis of CSG

Elemental analysis of vaccum dried CSG gels was carried out to determine the degree of deacetylation (DDA). The initial idea was, that if chitin was successfully deacetylated, then the absence of acetyl groups would lead to a higher nitrogen content. From this information and the now known chitin/glucan ratio it should be possible to obtain the DDA.
The general increase in nitrogen content with increasing time and concentration (see Table 4) suggests an increase of glucosamine-subunits in the material generated by cleavage of acetyl groups.
The content of nitrogen in pure chitin and chitosan is 6–7% and 7–9.5%, respectively [41]. The literature reports on calculating the DDA by elemental analysis [63]. Yet these publications refer to pure chitosan. Calculating the chitin fraction from the EA data is only possible under the assumption that during the reaction only chitin is deacetylated, but that no other reaction occurs that affects the ratio of chitin to glucan.
If assuming a glucan content of approximately 55%, the nitrogen values for the residual 45% were much too high for even pure chitosan. A possible cleavage of β-glucan, which was already discussed previously, might be responsible for this effect. Because of these reasons, calculating the DDA from EA is impossible.

4.3.3 FTIR-spectroscopy to investigate the effectiveness of the deacetylation reaction

FTIR-spectroscopy was performed to determine the DDA of chitosan-glucan. Figures 12 and 13 compare the infrared spectra of CG and CSG. The lines represent the average absorbance of five distinct measurements. The spectra of all samples can be found in the appendix.
The region between 3200 and 3600 cm^{-1} is caused by two overlapping vibrations: The -OH stretching vibration peaking at 3420 cm^{-1} and the -NH stretching peaking between 3260 cm^{-1} and 3280 cm^{-1}. The two peaks with the wavenumbers of 1650-1660 cm^{-1} and 1620 cm^{-1} both correspond to the C=O stretching of the amide and the band at 1550 - 1560 cm^{-1} to the -NH deformation. The peaks at 1425 cm^{-1} and 1370 cm^{-1} are caused by the scissoring vibration (in-plane bending) of CH_2 and CH, respectively. The small peak at 1300 cm^{-1} is due to the C-N stretching vibration and the prominent band between 1000 and 1100 cm^{-1} stems from the C-O and the C-O-C stretching vibrations. Peaking between 560 and 570 cm^{-1} we find the vibrations of the C-C backbone [119].

Interestingly, the band shape of the -OH and -NH region changes moving from milder to harsher procedures in terms of NaOH conc. and reaction time. For CSG20-1 a small plateau can be seen followed by a short adsorption band, whereas CSG60-1 displays a more centered band (3360 cm^{-1}), due to the stronger -NH vibrations.

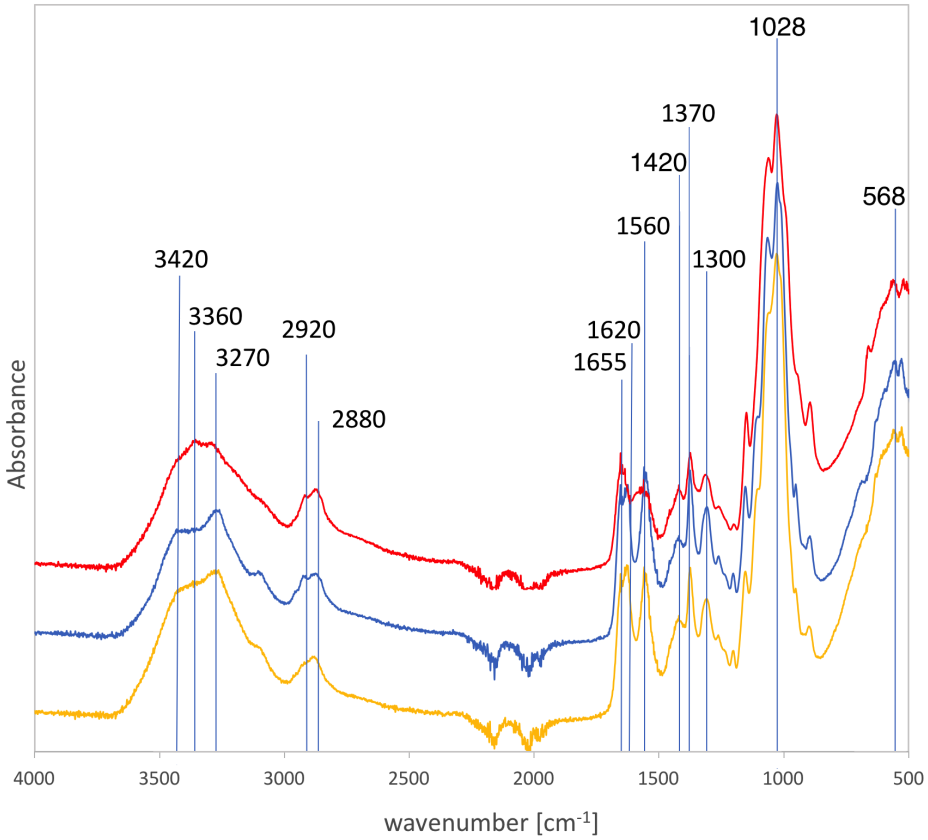

Figure 12: FTIR-spectrum of CG, CSG20-1 and CSG60-1.

In a study by Wu et al. [116] CG was extracted from *Aspergillus niger* and *Mucor rouxii*, two fungal mold species, by alkaline reflux and centrifugation. The resulting material was further purified with acetic acid, to separate chitosan from the chitin fraction. FTIR spectra of CG showed a band between 3200 and 3600 cm^{-1} that was very similar to the band for CG presented here. Yet the band of extracted chitosan was much more central and thus similar to CSG60-1. This suggests, that the -NH stretching band changes location, depending on the DDA and that the DDA of CSG60-1 might be comparable to that of extracted chitosan. One would expect the C=O bands to decrease with increasing DDA, as abundance of acetyl-groups should decrease. This phenomenon can be observed in Figure 12. The band height of CSG60-1 material in the region is greatly reduced in comparison to CG. This is also true for all other chitosan glucan synthesis procedures. Only CSG20-1 does not significantly differ from CG. The literature confirms this observation: FTIR spectra of CG from *Aspergillus niger* and *Mucor rouxii* showed strong sharp amide bands, while only two blunt and small bands in this region (1600 - 1660 cm^{-1}) could be observed in the spectra of extracted chitosan

from the same species [116]. The amide bands of CSG were still greater and sharper than the ones found in the literature for extracted chitosan, suggesting a lower DDA of the CSG compared to pure chitosan. Calculating the DDA from FTIR spectra is generally possible. Unfortunately from these (ATR-) spectra only qualitative information is given impeding the determination of the DDA.

Figure 13 shows the FTIR-spectra of CSG40 with a reaction time of 30 min, 1 h and 2 h, respectively. The assignment of bands is according to Figure 12. The similarity of CSG40-1 and CSG40-2 makes them almost interchangeable. The carbonyl stretching band of CSG40-0.5 is bigger than for the two other procedures. This suggests that the difference between 30 min of to 1 h of treatment had a bigger impact on the DDA than extending the reaction time from 1 h to 2 h. Also the EA indicated very similar compositions for both materials.

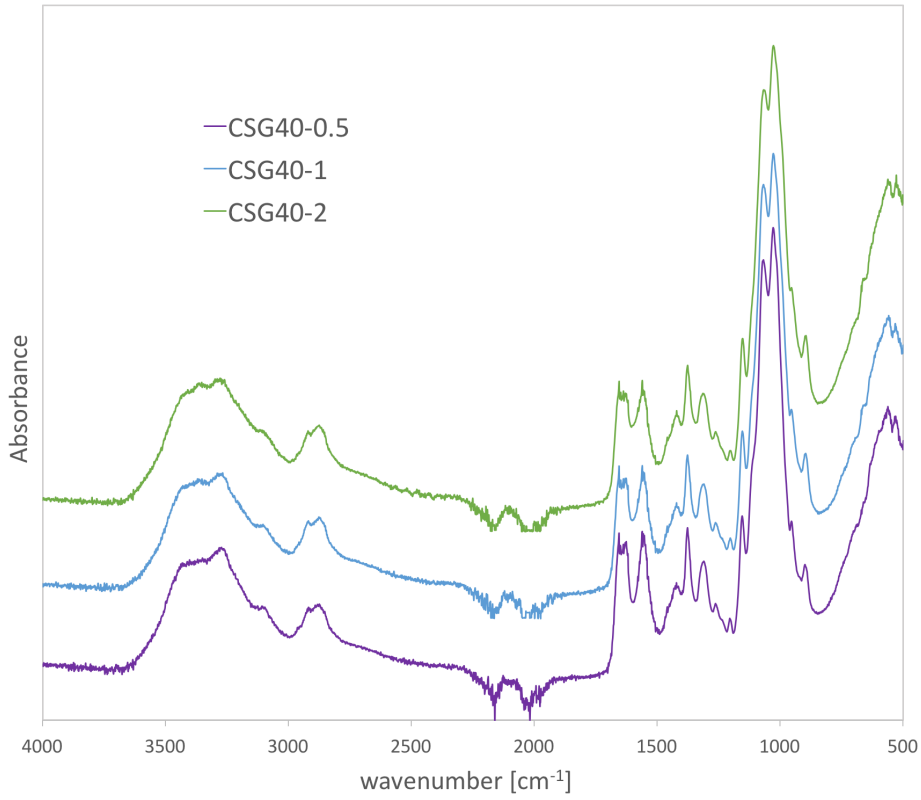

Figure 13: FTIR-spectrum of CSG40 with different reaction times.

4.3.4 ^{13}C-NMR-spectroscopy of CG and CSG

Solid state ^{13}C-NMR-spectroscopy was performed with the objective to calculate the DDA of CSG samples. The idea was based on the assumption that these spectra would contain more quantitative information than the FTIR spectra and that the DDA could be determined by comparing the integrals of the carbonyl- or methyl- carbons with a reference peak. Figure 14 shows a ^{13}C-NMR spectrum of CSG40-0.5.

The peaks at 173.5 ppm and 22.5 ppm belong to the carbonyl carbon and the CH_3-group

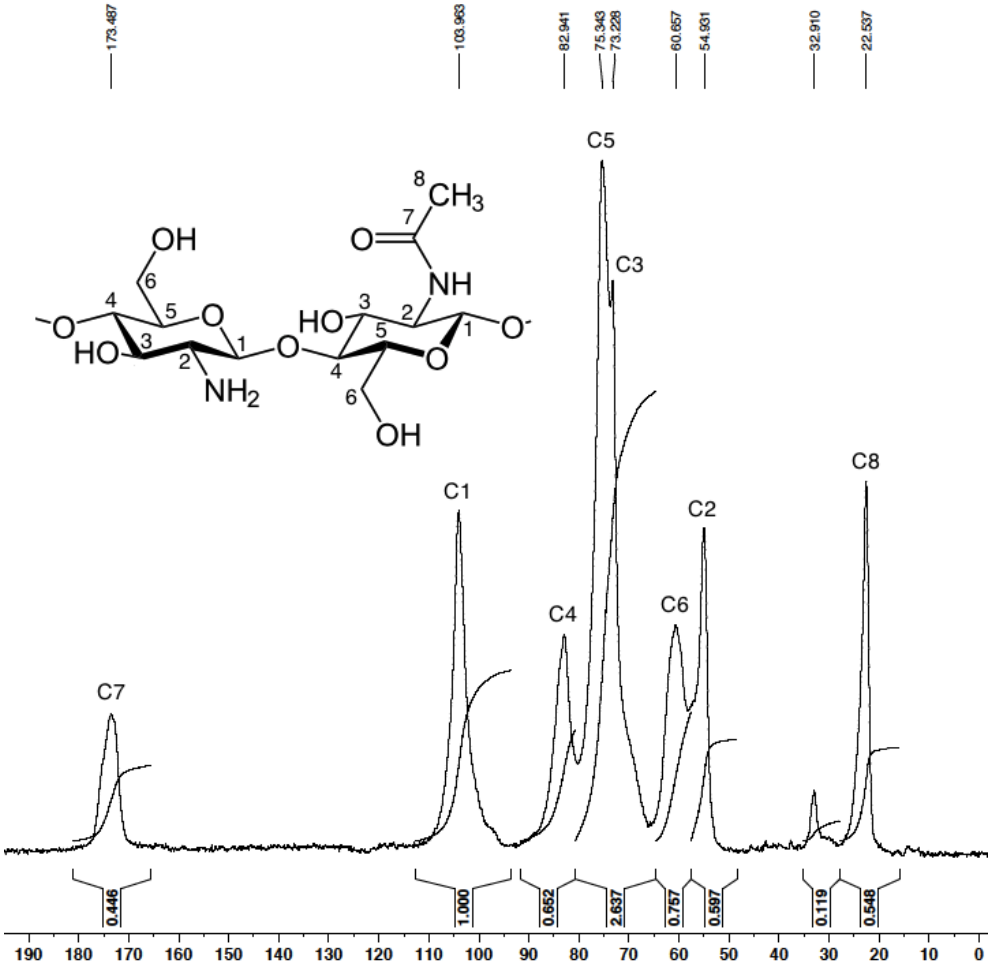

Figure 14: ^{13}C-NMR spectrum of CSG40-0.5: The assignment of peaks to the structure of chitin/chitosan ([65]) was done according to Roca et al. (2017) [120]

of the acetyl groups, respectively. The C2 has a nitrogen atom as its neighbor and therefore a lower chemical shift (54.9) than C3 (73.2 ppm), C4 (83.0), and C5 (75.3), which are also part of the ring system, as well as C6 (60.7). Because the C1 is bonded to two oxygen atoms it has a higher shift (104.0). As the C1 is present in all 3 polysaccharides (glucan, chitin, and chitosan) it is used as internal reference. The peak at 32.9 is common for CG and other biopolymer products and does neither stem from chitin/chitosan nor glucan. It may be attributed to residual amounts of lipids or proteins in the sample [120]. Interestingly with harsher deacetylation this peak increases in size and sharpness. It has to stem from alkali insoluble material that is enriched during the CSG preparation, while some of CG/CSG is lost.

The carbonyl- and the CH_3-peak represent the acetylated fraction in the material. The relative area integrals of these two peaks decreased with harsher reaction conditions, which indicates a higher DDA (see Figures 15a-d). If glucan were not affected by the alkaline treatment the DDA could simply be derived by comparison of the peak integrals. However, as

already mentioned above, it seems likely that some of the glucan fraction (and chitin/chitosan fraction) is cleaved off during the deacetylation procedure.

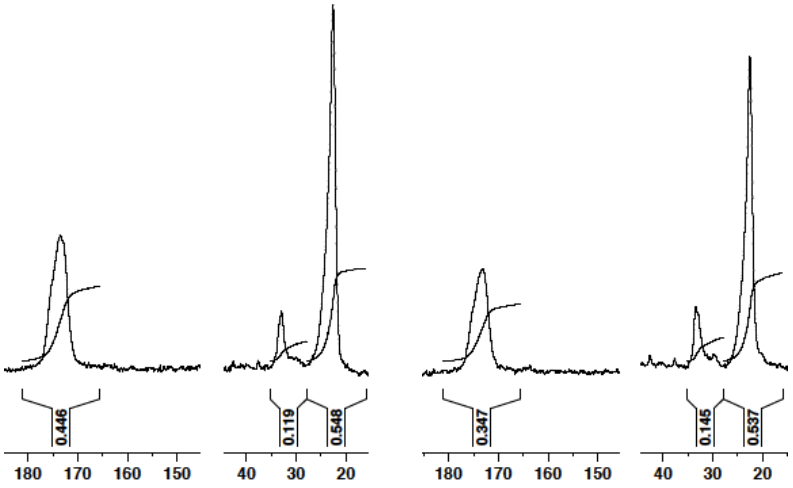

(a) ^{13}C-NMR spectrum of CSG40-0.5

(b) ^{13}C-NMR spectrum of CSG40-1

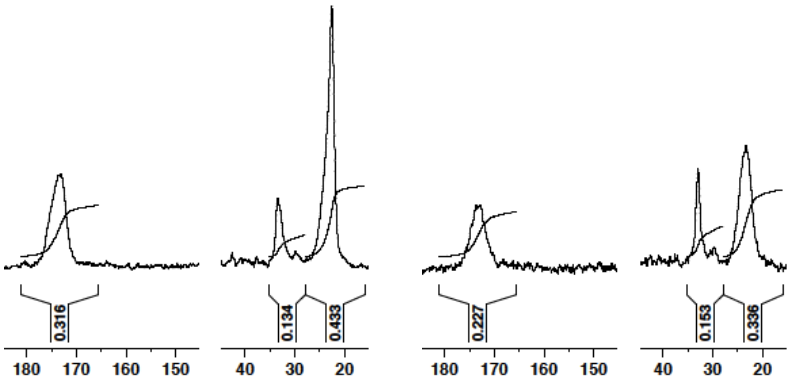

(c) ^{13}C-NMR spectrum of CSG40-2

(d) ^{13}C-NMR spectrum of CSG60-1

Figure 15: The integrals of CH_3 and $C=O$ peaks become smaller with harsher deacetylation conditions.

The ^{13}C-NMR spectra further proves this assumption: If the integral of the C1 carbon is assumed constant, then a comparison of the CG-spectra with CSG20-1 shows that the integrals of all peaks, including the ones representing the acetyl group, are larger for CSG20-1 than for untreated CG (see Figure 16).

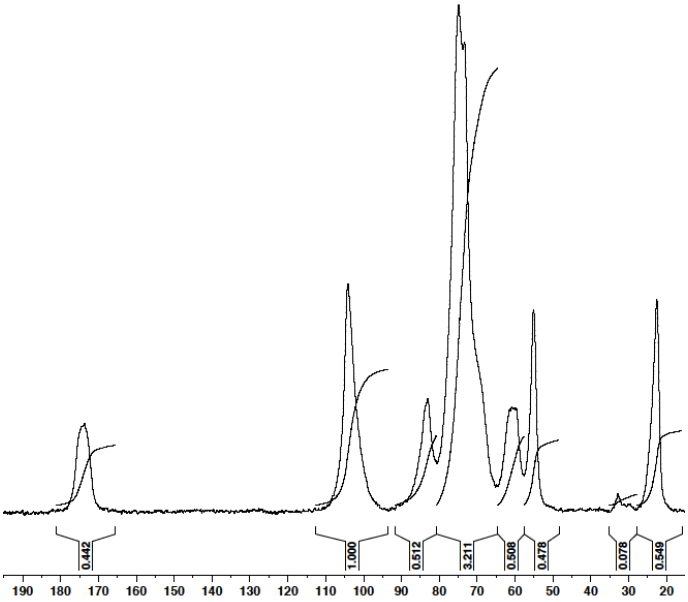

(a) ^{13}C-NMR spectrum of CG

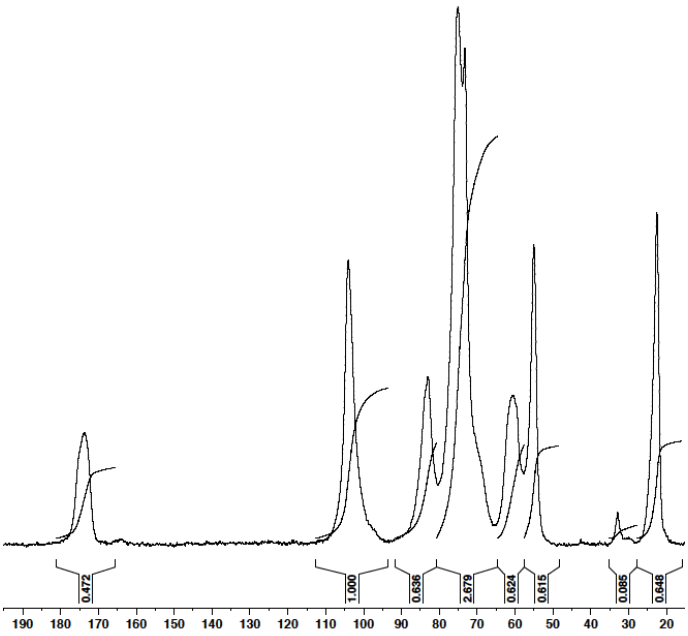

(b) ^{13}C-NMR spectrum of CSG20-1

Figure 16: The relative integrals of all peaks increase with respect to the C1 at 104 ppm.

As all peaks are affected by this increase, this cannot be attributed only to deacetylation. Loss of material that had contributed to the C1 in the CG spectrum could explain this effect. Hence, to determine the DDA first it is necessary to derive the exact content of glucan.

Heux et al. [121] conducted solid state ^{13}C-NMR-spectroscopy on CG extracted from *Aspergillus niger*, extracted with NaOH solution and purified by washing with several solvents. The spectrum they obtained very much resembles our spectra. However, they were also not

able to determine the DDA solely from solid state ^{13}C-NMR. The degree of deacetylation was evaluated from ^{15}N-NMR-spectroscopy, where the peak integrals of the amine and the amide correspond to the relative percentages of chitosan and chitin, respectively.
Although the data does not allow for the calculation of the DDA, the fraction of acetyl groups per monosaccharide unit (χ_{acetyl}) could be determined as the ratio of the averaged area integrals of C7 & C8 to the integral of C1, which had been chosen as a reference peak (Table 5).

Table 5: Fraction of acetylated monosaccharide units in CG and CSG

Sample	χ_{acetyl} [%]
CG	49.6
CSG20-1	51.0
CSG40-0.5	49.6
CSG40-1	44.2
CSG40-2	37.5
CSG60-1	28.2

The values for χ_{acetyl} of CG, CSG20-1, and CSG40-0.5 are all close to 50%. The acetylation per monosaccharide unit then drops with increasing reaction times or NaOH concentration (Table 5). It is save to say that there is an increase in DDA, based on these results combined with the increased nitrogen content determined by EA. This, however, is compensated by a loss of glucan, which explains, why χ_{acetyl} does not decrease for CSG20-1 and CSG40-0.5.
A splitting of the C4-peak is typical for a high DDA [121]. This cannot be found in any of the obtained spectra. One possible interpretation is that even for the harshest conditions (CSG60-1), total deacetylation did not take place. However it has been shown that when pure chitin (extracted from squid) was treated with 60% NaOH at 100°C for 1h, the DDA was 97.3 % [71]. The possible explanation why the peak splitting was not observed is masking by glucan.
Figure 17 shows the ^{13}C-NMR spectrum obtained by Heux et al. [121] for curdlan, a linear β-1,3-glucan. This illustrates how all peaks with the exception of $C = O$ and CH_3 are the result of both, chitin and glucan and makes clear why the determination of the DDA from ^{13}C-NMR-spectroscopy is not possible.

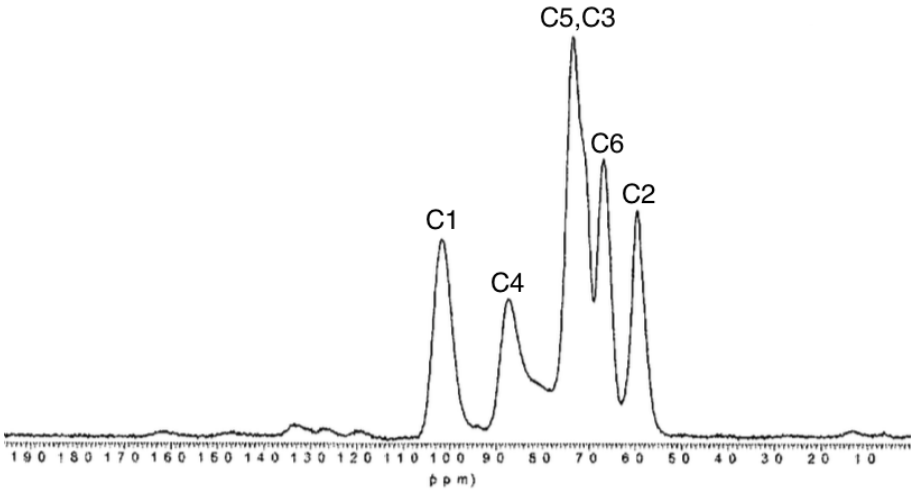

Figure 17: ^{13}C-NMR spectrum obtained for curdlan, a β-1,3-glucan. The spectrum was copied from Heux et al. [121] and the assignment of peaks added in this work.

4.4 Obstacles in the nanopaper production

Tensile tests can only be performed with free-standing nanopapers that are not attached to a filter. Because of this, the nanopaper was usually removed from the filter after the filtration process with the help of a spatula and a tweezer. This method worked fine for CG, but proved more difficult for CSG nanopapers, as they would often stick to the filter paper. In practice it proved impossible to remove CS60-1 from the filter paper. A possible explanation for this could be the higher density of charged groups which might interact with the hydroxy-groups of cellulose through hydrogen bonds. Because of these findings, we focused on CSG20-1, CSG40-1 and CSG40-2, leaving out CSG60-1 as free-standing nanopapers could not be produced.

The same problem also limited the lowest possible grammage that could be achieved for free-standing nanopapers. Using CG, nanopapers as thin as 10 g/m^2 could be easily prepared. The free-standing CSG nanopapers with the lowest grammage were 29.2, 32.6, and 37.7 g/m^2 for CSG20-1, CSG40-1 and CSG40-2, respectively. Nanopapers with a lower grammage could not be removed from the underlying filter without damage.

4.5 Grammage, thickness and density of CG & CSG nanopapers

CSG nanopapers were prone to shrinkage and did not retain their initial size during heat consolidation. Therefore, the grammage was measured by cutting discs of 49 mm in diameter from the final nanopapers and weighing them. Nanopapers with low grammage could not be removed from the filter paper because of sticking and are thus not shown here. This was the case for about half of all produced nanopapers. In Figure 18 the grammage is plotted against the thickness for all measured nanopapers. An almost linear relationship can be observed.

The red lines are to demonstrate that a 50 gsm nanopaper was roughly 45 - 55 µm thick.

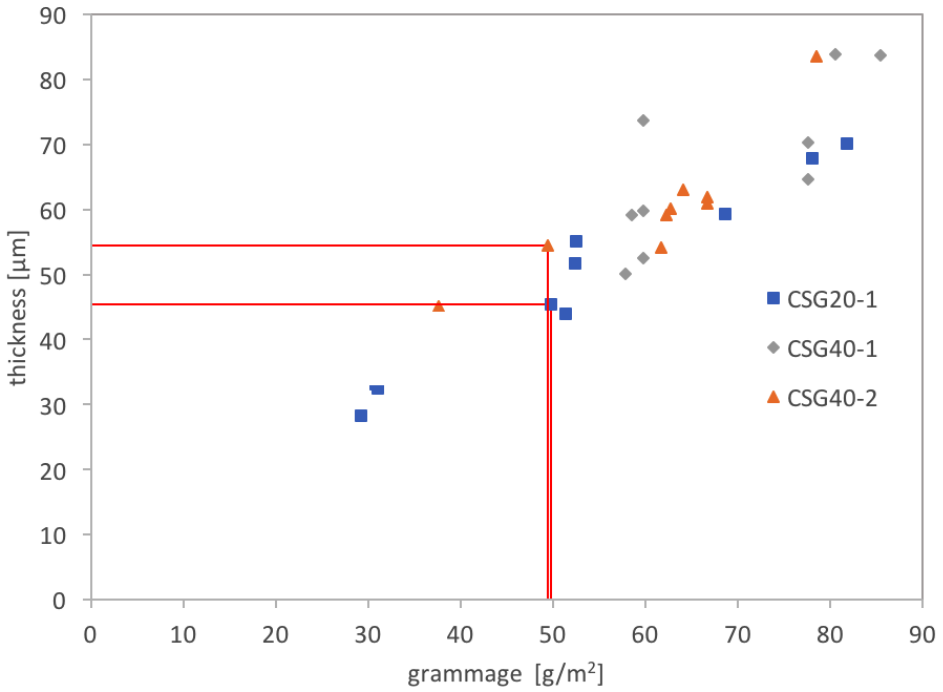

Figure 18: Thickness and grammage of CSG nanopapers.

The envelope density is the ratio between grammage and thickness and is summarized in Table 6. The envelope density was highest for CSG20-1 (1.05) and lowest for CSG40-2 (1.01). However, these differences were not significant.

Table 6: Density and Porosity of CSG nanopapers.

procedure	$\rho_{envelope}$ [g/cm^3]	$\rho_{skeletal}$ [g/cm^3]	porosity [%]
CSG20-1	1.05 ± 0.10	1.42 ± 0.06	25.8
CSG40-1	1.03 ± 0.12	1.43 ± 0.03	27.9
CSG40-2	1.01 ± 0.10	1.36 ± 0.03	25.5

Previous studies showed that the envelope density of CG nanopapers lies between 0.96 g/cm^3 and 1.14 g/cm^3 [36], depending on the grammage, and is therefore comparable with the envelope density of CSG nanopapers produced in this study.

Generally, the density of nanopapers produced from biomaterials is correlated to the degree of fibrillation and the fibril diameter: Both determine packaging efficiency and thus higher density. Dutta et al. [122] prepared chitosan nanofibers by mechanical treatment of chitosan powder in a Starburst system. The density of sheets did increase from 0.49 g/cm^3 (non-treated CS powder) to 0.66 g/cm^3 (10 passes). SEM analysis confirmed a decrease in fibril diameter after several passes, confirming that the density is controlled by fibril size.

The skeletal densities for CSG20-1, CSG40-1, and CSG40-2 as measured by pycnometry were 1.42, 1.43, and 1.36 g/cm^3, respectively. Previous studies found the skeletal density of

pure CG to be 1.47 g/cm^3 [57]. The slightly lower values for CSG could be attributed to the greater repulsion between the amine groups in chitosan. Furthermore, the skeletal densities of CSG and pure chitosan are comparable: For commercial chitosan (DDA approximately 85%) a skeletal density of 1.45 g was reported [123]. Deacetylation of lobster chitin (45% NaOH, 130 °C, 30 min) yielded chitosan (DDA 86 - 89%) with a skeletal density of 1.407 g/cm^3 [124].

The porosity Φ of the nanopapers in % was calculated from equation 7:

$$\Phi\ [\%] = \ 1 - \frac{\rho_{envelope}}{\rho_{skeletal}} \cdot 100\% \tag{7}$$

The porosity of all nanopapers was around 26% (table 6). In a study with nanopapers from CG the porosity was highly dependend on the grammage: It was as high as 35% for 30 g/m^2, but decreased to 22 - 26% for nanopapers of 50 - 100 g/m^2 [36]. Due to the lower envelope density the porosity of CSG nanopapers was generally higher than for CG nanopapers. With a porosity in the range of 20%, nanopapers from nanocellulose (NC) have a lower porosity than nanopapers from CG or CSG [125].

4.6 Surface morphology and fibril diameter of CSG nanopapers

Scanning electron microscopy was carried out to investigate the surface morphology of the nanopapers and to analyse the diameter of CG and CSG nanofibrils. Figure 19 shows SEM micrographs of CSG nanopapers prepared with various reaction times and NaOH conc. and one CG nanopaper at 500- and 1000-fold magnification. The surface of the CG nanopaper seems very smooth at this resolution, while the CSG nanopapers appear more structured.

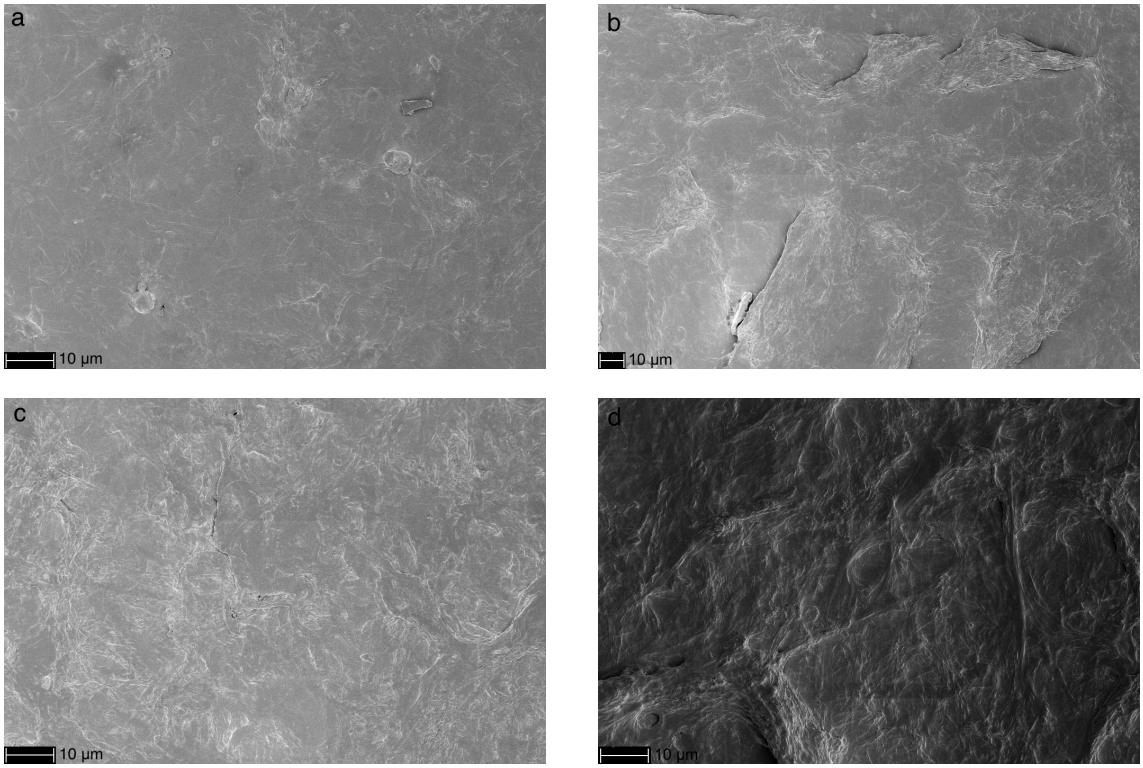

Figure 19: SEM images of CG (a), CSG20-1 (b), CSG40-1 (c) and CSG40-2 (d) at 500- (b) and 1000-fold (a, c, d) magnification

Figure 20 shows images of CG, CSG40-0.5, CSG20-1 and CSG40-1 at 10k- and 25k-fold magnification. At this magnification the single fibrils become visible.

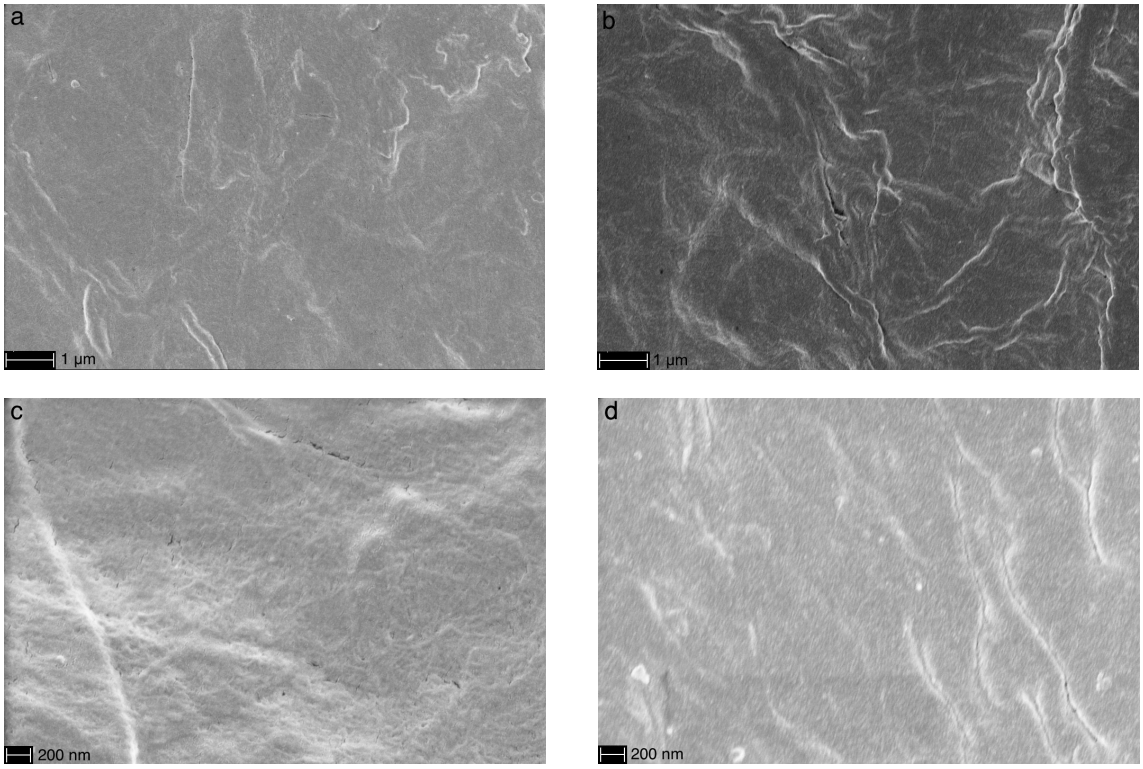

Figure 20: SEM images of CG (a), CSG40-0.5 (b), CSG20-1 (c), and CSG40-1 (d) at 10 k- (a,b) and 25 k-fold (c,d) magnification

Figure 21 shows a CG nanopaper at 100k-fold magnification, unfortunately at this magnification the resolution decreases. While the fibrils of CG samples can still be seen clearly, it is not possible to resolve nanofibrils in CSG nanopapers at 50k- and 100k- fold magnification. This is probably due to charging effects.

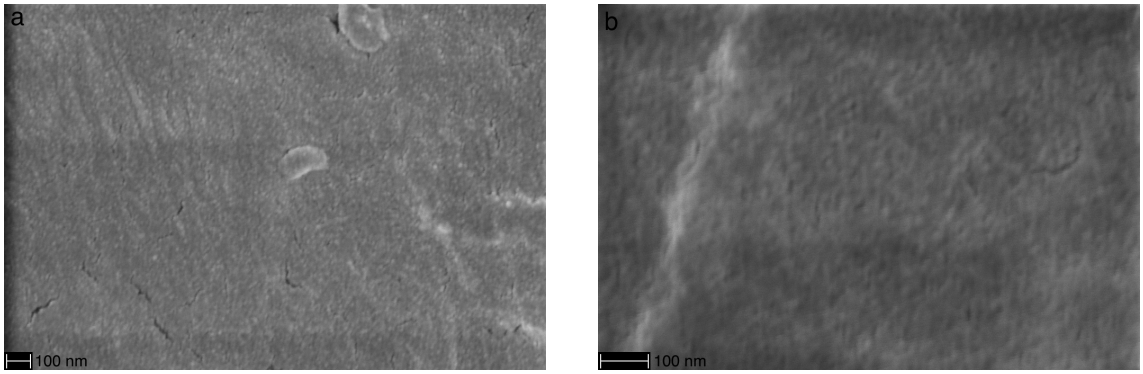

Figure 21: SEM Images of a CG nanopaper at 50k- (a) and 100k-fold (b) maginification-

From the images with the highest possible magnification the fibril diameter was determined (Table 7). The measurements revealed that the nanopapers were definitely structured on the nanometer scale. There seems to be no significant difference between fibril diameters among nanopapers from different procedures. Previous studies on CG nanopapers produced following the same protocol, found an average fibril diameter of 17.1 ± 3.0 nm [36], which is comparable to the results in this work.

Table 7: Fibril diameters of CG, CSG20-1, and CSG40-1 nanopapers.

procedure	diameter [nm]	maximum [nm]	minimum [nm]
CG	13.3 ± 3.1	20.1	8.93
CSG20-1 (a)	13.8 ± 2.0	16.9	11.2
CSG20-1 (b)	17.0 ± 3.0	22.3	12.6
CSG40-1	14.3 ± 2.2	16.1	10.0

4.7 Water permeance of CSG nanopapers

The permeance of membranes is one important parameter to assess their potential for filtration applications. The water permeance was tested in a dead end cell by placing a disc on top of a stainless-steel sintered filter and apply pressure to force water through the nanopaper. Figure 22 shows the pure water permeance for nanopapers of different grammages and different preparation procedures at a pressure of 5 bar.

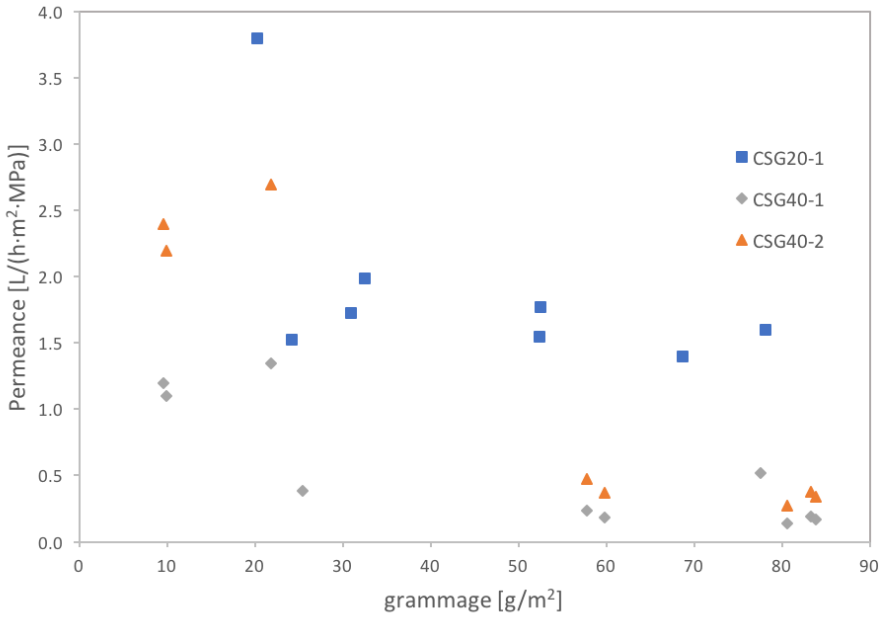

Figure 22: Water permeance for CSG20-1, CSG40-1, and CSG40-2 at different grammage

The water permeance of all CSG nanopapers was lower than for pure CG nanopapers, which at 50 g/m^2 had a permeance of 3.5 $L/h \cdot m^2 \cdot MPa$ [36]. For CSG20-1 at 50 g/m^2 the permeance was about half of a comparable CG nanopaper, CSG40-1 and CSG40-2 had even lower water permeance. Contrary to what one would expect CSG40-2 showed a better average performance than CSG40-1 for all tested grammages. This can potentially be explained by the slightly higher porosity of CSG40-1 nanopapers (27.9%) compared to CSG40-2 nanopapers (25.5%).

Although the porosity of CSG nanopapers was found to be higher than for CG nanopapers, CG nanopapers showed a better permeance in previous studies. In this, the DDA definitely plays a big part. One factor that may have a strong impact on the permeance of a membrane is its hydrophilicity. While chitin is insoluble in water because it is more hydrophobic [126] than chitosan, chitosan readily interacts with water, which may lead to a retention effect and thereby explain the general trend of lower permeance with higher DDA.

The permeance of commercially available NF membranes is about 50 to 100 times higher compared to our nanopapers. The membranes UTC20 (Toray) or NF270 (Dow/FilmTec3) have a molecular weight cut off (MWCO) of 180 kDa and 200-300 kDa, respectively. This means that they reject more than 90% of molecular species of that molecular weight. This converts to a pore size of less than 2 nm [127]. Still they have water permeances of 150 $L/(h \cdot m^2 \cdot MPa)$ (UTC20) and 110 $L/(h \cdot m^2 \cdot MPa)$ (NF270) [128].

4.8 Surface charge of CSG nanopapers

In Figure 23 the streaming potential is plotted against the pH and the IEP is the intersect of a curve with the x-axis.

The IEP of CSG40-1 and CSG40-2 nanopapers were found at pH 5.5 and 5.2, respectively. It is no coincidence that this pretty much resembles the streaming potential measurements of extracted chitin/chitosan of nanopapers from *Cancer Pagurus* (IEP 5.8) [57], which has a higher DDA than fungal CG and contains no glucan.

Potentiometric titration found the pKa of chitosan's $-NH_3^+$ group to be 6.2 [129]. The IEP of the two CSG40 nanopapers is thus slightly lower than this, which can be explained by the acidic nature of glucan. In previous studies the IEP of pure CG nanopapers had been found to be pH 3.1 [36]. The IEP of the CSG20-1 nanopaper in this work was measured to be pH 3.8 and is therefore between the IEP of CSG40 nanopapers and the one of pure CG nanopapers.

All nanopapers show a plateau at high pH. The plateau for nanopapers follows the order of the IEP: The CSG20-1 nanopaper showed the least negative plateau (-12.9 mV). This is followed by CSG40-2 (-22.0 mV) and CSG40-1 (-25.9 mV). Responsible for the plateau are the number of charged groups on a surface. An increase in the DDA explains the higher values for CSG40 nanopapers as compared to the CSG20-1 nanopaper. A loss of glucan in the deacetylation step could have caused the CSG40-1 nanopaper to display a higher density

of amino groups on its surface than the CSG40-2 nanopaper.

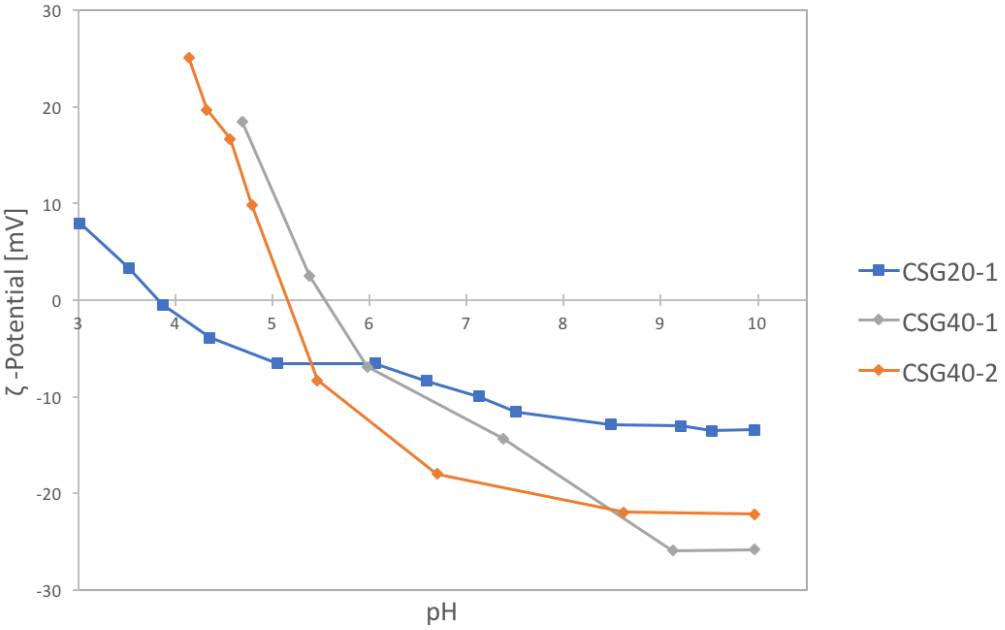

Figure 23: Streaming potential for chitosan-glucan nanopapers as function of pH

All of this is once again strong evidence that the deacetylation was successful. It suggests that the DDA of CSG nanopapers was higher than for CG nanopapers, and the DDA of CSG40 nanopapers higher than for the CSG20-1 nanopaper.

Streaming potential measurements of CSG40 nanopapers always failed when the pH was below 4. This might be due to the solubilization of chitosan in acidic environment. If the pH is lower than the IEP, all $-NH_2$ groups are protonated and chitosan solubilizes. Extraction protocols for chitosan therefore use a treatment with dilute acid [64].

4.9 Mechanical properties of CSG nanopapers

Figure 24 shows examples for the stress-strain curves of CSG20-1, CSG40-1 and CSG40-2 nanopapers. The highest point in the stress-strain curve represents the stress at failure, also called maximum tensile strength. It is a measure of how much stress a material can bear, before it breaks. From stress-strain curves also the Young's modulus can be derived. It is the slope of stress-strain curve in its linear part. The Young's modulus is a measure of how much stress is needed to be applied to a material to reach a certain deformation, thus it represents its stiffness.

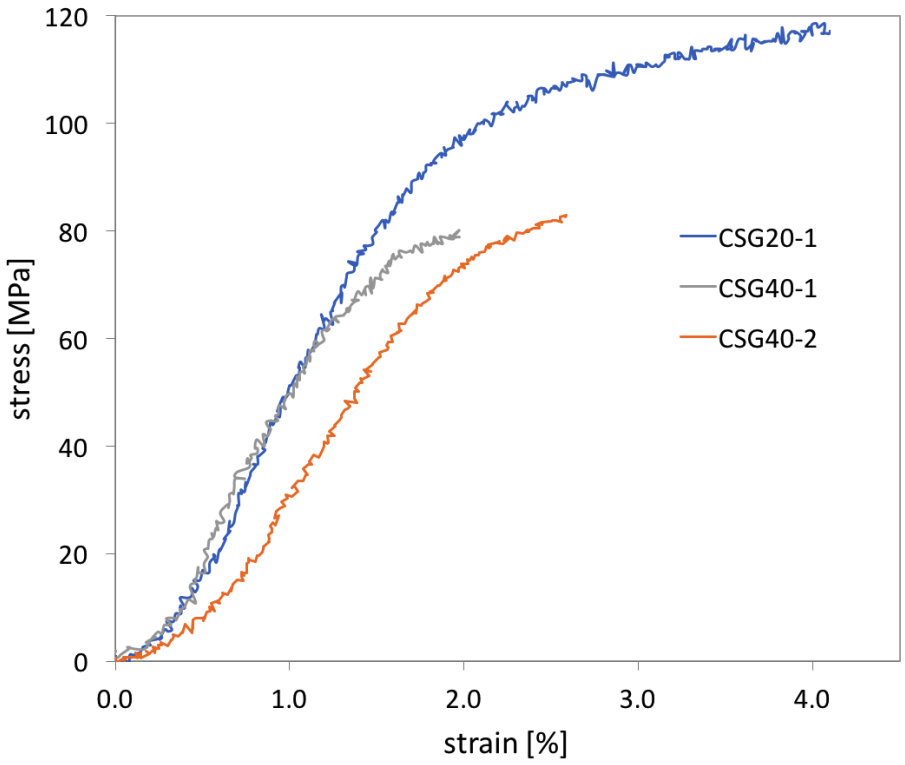

Figure 24: Representative stress-strain curves for CSG20-1, CSG40-1, and CSG40-2.

CSG20-1 nanopapers failed between 100 and 120 MPa, which is considerably stronger than CSG40-1 and CSG40-2 nanopapers (70 - 85 MPa). The average elongation at break was 4% for CSG20-1 and 2-3 % for CSG40-1 and CSG40-2. The Young's modulus is another important material property. Values of 6.34 GPa (CSG20-1), 5.02 GPa (CSG40-1) and 5.32 GPa (CSG40-2) were measured.

The results for the mechanical properties of nanopapers are depicted in Figure 25. It visualizes that higher NaOH concentrations did negatively affect the mechanical properties of CSG nanopapers, but that increasing the reaction time from 1 to 2 h did not have a big impact as can be seen by the similarity of CSG40-1 and CSG40-2 nanopapers.

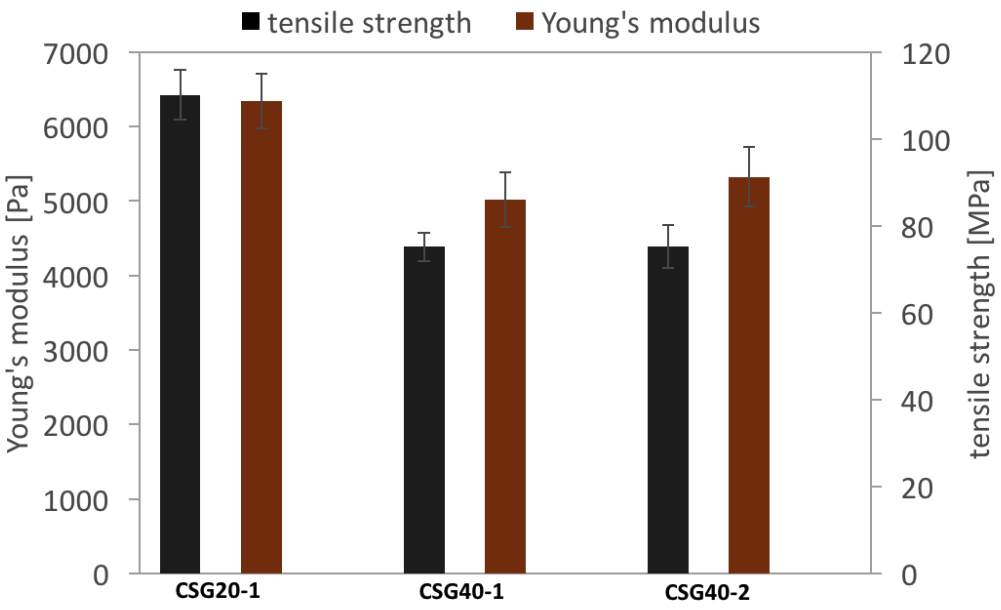

Figure 25: Mechanical properties of CSG20-1, CSG40-1, and CSG40-2 nanopapers

CG nanopapers prepared from CG extracted from stalks or caps of *Agaricus bisporus* have a reported tensile strength as high as 191.9 ± 10.6 MPa and 192.9 ± 12.0 MPa, respectively [57]. The deacetylation reaction caused the tensile strength to decrease. The Young's modulus of CSG40 nanopapers was similar to CG nanopapers (5.0 ± 0.3 GPa for stalks; 5.2 ± 0.5 GPa for caps). Interestingly CSG20-1 nanopapers showed an even higher Young's modulus (6.3 GPa) than CG nanopapers.

High molecular weight generally has a positive effect on the tensile strength of a material [130]. As noted in previous chapters, the harsh deacetylation conditions might have caused cleavage of covalent bonds in the material. The literature reports decrease of molecular weight for longer reaction times [70] and higher temperatures [69]. This would result in a product with lower molecular weight, which might explain the decrease in strength compared to CG. Another factor that might play a role is the lower density and higher porosity of CSG20-1, CSG40-1, and CSG40-2 compared to CG. Electrostatic repulsion of the functional groups in chitosan might be responsible for this effect, also resulting in a reduced tensile strength. Besides this factors also the network structure could be affected, resulting in a loser network than in the original CG.

Rivero et al. (2010) found tensile strength of chitosan films prepared by solution casting (dissolved in dilute acetic acid) at 73.8 MPa [131]. Besides this also the lower elongation at break of CSG nanopapers compared to CG nanopapers reflects a reduction in ductility

that might as well be due to lower average molecular weight, caused by cleavage of chemical bonds during the deacetylation reaction.
Chitosan films prepared by dissolving pure chitosan and treating it with different voltage found that depending on the procedure, films failed between 13 MPa (control) and 22 MPa (100 mV/cm^2) [84]. In another study films were made from pure chitosan by solution casting of CS (dissolved in lactic acid) in a petri dish. The ultimate tensile strength was found to be 34.1 MPa but the elongation at break was as high as 53.8 % [132]. The much higher ductility of the chitosan films illustrates that they are very different to CSG-papers in their tensile behaviour. Furthermore, it can be seen that the mechanical properties vary a lot depending on the exact procedure used to measure the mechanical properties. However, in general this shows that CSG nanopapers have a much higher tensile strength compared to chitosan films.

To evaluate the influence of heat consolidation procedure one CSG20-1 nanopaper was pressed in an hot-press at 120°C for 15 min under 1 t (CSG-HP). Figure 26 compares the stress-strain curves of CSG-HP to a nanopaper produced by pressing under 5 kg weight an oven.

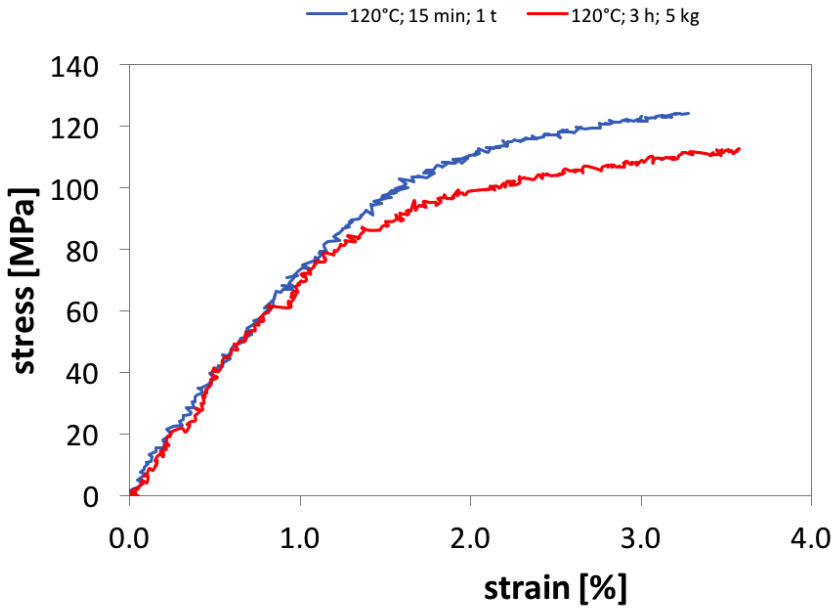

Figure 26: Tensile curves of a CSG20-1 nanopaper pressed under different conditions.

The maximum tensile strength of the hot-pressed nanopaper (120 ± 9 MPa) was slightly higher than of the nanopapers produced with the standard procedure, but still comparable. The good performance can be explained with better compaction under 1 t of weight, which did also lead to an increase in $\rho_{envelope}$ (1.18 g/cm^3 as opposed to 1.05 g/cm^3 for the standard procedure). Also the higher Young's modulus (7.7 ± 0.44 GPa) can be explained by the increased density. However, from this single measurement it is not possible to tell whether the improvement of mechanical properties was really a result of hot-pressing or a

stochastic effect.

4.10 Thermal stability of CSG nanopapers

Figure 27 shows thermograms of CSG20-1, CSG40-1, and CSG40-2 heated in air. The initial mass loss around 100 °C is associated to removal of water. The temperature of 280 °C is the the beginning of the first degradation step. At a temperature of 390 °C the curves start to flatten out, followed by a second mass degradation step around 490 °C. These two mass loss events indicate that there were two reactions taking place during thermal degradation of the material. In the second reaction all material was converted to gas. The curve drops to 0 % mass even before reaching 600 °C.

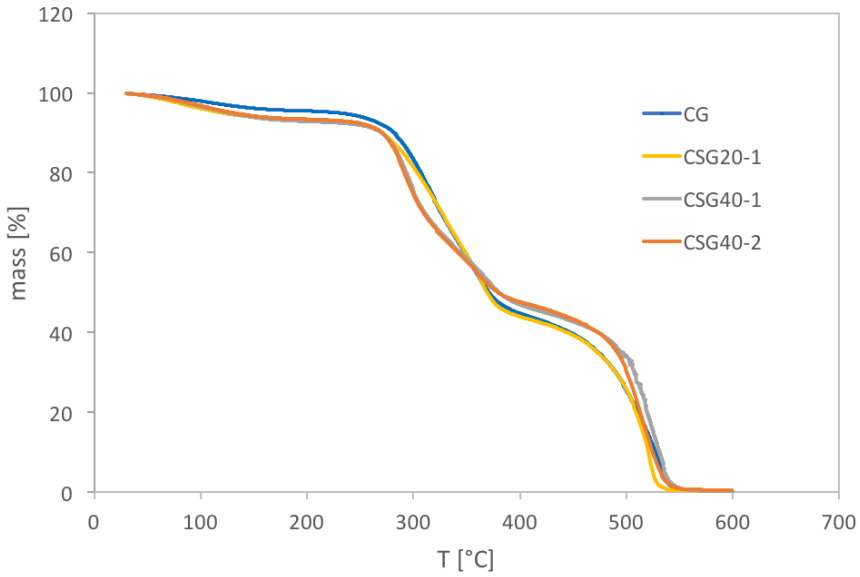

Figure 27: Thermograms of CG, CSG20-1, CSG40-1, and CSG40-2 nanopapers under air atmosphere

Figure 28 shows thermograms of the nanopapers heated in N_2. At low temperatures the mass is relatively stable followed by a sudden decline around 270 - 280 °C. At around 490 °C the degration reaction has stopped and the curves flatten out, leaving a char residue of around 30%.

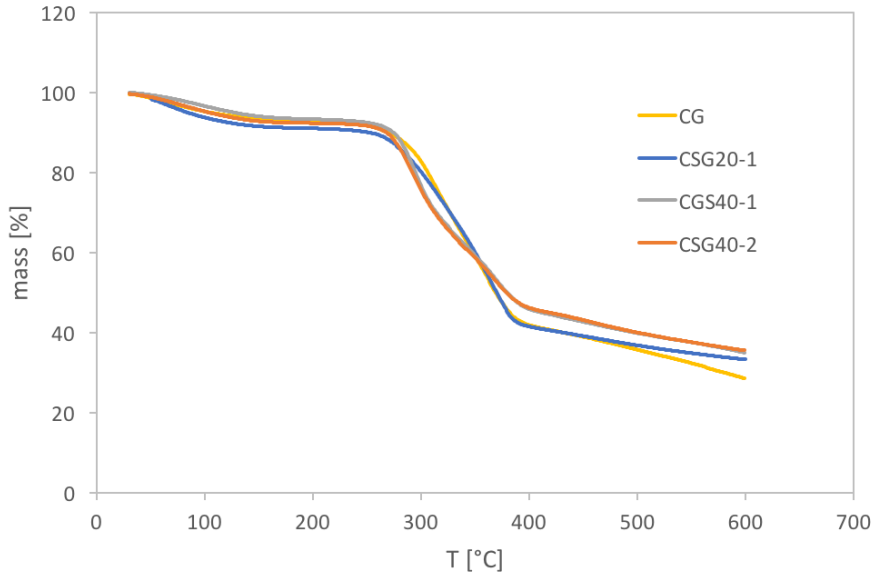

Figure 28: Thermograms of CG, CSG20-1, CSG40-1, and CSG40-2 nanopapers in a flow of nitrogen.

From this point on the rate of mass loss was greatly reduced. The mass did decrease slowly and at 600 °C residual material remained in the pans (table 8). While for CG only 28.6 % of initial material did not decompose, the values for the deacetylated nanopapers were 33.3%, 35.0%, and 36.0% for CSG20-1, CSG40-1, and CSG40-2, respectively. This demonstrates that longer reaction times and higher NaOH concentrations did increase the amount of produced char.

Table 8: Char residue of CSG nanopapers after heating to 600°C in N_2

paper	**mass @ 600°C** [%]
CG	28.6
CSG20-1	33.3
CSG40-1	35.0
CSG40-2	36.0

The first part of the thermogram of the nanopapers in N_2 (figure 28) resembles the thermograms of nanopapers in air (figure 27). However, while for heating in air two reactions could be observed decomposition in N_2 followed a single reaction. One indicator for the thermal stability is the onset temperature of the first degradation step, which was for all samples between 250 and 300 °C. Harsher reaction conditions generally led to material with lower onset temperature (Table 9). Such effects can often be attributed to autocatalysis.

Table 9: TGA onset temperatures of CG, CSG20-1, CSG40-1, CSG40-2, and CSG60-1 powder and nanopaper in air and N_2.

procedure	T_{onset} powder air [°C]	T_{onset} paper air [°C]	T_{onset} powder N_2 [°C]	T_{onset} paper N_2 [°C]
CG	242.7	281.4	255.9	287.6
CSG20-1	241.0	278.3	256.9	281.9
CSG40-1	-	271.7	262.7	275.6
CSG40-2	233.5	270.6	249.4	285.1
CSG60-1	233.5	-	254.4	-

Also reflected by the onset temperature is the higher stability of nanopapers versus powder which was true for all tested samples. The onset temperatures of papers in N_2 or air were found at 270 - 290 °C, while powders started to decompose already at 230 - 245 °C (air) and 255 - 265 °C (N_2). In addition to that, while nanopapers heated in N_2 left back around 30 - 40 % of residual material (figure 28), powders did fully decompose as shown in Figure 29. One factor that could explain this observation is that the dried material is more porous, so the contact area with a hot gas may be a lot greater than in a more compact nanopaper.

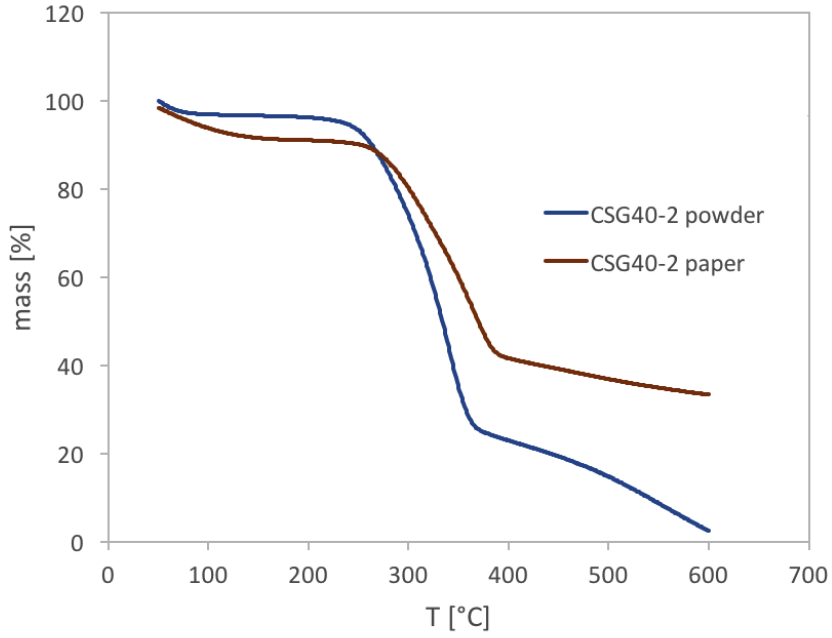

Figure 29: Thermograms of CSG40-2 powder and a CSG40-2 nanopaper in nitrogen atmosphere.

Heating curves of pure chitosan without glucan in nitrogen look similar to the heating curves of CSG in nitrogen. Figure 30 shows a thermograph obtained by Hong et al. [133] in a TGA study with chitosan extracted from shrimp shells. The material was heated to 650°C at heating rates of 10 °C/min, 14 °C/min, 18 °C/min, 22 °C/min, 26 °C/min, 30 °C/min[133], represented by lines 1-6.

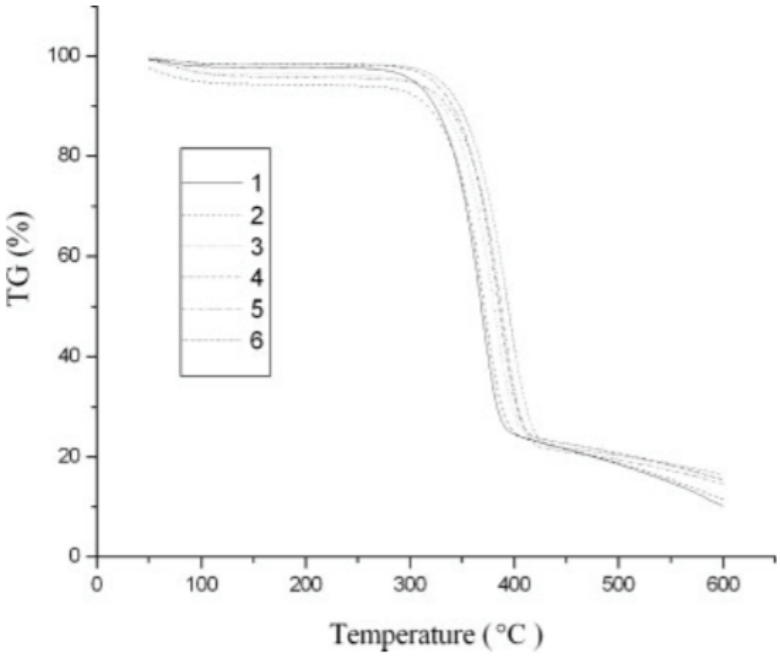

Figure 30: Thermograph obtained by heating chitosan in nitrogen atmosphere. The figure was copied from Hong et al. [133]

Line 1 (10 °C/min) has the same heating rate as the procedure used in this work. The graph very much resembles the heating curves obtained for CSG nanopapers in N_2. However, the most notable difference is the much later onset of the mass loss of around 300 °C in contrast to 280 °C for CG and CSG nanopapers or 250 - 260 °C for CG and CSG powder. Also chitin from *Cancer pagurus* heated in nitrogen was shown to have an onset temperature (at 10% mass loss) of 280 and 329 °C for powder and films, respectively, when heated in nitrogen. For CSG40-2 the onset temperature (at 10% mass loss) was 254 °C for both powder and films. It was found that in animal chitin the size of the chitin crystals was the factor that had the biggest impact on the degradation temperatures of chitin derived from different species [134]. The crystallite size was also described as causing the onset temperature of fungal CG to be lower compared to animal chitin [57]. This might also be true for CSG and explain why the onset temperature of CSG is much lower than that of shrimp shells or *Cancer pagurus*.

4.11 Specific surface area of CSG nanopapers

iGC measurements were performed using the BET model to determine the SSA of CSG nanopapers. The results are listed in Table 10. Values of dried CSG from all all procedures

were around 0.25 - 0.26 m^2/g with the only exception being CSG40-0.5 (0.232). However, this may be a stochastic effect, as the surface area was only measured once. It is noteworthy

Table 10: Surface specific area

Method	**SSA [m^2/g]**
CSG20-1	0.252
CSG40-0.5	0.232
CSG40-1	0.251
CSG40-2	0.255

that the values obtained for CSG are a lot higher than the SSA reported for CG nanopapers, which had been 0.11 and 0.17 m^2/g for stalk and cap, respectively [57]. An explanation for this could be the higher electrostatic repulsion due to the high abundance of free amines or the partial removal of glucan. Deacetylation of crab chitin yielded chitosan with a surface area of roughly 30 m^2/g [135]. This value is much higher than the results for CG and CSG. However the measurements refer to chitosan particles and not papers or films.
Comparison with conventional materials used for adsorption shows that CG and CSG do not have a particularily high SSA: For Bentonite (Çanakkale, Turkey), the major component of montmorillonite, 767 m^2/g have been reported [136] and one gram of activated carbon can have a surface of larger than 3000 m^2 [137]. Even fly ash, a waste product of thermal power stations, has a SSA 15.6 m^2/g [138].

4.12 Pore size of CSG nanopapers

The pore size of a paper specifies its properties in terms of size exclusion. For NF membranes it is typically below 1 nm. The smaller the pores the smaller can be the particles or neutral molecules, such as polymers, which can still be rejected by the membrane. Here the pore size was measured with a suspension of colloidal gold nanoparticles of approximately 10 nm in diameter.
After filtration the nanopapers were stained dark red, which is typical for gold nanoparticles (Figure 31 left). Also there was a clear visual difference between the suspensions before and after filtration (Figure 31 right).

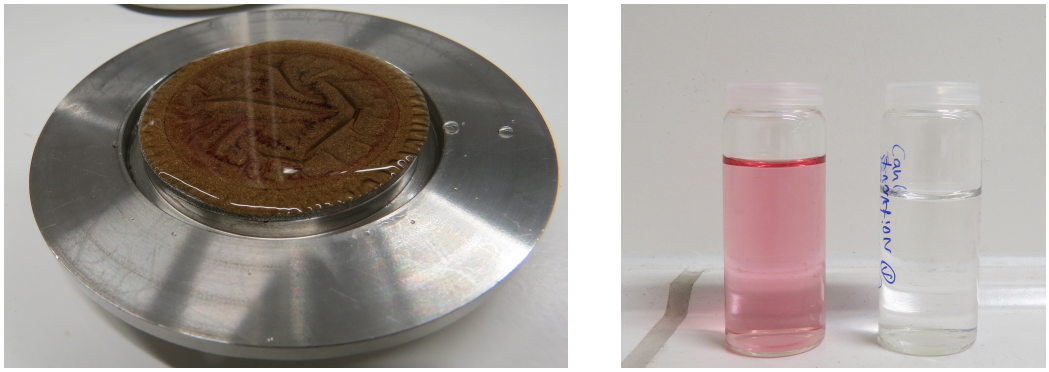

Figure 31: Nanopapers after gold NP filtration (left) and the NP suspension before and after filtration (right).

In Figure 32 the absorbance of the original nanoparticle suspension and the absorbance of the filtrate is plotted against the wavelength. The absorbance for gold nanoparticles of this size is typically between 515 and 520 nm.

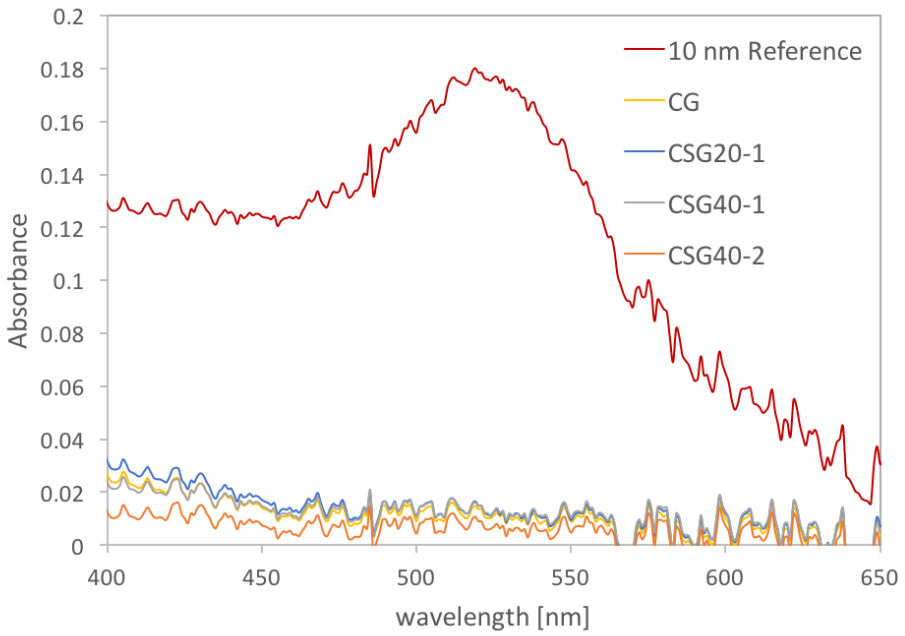

Figure 32: Absorbance before and after filtration of 10 nm gold NP-suspension through CG and CSG nanopapers

The results show that the NPs were completely rejected by the nanopapers. There was no absorbance of light at this wavelength for the permeate of any of the tested nanopapers. This lets conclude that the size of the pores is below 10 nm. The pore size of CG nanopapers prepared by the same method was determined by molecular weight cut-off (MWCO) of PEG in water and PS in THF and estimated to approximately 10 nm and 12 nm, respectively [36]. The result also confirms our observations from the fibril size measurements: there is no mechanical nor chemical treatment required to obtain fibers in the nanometer range for CG and this also holds true for CSG.

4.13 Adsorption of copper ions

Chitosan has high affinity towards heavy metal ions, especially copper(II) [88–92]. To investigate the effectiveness of CSG-papers for the removal of Cu^{2+} from water static adsorption experiments had been carried out in a previous study at this institute [139]. Briefly, CG- or CSG-suspensions (instead of nanopapers) were incubated with $Cu(NO_3)_2$ solutions. After 15 min the suspension was filtered and the concentration of copper in the permeate determined by titration with EDTA (0.5 mM) and compared to that of a reference sample. The experiment was done once with CG, twice with CSG40-1, and twice with CSG40-2. The results of the static adsorption capacities for different concentrations of Cu^{2+} are depicted in Figure 33.

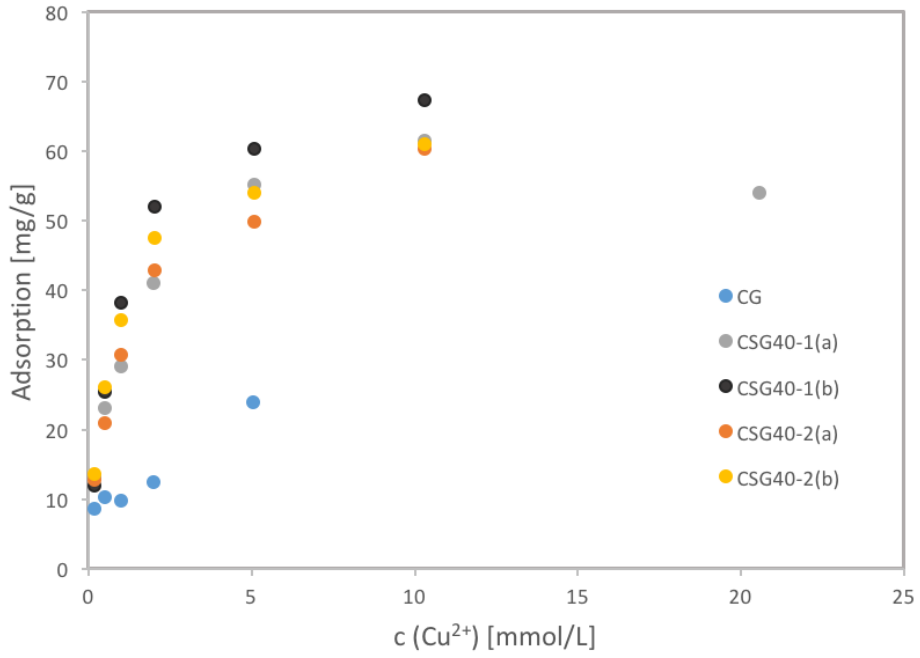

Figure 33: Comparison of the static adsorption of CG, CSG40-1, and CSG40-2 [139].

CSG40-1(a) and CSG40-2(a) were both produced from the same CG batch, and so were CSG40-1(b) and CSG40-2(b). CSG40 samples performed much better than the CG sample. The adsorption capacity generally increased with the concentration, being highest for CSG40-1(b) at 10.3 mM (73.3 mg/g). There was only one experiment carried out with 20 mM copper(II) solution and the result suggests a saturation of the membrane at this level of concentration. However, more measurements need to be carried out to confirm this.
Regarding the adsorption capacities of CSG40-1 and CSG40-2 the results clearly show that irregularities of starting material, extraction, or deacetylation seem to have a greater impact on the adsorption properties of the material than increasing the reaction time of CSG40 from 1 h to 2 h. Here CSG40-1(b) actually performed best, while CSG40-2(a) was worst on

average in terms of copper(II) adsorption.

Following these results, dynamic adsorption was carried out in a dead end cell at a driving pressure of 5 bar. The $Cu(NO_3)_2$ solution (1.92 mM) was filtered through the nanopapers and the permeate passing the membranes was titrated with EDTA. The use of EDTA was then compared to that of a reference sample. After the experiment the nanopapers were colored blue, caused by adsorbed copper (Figure 34).

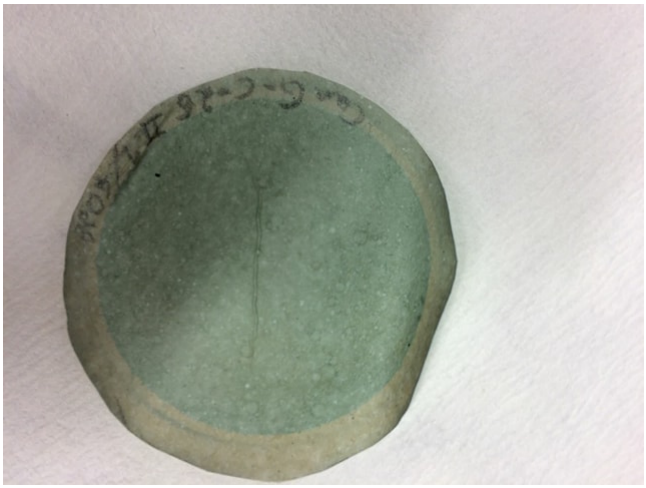

Figure 34: CSG nanopaper after filtration of a copper nitrate solution.

The adsorption curves for CG and CSG nanopapers are plotted in Figure 35.

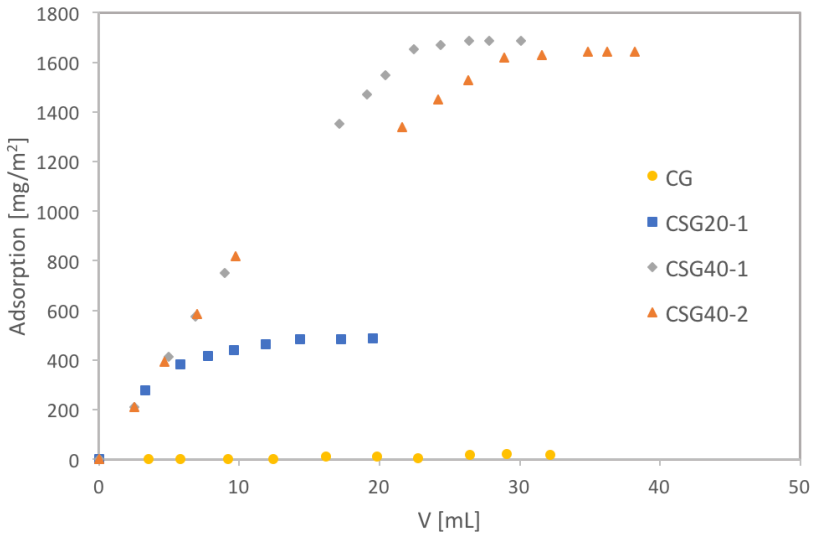

Figure 35: Total amount of Cu^{2+} in mg rejected by one m^2 of the nanopapers.

All data points for CG are close to 0 which indicates a low adsorption capacity. The CSG20-1 nanopaper is steep in the beginning that flattens out at 10 mL. After 20 mL of permeate had passed the membrane it was saturated with copper ions and the curve flattens out. The

adsorption capacities of CSG40-1 and CSG40-2 were very close to each other. Both curves overlap up to a volume of 10 mL. The following gap represents the night were no samples could be taken and the dead end cell was left under passive pressure that was 5 bar in the beginning (the connection valve to the nitrogen pressure was closed, yet the pressure in the system was not released). The earlier decline of the CSG40-2 curve could be attributed to the slightly higher grammage. Of all tested samples the CSG40 nanopapers performed best in terms of adsorption capacity. Also saturation was reached much later than for CSG20-1. The values for the maximum adsorption capacity are listet in Table 6. For CSG20-1 nanopapers it is was 555.3 mg/m^2 which correlates to 38.0 mg/g. Even higher than this were the adsorption capacities of CSG40 nanopapers: 1687.3 mg/m^2 (= 117.7 mg/g) and 1643.8 mg/m^2 (= 102.9 mg/g) for CSG40-1 and CSG40-2, respectively. This reflects the higher DDA in CSG40 related to CSG20-1, resulting in more free amino groups, that are capable of complexing Cu^{2+} ions.

The long filtration times (over night) could explain why maximum adsorption capacities of CSG40 at 2 mM Cu^{2+} measured in continuous adsorption were much higher, than the values obtained from static adsorption experiments (46 ± 5 mg/g) (figure 33), which did only take 15 min.

Table 11: Maximum adsorption for CG and CSG

Method	**Adsorption [mg/g]**	**Adsorption [mg/m^2]**
CG	2.8	17.5
CSG20-1	38.0	555.3
CSG40-1	117.7	1687.3
CSG40-2	102.9	1643.8

In terms of adsorption capacity the CG nanopapers (2.8 mg/g = 17.5 mg/m^2) were outperformed by the CSG nanopapers. The reason for this is the higher chitosan content in CSG. Next to the better chelation properties of chitosan versus chitin one reason for the better performance of CSG membrane might also be their larger surface area.

One continuous adsorption study with CG nanopapers of 40 g/m^2 showed an absorption capacity of 177 mg/m^2 [36]. This much higher value compared to the CG nanopaper investigated in this work could be explained by the higher grammage used in that study.

Ghaee et al. [140] prepared membranes by solution casting of chitosan (90 % DDA) from acetic acid and crossliking it with glutaraldehyde to enhance the stability. To increase the adsorption capacity for copper(II) they used silica gel as a porogen. Soaking the membranes for 24 h in a copper sulfate solution gave a maximum adsorption capacity for copper(II) of 46.98 mg/g for the most porous membrane. The CSG nanopapers of this work have the big advantage of already being porous. Furthermore, our nanopapers do not require

crosslinking, which is known to negatively affect the adsorption: In a study with crosslinked chitosan beads adsorption capacities were reduced from 80.71 mg/g (pure chitosan beads) to 59.67 mg (chitosan-glutaraldehyde beads), 62.47 mg/g (chitosan-epichlorohydrin beads), and 45.94 mg/g (chitosan-glycol diglycidyl ether beads) [112].

In another study porous chitosan membranes were prepared from chitosan by thermally induced phase separation. The maximum adsorption capacity as calculated from the Langmuir isotherms was 163.4 mg/g [141]. A chitosan/aluminium oxide composite prepared by casting from a chitosan suspension in toluene reached an adsorption capacity of 146 mg/g [142]. These values are somewhat higher but definitely comparable to CSG40 nanopapers (117.7 mg/g and 102.9 mg/g for CSG40-1 and CSG40-2, respectively). Electrospun chitosan can achieve higher copper adsorption capacities. In a study with electrospun CS nanofiber mats (86.7 % DDA) a maximum adsorption capacity of 485.4 mg/g was derived from Langmuir isotherms [97].

Generally, we can conclude that the copper(II) adsorption of CSG nanopapers (especially CSG40) is comparable to other modes of application of chitosan. The here presented methods provide a simple way to nanopapers that, if optimized, might lead to CSG nanopapers, with improved copper(II) adsorption that even outperform the already good adsorption capacities of the nanopapers here.

5 Conclusion and Outlook

In this work chitin-glucan (CG) was extracted from *Agaricus bisporus* and converted to chitosan-glucan (CSG) by a deacetylation reaction with NaOH. CSG was produced using 20% NaOH (CSG20), 40% NaOH (CSG40), and 60% NaOH (CSG60). While CSG40 was produced with reaction times of 0.5 h (CSG40-0.5), 1 h (CSG40-1), and 2 h (CSG40-2), CSG20 and CSG60 were both produced by reaction times of 1 h only (CSG20-1 and CSG60-1, respectively). Elemental analysis, Fourier-transform infrared spectroscopy, and ^{13}C-NMR-spectroscopy were used to characterize CSG. Furthermore, the skeletal density of CSG was measured. From this material nanopapers were prepared by filtration of aqueous suspensions of CSG over filter paper. The CSG film was pressed for 3h under a 5 kg weight in an oven at 120°C. The mechanical properties, the permeance of water, the ζ-potential, the specific surface area (SSA), as well as the retention of gold nanoparticles (10 nm diameter) were investigated. The fibril diameter of nanopapers was measured from micrographs obtained from SEM imaging. The adsorption capacities for copper(II) were determined in continuous adsorption experiments in a dead end cell.

Scanning electron microscope imaging showed that the nanopapers consisted of nanofibrils in the range of 10 - 20 nm. The skeletal density of CSG was between 1.36 and 1.43 g/cm^3 and the envelope densities were found between 1.01 and 1.05 g/cm^3. The permeance of the nanopapers was between 0.5 and 4 $L/h \cdot m^2 \cdot MPa$ for 10 - 20 gsm and dropped below 2 $L/h \cdot m^2 \cdot MPa$ for papers around 80 gsm. It was highest for CSG20-1 and lowest for CSG40-1. 10 nm gold nanoparticles were completely rejected by the nanopapers. The maximum tensile strength was 100 - 120 MPa for CSG20-1 nanopapers and 70 - 85 MPa for CSG40 nanopapers. The elongation at break decreased if harsher reaction conditions were applied. The SSA of all nanopapers was between 0.23 and 0.26 m^2/g. The isoelectric point (IEP) was found to be at pH 3.8, 5.54 and 5.15 for CSG20-1, CSG40-1, and CSG40-2 nanopapers, respectively. Continuous adsorption measurements found the maximum adsorption capacity for copper(II) increasing with NaOH concentration and reaction time: 2.8 mg/g, 38.0 mg/g, 117.7 mg/g and 102.9 mg/g for CG, CSG20-1, CSG40-1 and CSG40-2, respectively.

Higher concentrations of NaOH and longer reaction times led to an increase of the nitrogen content in the elemental analysis, which suggests a successful deacetylation. This observation is supported by ^{13}C-NMR-spectroscopy, where the peak integrals corresponding to the two carbon atoms of the acetyl group decrease with NaOH concentration and reaction time, compared to a reference peak. Based on these results the DDA increased in the order CG $<$ CSG20-1 $<$ CSG40-0.5 $<$ CSG40-1 $<$ CSG40-2 $<$ CSG60-1. This increase in amine groups opposed to acetamide groups on the nanopaper's surface was also backed by the streaming potential measurements. The IEP of CSG40 (ph 5 - 6) was found to be much closer to the

pKa of chitosan's NH_2-group than the IEP of CG and CSG20. Furthermore, the skeletal density of CSG was between 1.36 and 1.42 g/cm^3 and thus somewhat lower than for CG (1.47 g/cm^3). This may be attributed to the higher repulsion of charged groups in CSG and the partial removal of glucan, which aids paper formation.

Tensile tests revealed that the deacetylation reaction did somewhat decrease the tensile strength and the elongation at break. However, CSG nanopapers still reflect the good mechanical properties of CG and perform well compared to other nanopapers. They definitely outperform films prepared from pure chitosan extracted from marine animals.

SEM showed that CSG nanopapers maintained the nanostructured characteristics of the extracted CG. This property can be seen as an advantage of CG and CSG over many other biomaterials, where nanofibrils have to be produced, either mechanically or chemically. The successful production of CSG ultrafiltration membranes was proven by the full retention of 10 nm gold particles. This small pore size allows nanopapers to be used to remove viruses from water.

The SSA of CSG nanopapers was higher than the SSA of CG (0.11 - 0.17 m^2/g), but still low compared to traditional adsorbers, which was due to very dense nanopapers opposed to powders. Nevertheless, the CSG nanopapers showed good adsorption behavior. The maximum adsorption capacity for copper(II) did increase in the order CG $<$ CSG20-1 $<$ CSG40. This increase in adsorption performance also reflects the increase in the nitrogen content (and hence DDA). It can be assumed that the conversion from chitin to chitosan, a material who's outstanding chelation properties had been extensively investigated, has resulted in the high retention of copper(II) ions.

5.1 Future work

Unfortunately it was not possible to calculate the exact DDA from the applied methods. A way to obtain information on this could be sugar analysis. In this method polysaccharides are broken into their individual components, separated by HPLC, and quantified. A different approach would be to carry out solid state ^{15}N-NMR.

The low water permeance of nanopapers is definitely one of the big obstacles to overcome on the way to use them in real world applications [32]. It was shown, that the permeance of nanopapers can be tailored by selecting the nanofibril dimensions. This approach may be applied to CG and CSG nanopapers in future work. Proposing that the low permeance of nanocellulose ultrafiltration membranes was a result of their high density, Mautner et al. [143] successfully produced membranes using organic solvents instead of water. Using this approach, the authors were able achieve a significantly improved permeance. The idea of employing organic solvents might also be applicable to the manufacture of CG or CSG nanopapers. An alternative route could be the use of CSG in combination with other materials. As an example, a composite paper from highly deacetylated CSG and NC could potentially make benefit of chitosan's adsorption properties as well as from nanocellulose's

better permeance.

Furthermore, it has been demonstrated that it is possible to prepare nanopapers from nanocellulose with pore sizes as small as 10 nm and to influence the pore size of the nanopapers by combining different nanocellulose fibers. Also it was shown that the pore size is dependend on the fibril diameter, with the pore size being of the same order of magnitude as the fibril diameters. Hence it is possible by varying the fibril diameter to tailor the pore size [32]. This approach might also be applicable to CSG nanopapers.

A good adsorber is generally characterised by high specific surface area (SSA). Increasing the surface area could also lead to a better adsorption performance. Chitosan's adsorption peaks at pH 4.5 [96], however, the material dissolves in acidic media. Free chitosan, not linked to glucan, could thereby be lost. This could be addressed by crosslinking of chitosan in order to decrease its solubility.

Furthermore, other potential modes of application should be assessed. Although manufacture of filtration membranes is a cheap and easy way to apply CSG, the material might not be restricted to filtration. The successful use of CSG as an adsorber in suspension has already been proven. Other modes of application such as CSG-beads could be feasible.

Finally, we can conclude that CSG nanopapers have definitely promising potential to be applied in ultra- and nanofiltration as well as for the adsorbtion of pollutants, such as heavy metal ions. Research on this topic is still in its infancy. Future work will hopefully push the development of fungal chitosan nanopapers to a level, where they make their contribution to one of our greatest challenges: Provide sustainable methods to ensure access to clean water.

6 Glossary

ATR	attenuated total reflection
CG	chitin-glucan
CS	chitosan
CSG	chitosan-glucan
CSG20-1	CSG prepared with 20% NaOH and 1 h reaction time
CSG40-0.5	CSG prepared with 40% NaOH and 0.5 h reaction time
CSG40-1	CSG prepared with 40% NaOH and 1 h reaction time
CSG40-2	CSG prepared with 40% NaOH and 2 h reaction time
CSG60-1	CSG prepared with 60% NaOH and 1 h reaction time
DDA	degree of deacetylation
EA	elemental analysis
EDTA	ethylenediaminetetraacetic acid
FTIR-spectroscopy	Fourier-transfrom infrared spectroscopy
G	grammage [g/m^2]
IEP	isoelectric point
iGC	inverse gas chromatography
MWCO	molecular weight cut off
NC	nanocellulose
NF	nanofiltration
NMR-spectroscopy	nuclear magnetic resonance spectroscopy
RO	reverse osmosis
rpm	revolutions per minute
SEM	scanning electron microscopy
SSA	specific surface area
TEMPO	2,2,6,6-Tetramethylpiperidinyloxyl
TGA	thermogravimetric analysis
UF	ultrafiltration
Φ	porosity
$\rho_{envelope}$	envelope density/true density
$\rho_{skeletal}$	skeletal density

References

[1] S. Ahuja. *Water Challenges and Solutions on a Global Scale - Overview of Global Water Challenges and Solutions.* ACS Symposium Series, 1st edition. Americal Chemical Society, 2015. ISBN 9780841231061.

[2] WWAP (United Nations World Water Assessment Programme). *UN World Water Development Report, Wastewater: The Untapped Resource.* UNESCO, 2017.

[3] WHO. Drinking-water - fact sheet. *http://www.who.int/mediacentre/factsheets/fs391/en/*, accessed: 24/01/2018.

[4] C. Chartress and S. Varma. *Out of Water: From Abundance to Scarcity and How to Solve the World's Water Problems.* FT Press, Upper Saddle River, New Jersey, 2010. ISBN 0131367269.

[5] A. Pokharia and S.S. Ahluwalia. Isolation and screening of dye decolorizing bacterial isolates from contaminated sites. *Textiles and Light Industrial Science and Technology (TLIST)*, 2:54–61, 2013. doi: 10.1038/srep08716.

[6] V. Vaiano, G. Iervolino, L. Rizzo, and D. Sannino. Advanced oxidation processes for the removal of food dyes in wastewater. *Current Organic Chemistry*, 21:1068–1073, 2017. doi: 10.2174/1385272821666170102163307.

[7] Waterwise project. Causes of water pollution. *http://www.waterwise.co.za/site/water/environment/causes-of-water-pollution.html*, accessed: 22/12/2017.

[8] S.K. Nataraj, K.M. Hosamani, and T.M. Aminabhavi. Nanofiltration and reverse osmosis thin film composite membrane module for the removal of dye and salts from the simulated mixtures. *Desalination*, 249:12–17, 2009. doi: 10.1016/j.desal.2009.06.008.

[9] D. Zhou, L. Zhu, Y. Fu, M. Zhu, and L. Xue. Development of lower cost seawater desalination processes using nanofiltration technologies — a review. *Desalination*, 376: 109–116, 2015. doi: 10.1016/j.desal.2015.08.020.

[10] S. Ghizellaoui, A. Chibani, and S. Ghizellaoui. Use of nanofiltration for partial softening of very hard water. *Desalination*, 179:315–322, 2005. doi: 10.1016/j.desal.2004.11.077.

[11] N. Pagès, M. Reiga, O. Gilbert, and J.L. Cortina. Trace ions rejection tunning in nf by selecting solution composition: Ion permeances estimation. *Chemical Engineering Journal*, 308:126–134, 2017. doi: 10.1016/j.cej.2016.09.037.

[12] S.T. Muntha, A. Kausar, and M. Siddiq. Advances in polymeric nanofiltration membrane: A review. *Polymer-Plastics Technology and Engineering*, 56:841–856, 2016. doi: 10.1080/03602559.2016.1233562.

[13] R.R. Choudhury, Gohil J.M, Mohantya S., and Nayak S.K. Antifouling, fouling release and antimicrobial materials for surface modification of reverse osmosis and nanofiltration membranes. *Journal of Material Chemistry*, 6:313–333, 2018. doi: 10.1039/C7TA08627J.

[14] Y. Ji, W. Qian, Q. Yu, Y.and An, L. Liu, Y. Zhou, and C. Gao. Recent developments in nanofiltration membranes based on nanomaterials. *Chinese Journal of Chemical Engineering*, 25:1639–1652, 2017. doi: 10.1016/j.cjche.2017.04.014.

[15] T. Jesionowski et al. Removal of nickel(ii) and lead(ii) ions from aqueous solution using peat as a low-cost adsorbent: A kinetic and equilibrium study. *Arabian Journal of Chemistry*, article in press, 2015. doi: 10.1016/j.arabjc.2015.07.018.

[16] T.K. Naiya, A.K. Bhattacharya, and S.K. Das. Adsorption of cd(ii) and pb(ii) from aqueous solutions on activated alumina. *Journal of Colloid and Interface Science*, 333: 14–26, 2009. doi: 10.1016/j.jcis.2009.01.003.

[17] M. Jaishankar, T. Tseten, N. Anbalagan, B.B. Mathew, and K.N. Beeregowda. Toxicity, mechanism and health effects of some heavy metals. *Interdisciplinary Toxicology*, 7:60–72, 2014. doi: 10.2478/intox-2014-0009.

[18] R. Uauy, M. Olivares, and M. Gonzalez. Essentiality of copper in humans. *The American Journal of Clinical Nutrition*, 67:952–959, 1998. doi: 10.1093/ajcn/67.5.952S.

[19] S.N. Padrilah et al. Toxic effects of copper on liver and cholinesterase of clarias gariepinus. *Environmental Science and Pollution Research*, 24:22510–22523, 2017. doi: 10.2478/intox-2014-0009.

[20] M.A. Barakat. New trends in removing heavy metals from industrial wastewater. *Arabian Journal of Chemistry*, 4:361–377, 2011. doi: 10.1016/j.arabjc.2010.07.019.

[21] H.-J. Choi, S.-W. Yu, and K.H. Kim. Efficient use of mg-modified zeolite in the treatment of aqueous solution contaminated with heavy metal toxic ions. *Journal of the Taiwan Institute of Chemical Engineers*, 63:482–489, 2016. doi: 10.1016/j.jtice.2016.03.005.

[22] A.E. Burakov, E.V. Galunin, I.V. Burakova, S. Agarwal, A.G. Tkachev, and V.K. Gupta. Adsorption of heavy metals on conventional and nanostructured materials for wastewater treatment purposes: A review. *Ecotoxicology and Environmental Safety*, 148:702–712, 2018. doi: 10.1016/j.ecoenv.2017.11.034.

[23] T.S. Anirudhan and S.S. Sreekumari. Adsorptive removal of heavy metal ions from industrial effluents using activated carbon derived from waste coconut buttons. *Journal of Environmental Sciences*, 23:1989–1998, 2011. doi: 10.1016/S1001-0742(10)60515-3.

[24] N.K.E.M. Yahayaa, M.F.P.M. Latiffa, I. Abustana, and M.A. Ahmad. Effect of preparation conditions of activated carbon prepared from rice husk by zncl2 activation for removal of cu (ii) from aqueous solution. *International Journal of Engineering & Technology*, 10:28–32, 2010. doi: 10.1063/1.4965057.

[25] T. Karthikeyan, S. Rajgopal, and L.R. Miranda. Chromium (vi) adsorption from aqueous solution by hevea brasilinesis sawdust activated carbon. *Journal of Hazardous Materials*, 124:192–199, 2005. doi: 10.1016/j.jhazmat.2005.05.003.

[26] M. Ahmaruzzaman. Industrial wastes as low-cost potential adsorbents for the treatment of wastewater laden with heavy metals. *Advances in Colloid and Interface Science*, 166:36–599, 2011. doi: 10.1016/j.cis.2011.04.005.

[27] G.S. Dhillon, S. Kaur, S.J. Sarma, and S.K. Brar. Integrated process for fungal citric acid fermentation using apple processing wastes and sequential extraction of chitosan from waste stream. *Industrial Crops and Products*, 50:346–351, 2013. doi: 10.1016/j.indcrop.2013.08.010.

[28] M. Parmar and L.S. Thakur. Heavy metal cu, ni and zn: Toxicity, health hazards and their removal techniques by low cost adsorbents: A short overview. *International Journal of Plant, Animal and Environmental Sciences*, 3:143–157, 2013.

[29] I. Koyuncu, R. Sengur, T. Turken, S. Guclu, and M.E. Pasaoglu. *Advances in Membrane Technologies for Water Treatment - Advances in water treatment by microfiltration, ultrafiltration, and nanofiltration.* Woodhead Publishing Series in Energy. Elsevier Ltd, 2015. Sawston. ISBN 978-1-78242-121-4.

[30] A.G. Boricha and Z.V.P. Murthy. Preparation of n,o-carboxymethyl chitosan/cellulose acetate blend nanofiltration membrane and testing its performance in treating industrial wastewater. *Chemical Engineering Journal*, 157:293–400, 2010. doi: 10.1016/j.cej.2009.11.025.

[31] G. Metreveli, L. Wågberg, E. Emmoth, S. Belák, M. Strømme, and A. Mihranyan. A size-exclusion nanocellulose filter paper for virus removal. *Advanced Healthcare Materials*, 3:1546–1550, 2014. doi: 10.1002/adhm.201300641.

[32] A. Mautner, K.-Y. Lee, P. Lahtinen, T. Tammelin, K. Li, and A. Bismarck. Nanopapers for organic solvent nanofiltration. *Chemical Communications*, 50:5778–5781, 2014. doi: 10.1039/C4CC00467A.

[33] S. Mondal. Preparation, properties and applications of nanocellulosic materials. *Carbohydrate Polymers*, 163:301–316, 2017. doi: 10.1016/j.carbpol.2016.12.050.

[34] A. Mautner, K.-Y. Lee, T. Tammelin, A.P. Mathew, A.J. Nedoma, K. Lie, and A. Bismarck. Cellulose nanopapers as tight aqueous ultra-filtration membranes. *Reactive and Functional Polymers*, 86:209–214, 2015. doi: 10.1016/j.reactfunctpolym.2014.09.014.

[35] H. Voisin, L. Bergström, P. Liu, and A.P. Mathew. Nanocellulose-based materials for water purification. *Nanomaterials (Basel)*, 7:57, 2017. doi: 10.3390/nano7030057.

[36] N. Yousefi. Chitin membranes for water purification, Master thesis, University of Vienna, 2017.

[37] I. Tsigos, A. Martinou, D. Kafetzopoulos, and V. Bouriotis. Chitin deacetylases: new, versatile tools in biotechnology. *Trends in Biotechnology*, 18:305–312, 2000. doi: 10.1016/S0167-7799(00)01462-1.

[38] X. Shen, J.L. Shamshina, P. Berton, G. Gurau, and R.D. Rogers. Hydrogels based on cellulose and chitin: fabrication, properties, and applications. *Green Chem.*, 18:53–75, 2016. doi: 10.1039/C5GC02396C.

[39] Cellulose_sessel. *https://upload.wikimedia.org/wikipedia/commons/0/07/ Cellulose_Sessel.svg*, accessed: 05/12/2017.

[40] Chitin. *https://upload.wikimedia.org/wikipedia/commons/1/13/Chitin. svg*, accessed: 05/12/2017.

[41] F. Khoushab and M. Yamabhai. Chitin research revisited. *Marine Drugs*, 8:1988–2012, 2010. doi: 10.3390/md8071988.

[42] P. Sikorski, R. Hori, and M. Wada. Revisit of -chitin crystal structure using high resolution x-ray diffraction data. *Biomacromolecules*, 10:1100–1105, 2009. doi: 10.1021/bm801251e.

[43] I. Hamed, F. Özogul, and J.M. Regenstein. Industrial applications of crustacean by-products (chitin, chitosan, and chitooligosaccharides): A review. *Trends in Food Science Technology*, 48:40–50, 2016. doi: 10.1016/j.tifs.2015.11.007.

[44] Muzzarelli R. *Chitin - Chitin Nanostructures in Living Organisms.* Geobiology book series. Springer, Dordrecht. 2010.

[45] I. Younes and Rinaudo M. Chitin and chitosan preparation from marine sources. structure, properties and applications. *Marine Drugs*, 13:1133–1174, 2015. doi: 10.3390/md13031133.

[46] I. Younes and Rinaudo M. Studies on extraction methods of chitin from crab shell and investigation of its mechanical properties. *Marine Drugs*, 8:220–231, 2017.

[47] A. Bhatnagar and M. Sillanpää. Applications of chitin- and chitosan-derivatives for the detoxification of wate and wastewater — a short review. *Advances in Colloid and Interface Science*, 152:26–38, 2009. doi: 10.1016/j.cis.2009.09.003.

[48] C.M. Stagg and S. Feather. The characterization of a chitin-associated d-glucan from the cell walls of aspergillus niger. *Biochimica et Biophysica Acta (BBA) - General Subjects*, 320:64–72, 1973. doi: 10.1016/0304-4165(73)90166-9.

[49] K. Beran, Z. Holan, and J. Baldrian. he chitin-glucan complex in saccharomyces cerevisiae. ir and x-ray observations. *Folia Microbiologica*, 17:322–30, 1972.

[50] J.H. Sietsma and J.G.H. Wessels. Solubility of (1-3)--d/(1-6)--d-glucan in fungal walls: Importance of presumed linkage between glucan and chitin. *Microbiology*, 125:209–212, 1973. doi: 10.1099/00221287-125-1-209.

[51] S. Ifuku, R. Nomura, M. Morimoto, and H. Saimoto. Preparation of chitin nanofibers from mushrooms. *Materials (Basel)*, 4:1417–1425, 2011. doi: 10.3390/ma4081417.

[52] A. Beauvais, T. Fontaine, V. Aimani, and J.-P. Latgé. Aspergillus cell wall and biofilm. *Mycopathologia*, 178:371–377, 2014. doi: 10.1007/s11046-014-9766-0.

[53] J.H. Sietsma and J.G.H. Wessels. Evidence for covalent linkages between chitin and beta-glucan in fungal wall. *Journal of General Microbiology*, 114:99–108, 1979.

[54] J.P. Latgé. The cell wall: a carbohydrate armour for the fungal cell. *Molecular Microbiology*, 66:279–290, 2007.

[55] β-1,3-glucan. *https://upload.wikimedia.org/wikipedia/commons/6/62/Curdlan_haworth.png*, accessed: 03/02/2018.

[56] R. Kollár et al. Architecture of the yeast cell wall (1-6)-glucan interconnects mannoprotein, (1-3)-glucan, and chitin. *Journal of Biological Chemistry*, pages 17762–17775, 1997. doi: 10.1074/jbc.272.28.17762.

[57] M.W.F.W. Nawawi. *Renewable chitin based nanomaterials from fungi.* PhD thesis, Imerial College London. 2016.

[58] I. Farinha, P. Duarte, A. Pimentel, E. Plotnikova, B. Chagas, L. Mafra, C. Grandfils, F. Freitas, E. Fortunato, and M.A.M. Reis. Chitin–glucan complex production by komagataella pastoris: Downstream optimization and product characterization. *Carbohydrate Polymers*, 130:455–464, 2015. doi: 10.1016/j.carbpol.2015.05.034.

[59] S. Gautier, E. Xhauflaire-Uhoda, and GE. Piérard. Chitin-glucan, a natural cell scaffold for skin moisturization and rejuvenation. *International Journal of Cosmetic Science*, 30:459–69, 2008. doi: 10.1111/j.1468-2494.2008.00470.x.

[60] A. Percot, C. Viton, and A. Domard. Optimization of chitin extraction from shrimp shells. *Biomacromolecules*, 4:12–18, 2003. doi: 10.1021/bm025602k.

[61] A. Bornet and P.L. Teissedre. Chitosan, chitin-glucan and chitin effects on minerals (iron, lead, cadmium) and organic (ochratoxin a) contaminants in wines. *European Food Research and Technology*, 226:681–689, 2008. doi: 10.1007/s00217-007-0577-0.

[62] Y.A. Skorik, A.V. Pestov, and Y.G. Yatluk. Evaluation of various chitin-glucan derivatives from aspergillus niger as transition metal adsorbents. *Bioresource Technology*, 101:1769–1775, 2010. doi: 10.1016/j.biortech.2009.10.033.

[63] Z.M. dos Santos, A.L.P.F. Caroni, M.R. Pereira, D.R. da Silva, and J.L.C. Fonseca. Determination of deacetylation degree of chitosan: a comparison between conductometric titration and chn elemental analysis. *Carbohydrate Research*, 344:145–156, 2009. doi: 10.1016/j.carres.2009.08.030.

[64] M. Rinaudo. Chitin and chitosan: Properties and applications. *Progress in Polymer Science*, 31:603–632, 2006. doi: 10.1016/j.progpolymsci.2006.06.001.

[65] Wikipedia. Chitosan. *https://de.wikipedia.org/wiki/Chitosan*, accessed: 05/12/2017.

[66] F. Heidari, M. Razavi, M.E. Bahrololoom, M. Tahriri, M. Rasoulianboroujeni, H. Koturi, and L. Tayebi. Preparation of natural chitosan from shrimp shell with different deacetylation degree. *Materials Research Innovations*, 44:1–5, 2016. doi: 10.1080/14328917.2016.1271591.

[67] S. Kumari and P.K. Rath. Extraction and characterization of chitin and chitosan from (labeo rohit) fish scales. *Procedia Materials Science*, pages 482–489, 2014. doi: 10.1016/j.mspro.2014.07.062.

[68] M.-W. Kim et al. Production of chitin and chitosan from the exoskeleton of adult two-spotted field crickets (gryllus bimaculatus). *Entomological Research*, 47:279–28, 2017. doi: 10.1111/1748-5967.12239.

[69] A Muxika, A. Etxabide, J. Uranga, P. Guerrero, and K. de la Caba. Chitosan as a bioactive polymer: Processing, properties and applications. *International Journal of Biological Macromolecules*, 105:1358–1368, 2017. doi: 10.1016/j.ijbiomac.2017.07.087.

[70] P.R. Sivashankari and M. Prabaharan. *Chitosan Based Biomaterials Volume 1: 5 - Deacetylation modification techniques of chitin and chitosan.* Woodhead Publishing, Amsterdam, Netherlands, 2017. ISBN 978-0-08-100230-8.

[71] P. Methacanona, M. Prasitsilp, T. Pothsreea, and J. Pattaraarchachai. Heterogeneous n-deacetylation of squid chitin in alkaline solution. *Carbohydrate Polymers*, 52:119–123, 2003. doi: 10.1016/S0144-8617(02)00300-4.

[72] A.M. Abdel-Mohsen, J. Jancar, D. Massoud, Z. Fohlerova, H. Elhadidy, Z. Spotz, and A. Hebeish. Novel chitin/chitosan-glucan wound dressing: Isolation, characteri-

zation, antibacterial activity and wound healing properties. *International Journal of Pharmaceutics*, 510:86–99, 2016. doi: 10.1016/j.ijpharm.2016.06.003.

[73] D Tahtat, C. Uzun, M. Mahlous, and O. Güven. Beneficial effect of gamma irradiation on the n-deacetylation of chitin to form chitosan. *Nuclear Instruments and Methods in Physics Research Section B: Beam Interactions with Materials and Atoms*, 265: 425–428, 2007. doi: 10.1016/j.nimb.2007.09.016.

[74] T. Lertwattanaseri, N. Ichikawa, T. Mizoguchi, Y. Tanaka, and S. Chirachanchai. Microwave technique for efficient deacetylation of chitin nanowhiskers to a chitosan nanoscaffold. *Current Organic Chemistry*, 344:331–335, 2009. doi: 10.1016/j.carres.2008.10.018.

[75] S.N. Hamer, S. Cord-Landwehr, X. Biarnés, A. Planas, H. Waegeman, B.M. Moerschbacher, and S. Kolkenbrock. Enzymatic production of defined chitosan oligomers with a specific pattern of acetylation using a combination of chitin oligosaccharide deacetylases. *Scientific Reports*, 5:1–9, 2015. doi: 10.1038/srep08716.

[76] M. Pogorielov, A. Kravtsova, and G. Reilly et al. Experimental evaluation of new chitin–chitosan graft for duraplasty. *Journal of Materials Science: Materials in Medicine*, 28:12–18, 2017. doi: 10.1007/s10856-017-5845-3.

[77] S.K. Samal. Cationic polymers and their therapeutic potential. *Chemical Society Reviews*, 41:7147–7194, 2012. doi: 10.1039/c2cs35094g.

[78] J.M. Chupa, A.M. Foster, S.R. Sumner, S.V. Madihally, and H.W. Matthew. Vascular cell responses to polysaccharide materials: in vitro and in vivo evaluations. *Biomaterials*, 21:2315–2322, 2000. doi: 10.1016/S0142-9612(00)00158-7.

[79] K. Tomihata and Y. Ikada. In vitro and in vivo degradation of films of chitin and its deacetylated derivatives. *Biomaterials*, 18:567–75, 1997.

[80] J. Venkatesan, S. Anil, K. Se-Kwon, and M.S. Shima. Chitosan as a vehicle for growth factor delivery: Various preparations and their applications in bone tissue regeneration. *International Journal of Biological Macromolecules*, 104:1383–1397, 2017. doi: 10.1016/j.ijbiomac.2017.01.072.

[81] T.M. Crizel, A. de Oliveira Rios, V.D. Alves, N. Bandarra, S.H. Moldão-Martins, and Flôres. Active food packaging prepared with chitosan and olive pomace. *Food Hydrocolloids*, 74:139–150, 2018. doi: 10.1016/j.foodhyd.2017.08.007.

[82] M. Guo, M.P. Yadav, and T.Z. Jin. Antimicrobial edible coatings and films from microemulsions and their food applications. *International Journal of Food Microbiology*, 263: 9–16, 2017. doi: 10.1016/j.ijfoodmicro.2017.10.002.

[83] M. Aider. Chitosan application for active bio-based films production and potential in the food industry: Review. *LWT - Food Science and Technology*, 43:837–842, 2010. doi: 10.1016/j.lwt.2010.01.021.

[84] B.W.S. Souza, M.A. Cerqueira, J.T. Martins, A. Casariego, J.A. Teixeira, and A. Vicente. Influence of electric fields on the structure of chitosan edible coatings. *Food Hydrocolloids*, 24:330–335, 2010. doi: 10.1016/j.foodhyd.2009.10.011.

[85] B.W.S. Souza, M.A. Cerqueira, A. Casariego, A.M.P. Lima, J.A. Teixeira, and A.A. Vicente. Effect of moderate electric fields in the permeation properties of chitosan coatings. *Food Hydrocolloids*, 23:2110–2115, 2009. doi: 10.1016/j.foodhyd.2009.03.021.

[86] H. Liu, J. Du, X. Wang, and L. Sun. Chitosan kills bacteria through cell membrane damage. *International Journal of Food Microbiology*, 95:147–155, 2004. doi: 10.1016/j.ijfoodmicro.2004.01.022.

[87] I.M. Helander, E.-L. Nurmiaho-Lassila, R. Ahvenainen, J. Rhoades, and S. Roller. Chitosan disrupts the barrier properties of the outer membrane of gram-negative bacteria. *International Journal of Food Microbiology*, 71:235–244, 2001. doi: 10.1016/S0168-1605(01)00609-2.

[88] S. Babel and T.A. Kurniawan. Low-cost adsorbents for heavy metals uptake from contaminated water: a review. *Journal of Hazardous Materials*, 97:219–243, 2003. doi: 10.1016/S0304-3894(02)00263-7.

[89] M.N.V.R. Kumar. A review of chitin and chitosan applications. *Reactive and Functional Polymers*, 46:1–27, 2000. doi: 10.1016/S1381-5148(00)00038-9.

[90] E. Guibal. Separation and purification technology interactions of metal ions with chitosan-based sorbents: a review. *Separation and Purification Technology*, 38:43–74, 2004. doi: 10.1016/j.seppur.2003.10.004.

[91] A.J. Varma, S.V. Deshpande, A.J. Varma, and J.F. Kennedy. Metal complexation by chitosan and its derivatives: a review. *Carbohydrate Polymers*, 55:77–93, 2004. doi: 10.1016/j.carbpol.2003.08.005.

[92] G. Crini and P.M. Badot. Application of chitosan, a natural aminopolysaccharide, for dye removal from aqueous solutions by adsorption processes using batch studies: A review of recent literature. *Progress in Polymer Science*, 33:399–447, 2008. doi: 10.1016/j.progpolymsci.2007.11.001.

[93] S.T. Lee, F.-L. Mi, Y.J. Shen, and S.S. Shyu. Equilibrium and kinetic studies of copper(ii) ion uptake by chitosan-tripolyphosphate chelating resin. *Polymer*, 42:1879–1892, 2001. doi: 10.1016/S0032-3861(00)00402-X.

[94] J. Wang and C. Chen. Chitosan-based biosorbents: Modification and application for biosorption of heavy metals and radionuclides. *Bioresource Technology*, 160:129–141, 2014. doi: 10.1016/j.biortech.2013.12.110.

[95] R. Schmuhl, H.M. Krieg, and K. Keizer. Adsorption of cu(ii) and cr(vi) ions by chitosan: Kinetics and equilibrium studies. *Water SA*, 27:1–8, 2001.

[96] N. Prakash and S.A. Vendan. Biodegradable polymer based ternary blends for removal of trace metals from simulated industrial wastewater. *International Journal of Biological Macromolecules*, 83:198–208, 2016. doi: 10.1016/j.ijbiomac.2015.09.050.

[97] S. Haider and S.-Y. Park. Preparation of the electrospun chitosan nanofibers and their applications to the adsorption of cu(ii) and pb(ii) ions from an aqueous solution. *Journal of Membrane Science*, 328:90–96, 2009. doi: 10.1016/j.memsci.2008.11.046.

[98] M.M. Rao, A. Ramesh, G.P.C. Rao, and K. Seshaiah. Removal of copper and cadmium from the aqueous solutions by activated carbon derived from ceiba pentandra hulls. *Journal of Hazardous Materials*, 129:123–129, 2006. doi: 10.1016/j.jhazmat.2005.08.018.

[99] S.M. Lee and A.P. Davis. Removal of cu(ii) and cd(ii) from aqueous solution by seafood processing waste sludge. *Water Research*, 35:534–540, 2001. doi: 10.1016/S0043-1354(00)00284-0.

[100] S. Yu, Y. Ai, X. Wang, Y. Liang, Y. Ji, J. Li, T. Hayat, A. Alsaedi, and X. Wang. Spectroscopic and theoretical studies on the counterion effect of cu(ii) ion and graphene oxide interaction with titanium dioxide. *Environmental Science: Nano*, 3:1361–1368, 2016. doi: 10.1039/C6EN00297H.

[101] S.A. Al-Saydeha, M.H. El-Naas, and S.J. Zaidi. Copper removal from industrial wastewater: A comprehensive review. *Journal of Industrial and Engineering Chemistry*, 56:35–44, 2017. doi: 10.1016/j.jiec.2017.07.026.

[102] E. Onsosyen and O. Skaugrud. Metal recovery using chitosan. *Journal of Chemical Technology and Biotechnology*, 49:395–404, 1990. doi: 10.1002/jctb.280490410.

[103] M. Rhazi, J. Desbrières, A. Tolaimate, M. Rinaudo, P. Vottero, and A. Alagui. Contribution to the study of the complexation of copper by chitosan and oligomers. *Polymer*, 43:1267–1276, 2002. doi: 10.1016/S0032-3861(01)00685-1.

[104] J. Desbrières and E. Guibal. Chitosan for wastewater treatment. *Polymer International.*, 67:7–14, 2017. doi: 10.1002/pi.5464.

[105] R.P. Srinivasa, Y. Vijaya, V.M. Boddu, and K. Abburi. Adsorptive removal of copper and nickel ions from water using chitosan coated pvc beads. *Bioresource Technology*, 100:194–199, 2009. doi: 10.1016/j.biortech.2008.05.041.

[106] W.S. Wan Ngah and S. Fatinathan. Adsorption of cu(ii) ions in aqueous solution using chitosan beads, chitosan–gla beads and chitosan–alginate beads. *Chemical Engineering Journal*, 143:62–72, 2008. doi: 10.1016/j.cej.2007.12-006.

[107] F.-L. Mi, S.J. Wu, and F.M. Lin. Adsorption of copper(ii) ions by a chitosan–oxalate complex biosorbent. *International Journal of Biological Macromolecules*, 72:136–144, 2015. doi: 10.1016/j.ijbiomac.2014.08.006.

[108] W.S Wan Ngah, A. Kamari, and Y.J. Koay. Equilibrium and kinetics studies of adsorption of copper (ii) on chitosan and chitosan/pva beads. *International Journal of Biological Macromolecules*, 34:155–161, 2004. doi: 10.1016/j.ijbiomac.2004.03.001.

[109] F. Shahidi, J.K.V. Arachchi, and Y.-J. Jeon. Food applications of chitin and chitosans. *Trends in Food Science Technology*, 10:37–51, 1999. doi: 10.1016/S0924-2244(99)00017-5.

[110] T.K. Varun, S. Senani, N. Jayapal, J. Chikkerur, S. Roy, V.B. Tekulapally, M. Gautam, and N. Kumar. Extraction of chitosan and its oligomers from shrimp shell waste, their characterization and antimicrobial effect. *Veterinary World*, 10:170–175, 2017. doi: 10.14202/vetworld.2017.170-175.

[111] S. Kheirandish, M. Ghaedi, K. Dashtian, F. Heidari, F. Pourebrahim, and S. Wang. Chitosan extraction from lobster shells and its grafted with functionalized mwcnt for simultaneous removal of pb2+ ions and eriochrome cyanine r dye after their complexation. *International Journal of Biological Macromolecules*, 102:181–191, 2017. doi: 10.1016/j.ijbiomac.2017.03.035.

[112] W.S. Wan Ngah, C.S. Endud, and R. Mayanar. Removal of copper(ii) ions from aqueous solution onto chitosan and cross-linked chitosan beads. *Reactive and Functional Polymers*, 50:181–190, 2002. doi: 10.1016/S1381-5148(01)00113-4.

[113] M. Vakili, M. Rafatullah, B. Salamatinia, A.Z. Abdullah, M.H. Ibrahim, K.B. Tan, Z. Gholami, and P. Amouzgar. Application of chitosan and its derivatives as adsorbents for dye removal from water and wastewater: A review. *Carbohydrate Polymers*, 113: 115–130, 2014. doi: 10.1016/j.carbpol.2014.07.007.

[114] W.S.W. Ngah, C.S. Endud, and R. Mayanar. Removal of copper(ii) ions from aqueous solution onto chitosan and cross-linked chitosan beads. *Reactive and Functional Polymers*, 50:181–190, 2002. doi: 10.1016/S1381-5148(01)00113-4.

[115] K.M. Abdel-Gawad, A.F. Hifney, M.A. Fawzy, and M. Gomaa. Technology optimization of chitosan production from aspergillus niger biomass and its functional activities. *Food Hydrocolloids*, 63:593–601, 2017. doi: 10.1016/j.foodhyd.2016.10.001.

[116] T. Wu, S. Zivanovic, A. Draughon, W.S. Conway, and C.E. Sams. Physicochemical properties and bioactivity of fungal chitin and chitosan. *J. Agric. Food Chem.*, 53: 3888–3894, 2005. doi: 10.1021/jf048202s.

[117] R.H. Perry and D. Green. *Perry's Chemical Engineers' Handbook, 6th Edition.* McGraw-Hill Book Co, 1985.

[118] Filomena Freitas and Christophe Roca. *Handbook of Polymers for Pharmaceutical Technologies: Biodegradable Polymers, Volume 3 - 3. Fungi as Sources of Polysaccharides for Pharmaceutical and Biomedical Applications.* Hoboken, New Jersey, Scrivener Publishing, 2015. ISBN 9781119041429.

[119] G. Cárdenas, G. Cabrera, E. Taboada, and S.P. Miranda. Chitin characterization by sem, ftir, xrd, and 13c cross polarization/mass angle spinning nmr. *Journal of Applied Polymer Science*, 93:1876–1885, 2004. doi: DOI 10.1002/app.20647.

[120] C. Roca, B. Chagasa, I. Farinhaa, F. Freitas, L Mafra, F. Aguiar, R. Oliveira, and M.A.M Reis. Production of yeast chitin–glucan complex from biodiesel industry byproduct. *Process Biochemistry*, 47:1670–1675, 2012. doi: 10.1016/j.procbio.2012.04.004.

[121] L. Heux, J. Brugnerotto, J. Desbrières, M.F. Versali, and M. Rinaudo. Solid state nmr for determination of degree of acetylation of chitin and chitosan. *Biomacromolecules*, 1:746–751, 2000. doi: 10.1021/bm000070y.

[122] A.K. Dutta, N. Kawamoto, G. Sugino, H. Izawa, M. Morimoto, H. Saimoto, and S. Ifuku. Simple preparation of chitosan nanofibers from dry chitosan powder by the star burst system. *Carbohydrate Polymers*, 97:363–367, 2013. doi: 10.1016/j.carbpol.2013.05.010.

[123] H.-S. Tsai and Y.-Z. Wang. Properties of hydrophilic chitosan network membranes by introducing binary crosslink agents. *Polymer Bulletin*, 60:103–113, 2008. doi: 10.1007/s00289-007-0846-x.

[124] M.F. Cervera, J. Heinämäki, M. Räsänen, S.L. Maunu, M. Karjalainen, O.M.N. Acosta, A.I. Colarte, and J. Yliruusi. Solid-state characterization of chitosans derived from lobster chitin. *Carbohydrate Polymers*, 58:401–408, 2004. doi: 10.1016/j.carbpol.2004.08.017.

[125] M. Henriksson, L.A. Berglund, P. Isaksson, T. Lindström, and T. Nishino. Cellulose nanopaper structures of high toughness. *Biomacromolecules*, 9:1579–1585, 2008. doi: 10.1021/bm800038n.

[126] P.K. Dutta, J. Dutta, and V.S. Tripathi. Chitin and chitosan: Chemistry, properties and applications. *Journal of Scientific Industrial Research*, 63, 2004. doi: 10.1016/j.progpolymsci.2006.06.001.

[127] Andreas F. von Recum. *Handbook of Biomaterials Evaluation. Scientific, Technical, and Clinical Testing of Implant Materials.* MacMillan, New York, 1998. ISBN 1-56032-479-1.

[128] K. Boussu. *Influence of Membrane Characteristics on Flux Decline and Retention in Nanofiltration.* PhD thesis, Katholieke Universiteit Leuven, 2007.

[129] J.W. Parl and K.H. Choi. Acid-base equilibria and related properties of chitosan. *Bulletin of Korean Chemical Society*, 4:68–72, 1983.

[130] M.C. Sobieraj and C.M. Rimnac. Ultra high molecular weight polyethylene: Mechanics, morphology, and clinical behavior. *Journal of the Mechanical Behavior of Biomedical Materials*, 2:433–443, 2008. doi: 10.1016/j.jmbbm.2008.12.006.

[131] S. Rivero, M.A. García, and A. Pinotti. Crosslinking capacity of tannic acid in plasticized chitosan films. *Carbohydrate Polymers*, 82:270–276, 2010. doi: 10.1016/j.carbpol.2010.04.048.

[132] J.T. Martins, M.A. Cerqueira, and A.A. Vicente. Influence of -tocopherol on physicochemical properties of chitosan-based films. *Food Hydrocolloids*, 27:220–227, 2012. doi: 10.1016/j.foodhyd.2011.06.011.

[133] P.-Z. Hong, S.D. Li, C.Y. Ou, C.P. Li, L. Yang, and C.H. Zhang. Thermogravimetric analysis of chitosan. *Journal of Applied Polymer Science*, 105:547–551, 2007. doi: 10.1002/app.25920.

[134] D. Stawski, S. Rabiej, L. Herczynska, and Z. Draczynski. Thermogravimetric analysis of chitins of different origin. *Journal of Thermal Analysis and Calorimetry*, 93:489–494, 2008. doi: 10.1007/s10973-007-8691-6.

[135] J.R. Evans, W.G. Davids, J.D. MacRae, and A. Amirbahman. Kinetics of cadmium uptake by chitosan-based crab shells aria. *Water Research*, 36:3219–3226, 2002. doi: 10.1016/S0043-1354(02)00044-1.

[136] A.S. Özcan, B. Erdem, and A. Özcan. Adsorption of acid blue 193 from aqueous solutions onto na–bentonite and dtma–bentonite. *Journal of Colloid and Interface Science*, 280:44–54, 2004. doi: 10.1016/j.jcis.2004.07.035.

[137] E.C. Dillon Jr, J.H. Wilton, J.C. Barlow, and W.A. Watson. Large surface area activated charcoal and the inhibition of aspirin absorption. *Annals of Emergency Medicine*, 18:547–552, 1989. doi: http://dx.10.1016/S0196-0644(89)80841-8.

[138] S. Wang, Y. Boyjoo, A. Choueib, and Z.H. Zhu. Removal of dyes from aqueous solution using fly ash and red mud. *Water Research*, 39:129–138, 2005. doi: 10.1016/j.watres.2004.09.011.

[139] M. Holzmann. *BSc. thesis, Institut für Materialchemie und Forschung, Universität Wien*, 2018.

[140] A. Ghaee, M. Shariaty-Niassar, J. Barzin, and T. Matsuura. Effects of chitosan membrane morphology on copper ion adsorption. *Chemical Engineering Journal*, 165:46–55, 2010. doi: 10.1016/j.cej.2010.08.051.

[141] W. Qin, J. Li, J. Tu, H. Yang, Q. Chen, and H. Liu. Fabrication of porous chitosan membranes composed of nanofibers by low temperature thermally induced phase separation, and their adsorption behavior for cu2+. *Carbohydrate Polymers*, 178:338–346, 2017. doi: 10.1016/j.carbpol.2017.09.051.

[142] Y. Yang, S. Zhao, C. Song, and M. Gao. The adsorption of cu2+ onto chitosan-aluminium oxide composite material. *Advanced Materials Research*, 1015:643–646, 2014. doi: 10.4028/www.scientific.net/AMR.1015.643.

[143] A. Mautner, K.-Y. Lee, K. Li, and A. Bismarck. Designing the porosity of bacterial cellulose nanopapers. *Abstracts of Papers, 249th ACS National Meeting & Exposition, Denver, CO, United States*, 2015.

7 Appendix

7.1 Abstract

Chitin is the second most abundant renewable macromolecule on the planet after cellulose. In contrast to that it is still an underused biomass. Chitosan, which can easily be obtained from chitin by deacetylation, has outstanding chelation properties and is one of the most promising molecules for the removal of heavy metal ions from wastewater. Here I present the production of a chitosan-based ultrafiltration membrane from mushrooms, that also shows high affinity for Cu(II) ions.

A chitin-glucan complex (CG) was extracted from *Agaricus bisporus*, the common mushroom, by mild alkaline treatment. The obtained suspension was stirred at 100°C in a NaOH-solution at concentrations of 20%, 40% and 60% (w/v) (CSG20, CSG40, CSG60, respectively). The obtained chitosan-glucan complex (CSG) was characterised by elemental analysis, Fourier-transform infrared spectroscopy, solid state ^{13}C-NMR-spectroscopy and thermogravimetric analysis. From this material, nanopapers were prepared by pressing for 3 h at 120°C under a 5 kg weight in an oven. The mechanical properties, the ζ-potential as well as the permeance for water and the adsorption capacity for Cu(II) ions were determined. Furthermore, the nanopapers were tested for their ability to reject gold nanoparticles from water to demonstrate feasibility for the removal of viruses.

It was shown that longer reaction times and higher NaOH concentrations did both have a positive effect on the nitrogen content of the sample, suggesting a successful deacetylation. However, tensile strength and Young's modulus of nanopapers did decrease if harsher deacetylation conditions were applied. SEM-Imaging showed a nanostructured surface with fibril diameters ranging from 13 to 17 nm. The isoelectric point (IEP) of CSG20 nanopapers as determined by streaming potential measurements was at pH 3.8 and thus slightly higher than the IEP of CG nanopapers, which was at pH 3.1. The IEP of CSG40-papers was found at pH 5.5 for 1 h and pH 5.2 for 2 h reaction time in NaOH-solution, respectively, and was therefore close to the pKa of chitosan's amino group (6.2), demonstrating successful deacetylation. The permeance of nanopapers was determined in a dead end cell, whereby values of up to 4 $L/(h \cdot m^2 \cdot MPa)$ were reached. Continuous adsorption measurements showed a maximum adsorption capacity of 18 mg/g, 555 mg/g and 1687 mg/g for CG nanopapers, CSG20 nanopapers and CSG40 nanopapers, respectively. This demonstrated that CSG had much higher affinity to Cu(II) than CG. Gold nanoparticles of 10 nm in diameter were completely rejected by the membranes, demonstrating their applicability for ultrafiltration.

7.2 Zusammenfassung

Nach Cellulose ist Chitin ist das zweithäufigste Biopolymer. Im Gegensatz zur enormen Menge dieser Biomasse stehen die vergleichsweise geringen Einsatzgebiete. Chitosan, das aus Chitin durch einen einfachen Deacetylierungsschritt erhalten wird, ist aufgrund seiner ausgezeichneten Chelationseigenschaften eines der vielversprechendsten Materialien um Wasser von Schwermetallionen zu reinigen. In dieser Arbeit präsentiere ich die Herstellung von Nanopapieren, hergestellt aus Chitosan auf Basis von Pilzextrakten.

Aus *Agaricus bisporus* (Champignon) wurde durch basische Extraktion ein Chitin-Glucan-Komplex (CG) gewonnen. Die erhaltene Suspension wurde bei 100°C mit 20% (CSG20), 40% (CSG40) oder 60% (CSG60) NaOH reagiert. Der gewonnene Chitosan-Glucan-Komplex (CSG) wurde mittels Elementaranalyse, Fourier-Transform- Infrarotspektroskopie, Festphasen-^{13}C-NMR-Spektroskopie und Thermogravimetrie charakterisiert. Aus diesem Material wurden über 3 h bei 120°C unter einem Gewicht von 5 kg Papiere gepresst. Die mechanischen Eigenschaften, das ζ-Potential, die Permeanz für Wasser und die Adsorptionskapazität für Cu(II)-Ionen wurden gemessen. Außerdem wurden Gold-Nanopartikel (10 nm Durchmesser) filtriert, um die Anwendbarkeit als Membran zur Virus-Filtration zu demonstrieren.

Die Elementaranalyse zeigte, dass längere Reaktionszeiten und höhere NaOH- Konzentrationen zu einer allgemeinen Erhöhung des Stickstoffanteils führten, was als Zeichen für die erfolgreiche Durchführung der Deacetylierungsreaktion interpretiert wird. Die maximale Zugfestigkeit von Papieren nahm mit höherer NaOH-Konzentration und längeren Reaktionszeiten ab. SEM-Bilder zeigten eine nanostrukturierte Oberfläche mit Fibrillen von 13 bis 17 nm Durchmesser. Der isoelektrische Punkt (IEP) von CSG40-Papieren lag bei pH 5.5 (1 h Reaktionszeit) und pH 5.2 (2 h Reaktionszeit) und damit nahe am pKa von Chitosans Aminogruppe (6.2). Der IEP von CSG20 Papieren (3.8) ähnelte hingegen eher dem IEP von CG (3.1), was die Deacetylierung in Abhängigkeit von NaOH-Konzentration und Deacetylierungsdauer unterstreicht. Die Permeanz von H_2O erreichte Werte bis zu 4 $L/(h \cdot m^2 \cdot MPa)$. Die maximale Adsorption von Cu(II)-Ionen auf Papieren lag bei 18 mg/g (CG), 555 mg/g (CSG20) und 1687 mg/g (CSG40), was beweist, dass CSG eine viel stärkere Affinität zu Cu(II)-Ionen aufweist als CG. Des weiteren konnten Gold-Nanopartikel von 10 nm Durchmesser zu 100% von den Membranen gefiltert werden, was die Möglichkeit zur Filtration von Viren demonstriert.

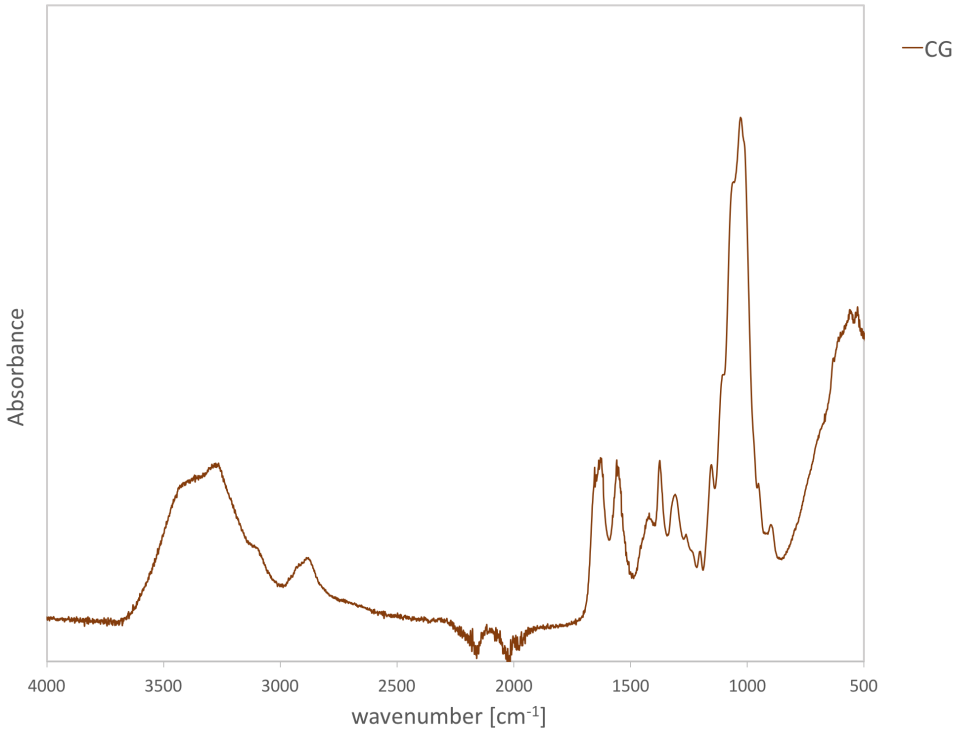

Figure 36: FTIR spectrum of CG

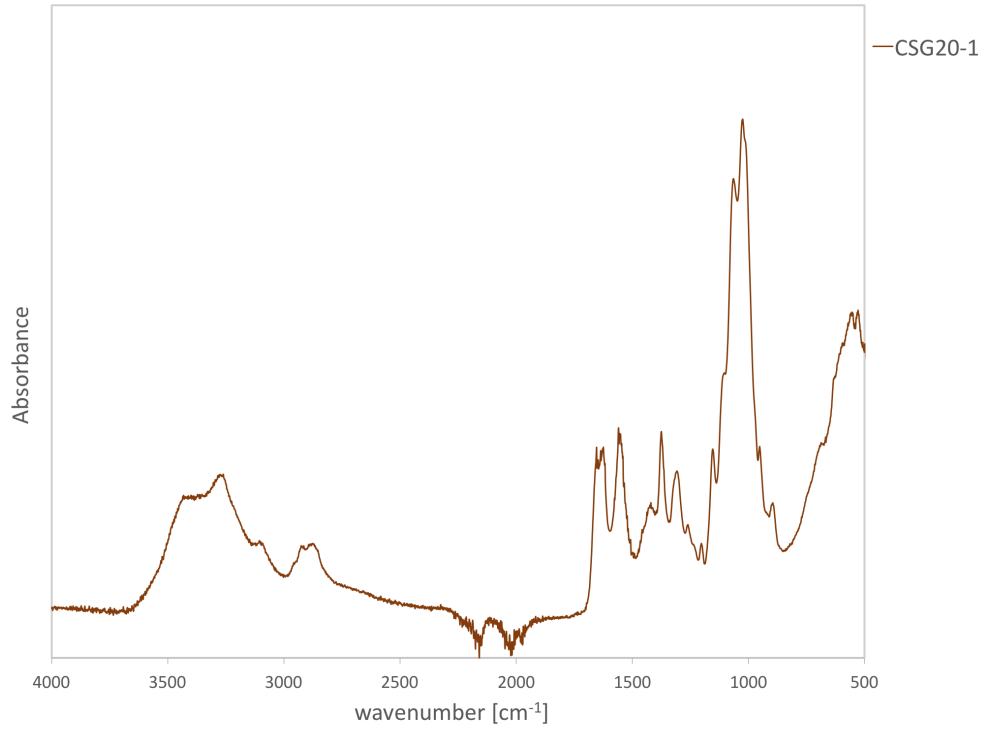

Figure 37: FTIR spectrum of CSG20-1

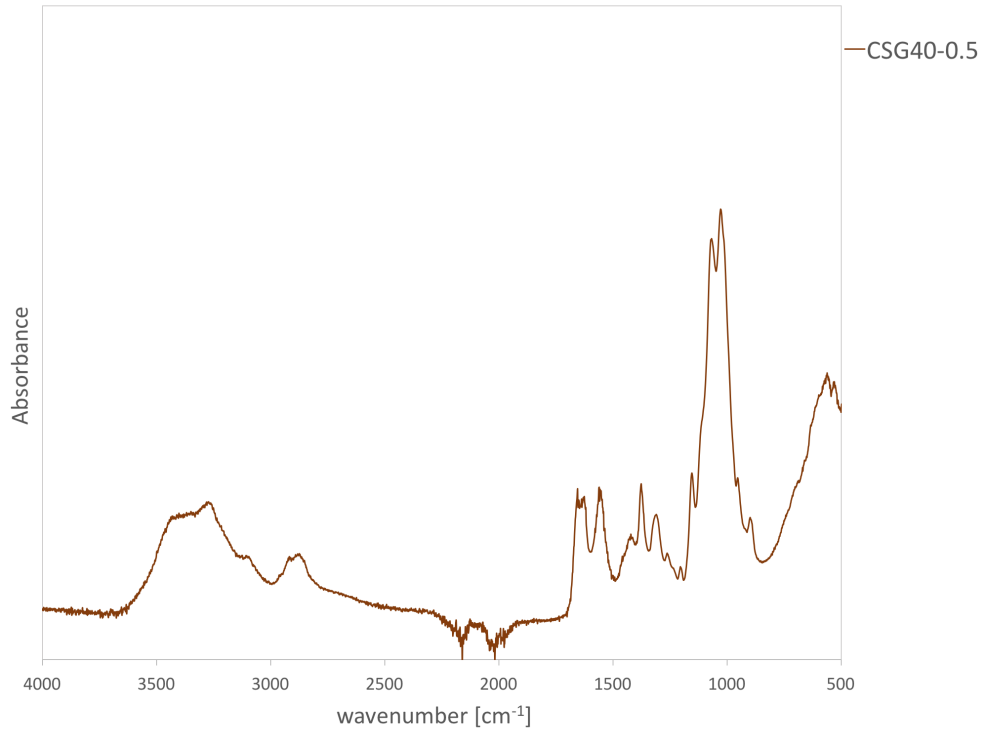

Figure 38: FTIR spectrum of CSG40-0.5

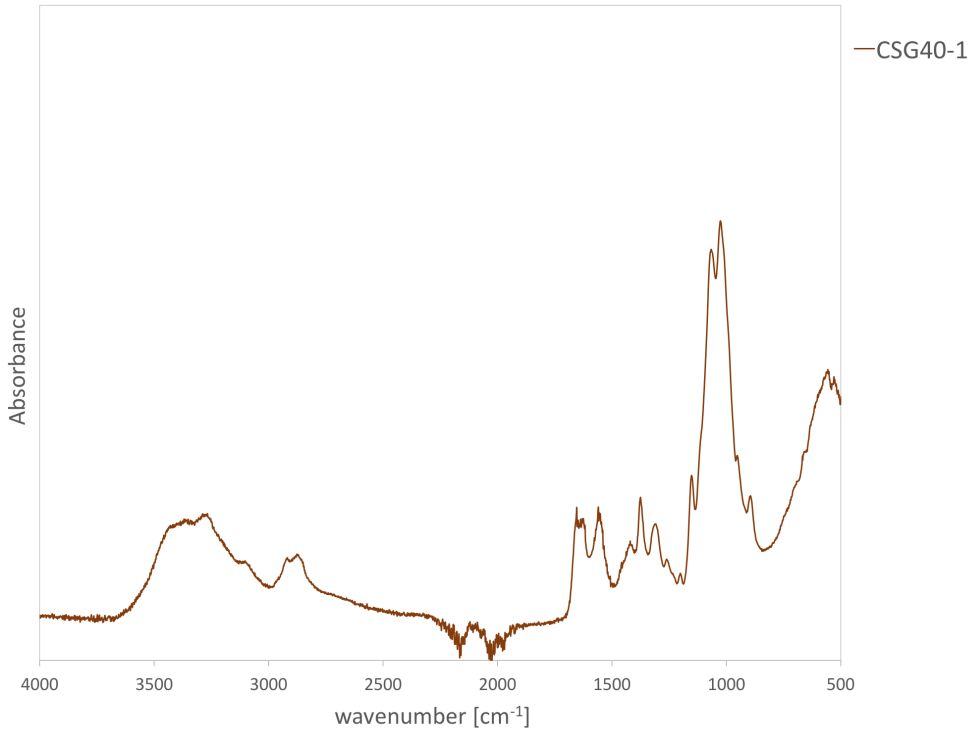

Figure 39: FTIR spectrum of CSG40-1

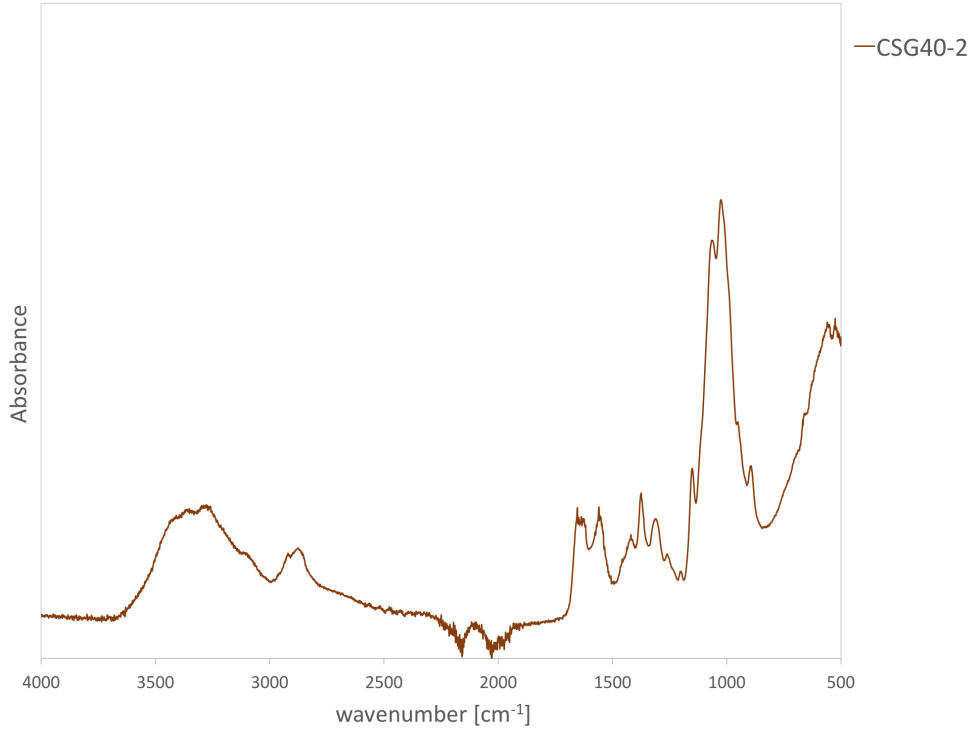

Figure 40: FTIR spectrum of CSG40-2

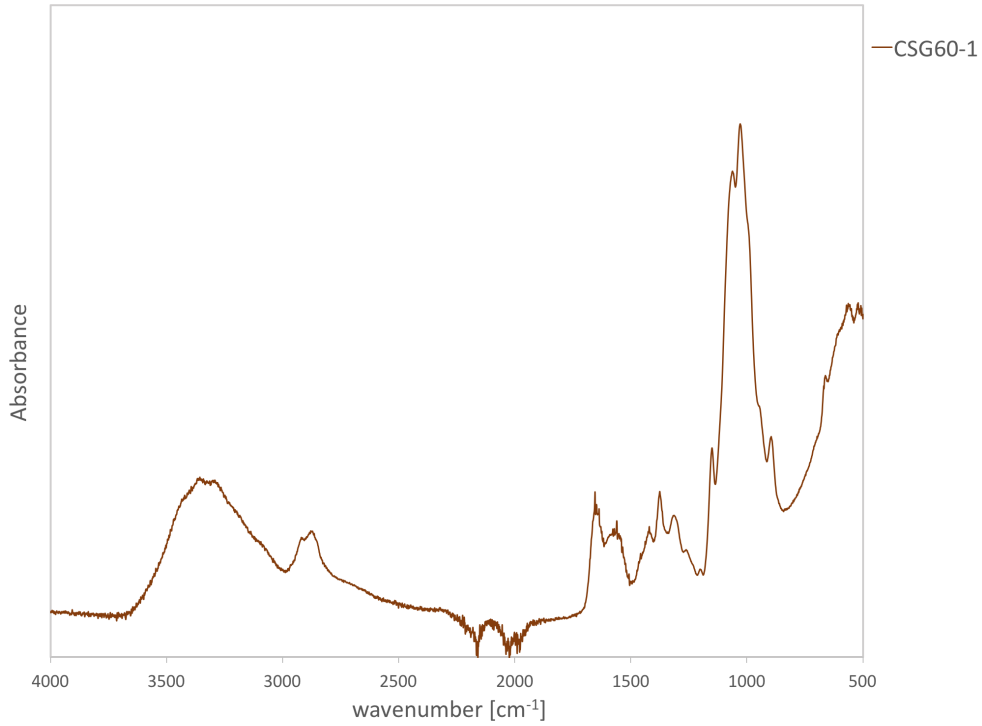

Figure 41: FTIR spectrum of CSG60-1

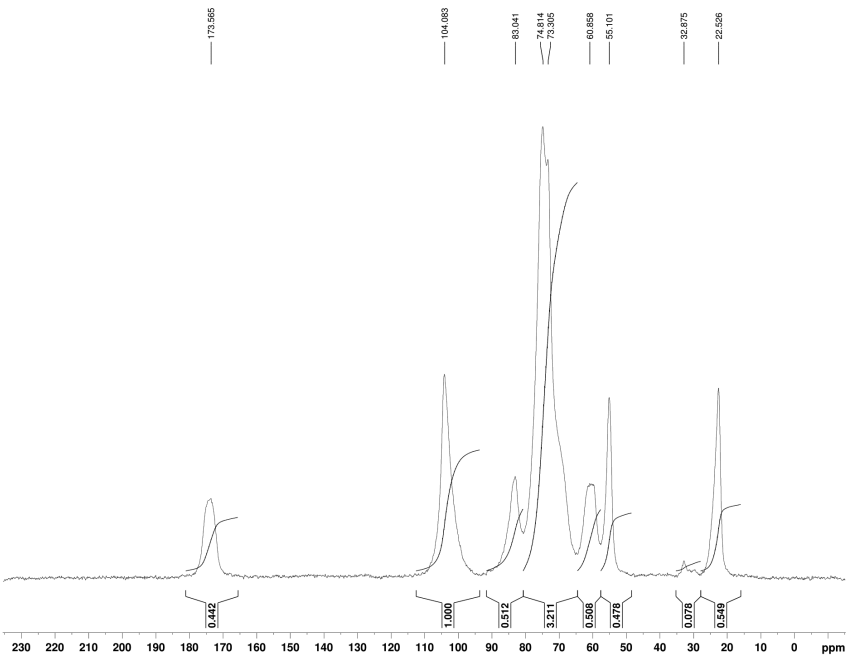

Figure 42: NMR spectrum of CG

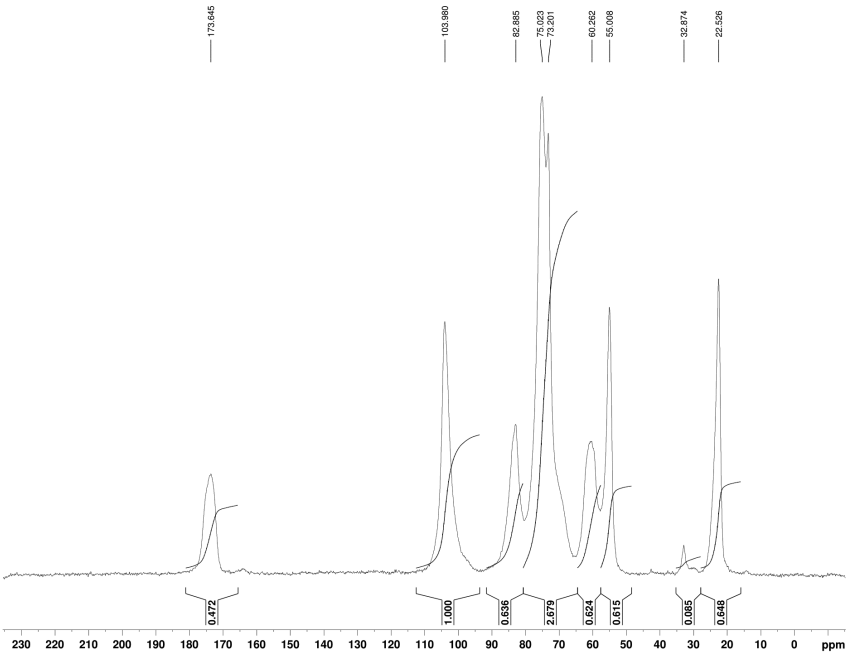

Figure 43: NMR spectrum of CSG20-1

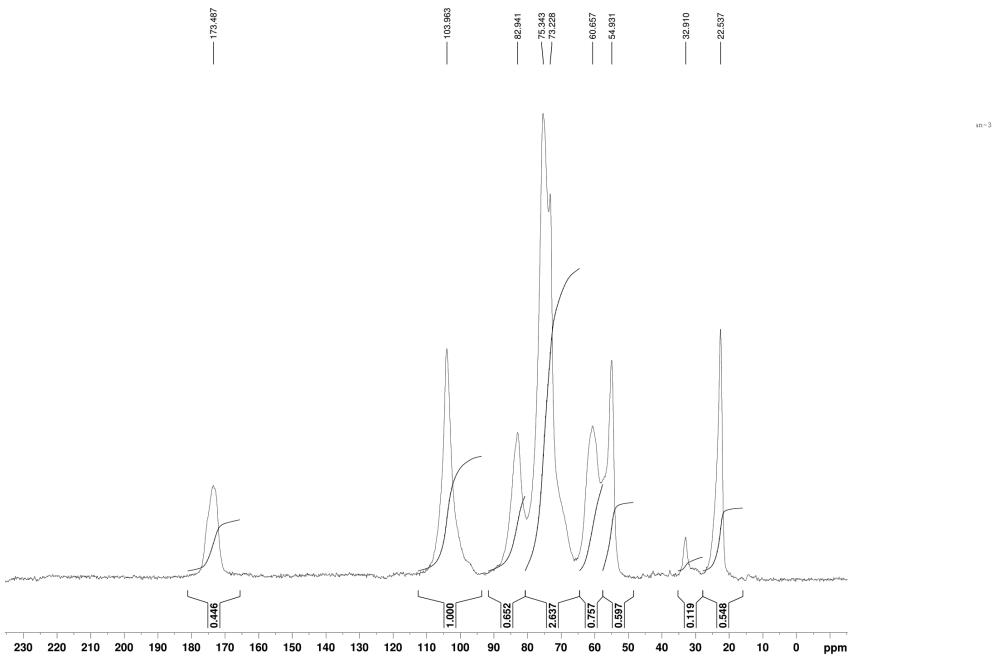

Figure 44: NMR spectrum of CSG40-0.5

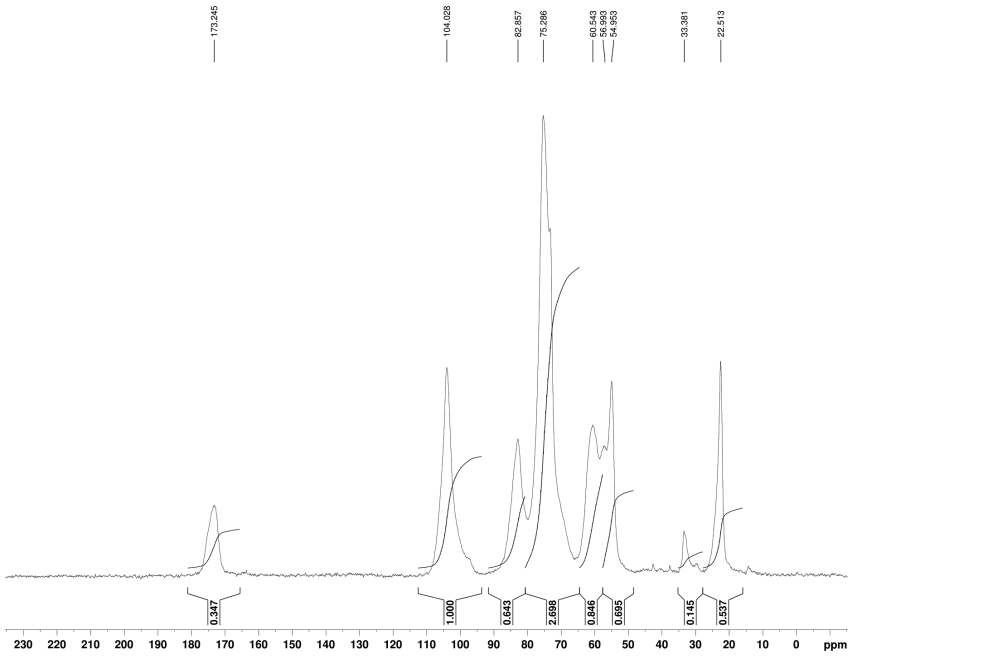

Figure 45: NMR spectrum of CSG40-1

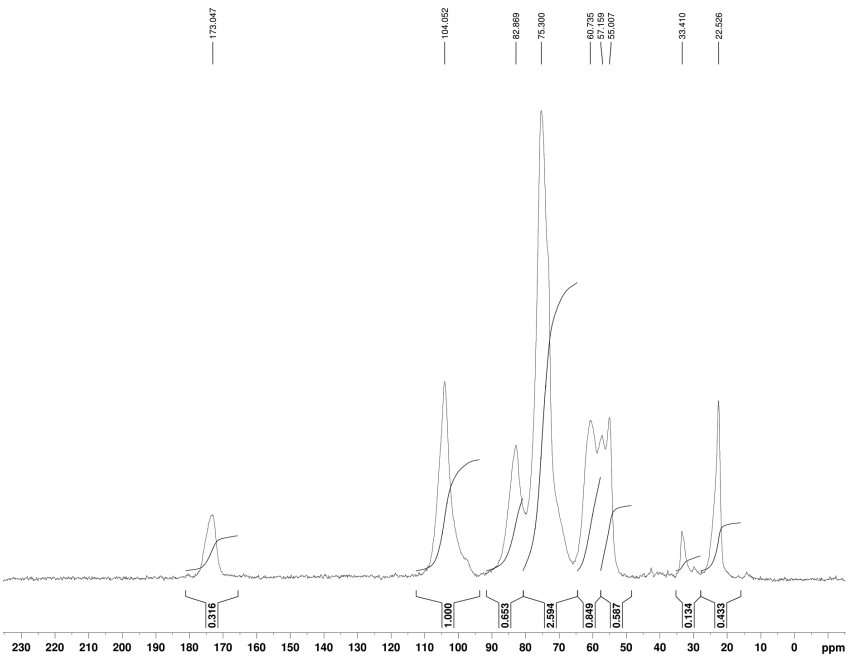

Figure 46: NMR spectrum of CSG40-2

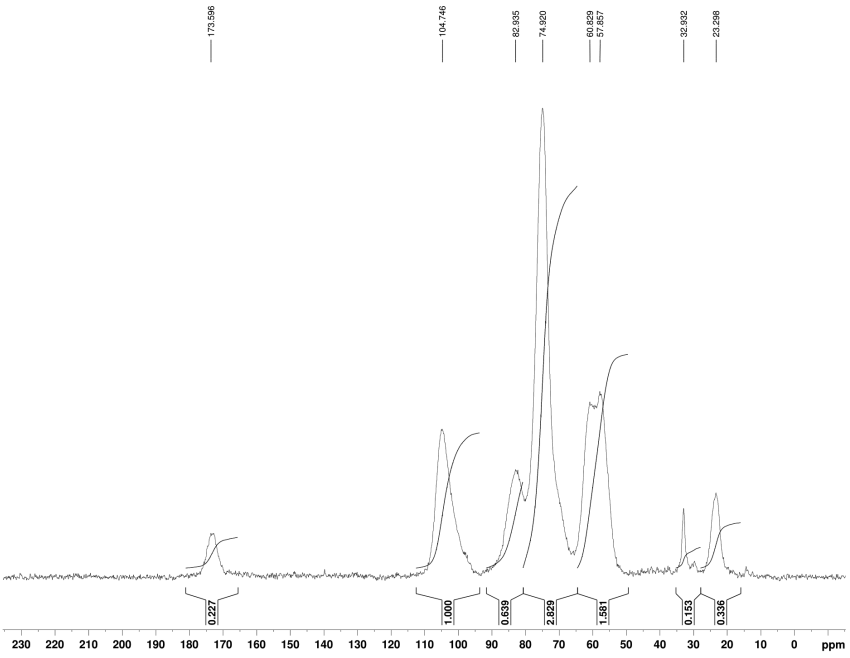

Figure 47: NMR spectrum of CSG60-1